Copyright Warning & Restrictions

The copyright law of the United States (Title 17, United States Code) governs the making of photocopies or other reproductions of copyrighted material.

Under certain conditions specified in the law, libraries and archives are authorized to furnish a photocopy or other reproduction. One of these specified conditions is that the photocopy or reproduction is not to be "used for any purpose other than private study, scholarship, or research." If a, user makes a request for, or later uses, a photocopy or reproduction for purposes in excess of "fair use" that user may be liable for copyright infringement,

This institution reserves the right to refuse to accept a copying order if, in its judgment, fulfillment of the order would involve violation of copyright law.

Please Note: The author retains the copyright while the New Jersey Institute of Technology reserves the right to distribute this thesis or dissertation

Printing note: If you do not wish to print this page, then select "Pages from: first page # to: last page #" on the print dialog screen

ABSTRACT

CONCURRENT EVAPORATING SPRAY JETS IN DILUTE GAS-SOLIDS PIPE FLOWS

by
Xiaohua Wang

Evaporating spray jets into gas-solids suspensions are encountered in many industrial applications. The rapid evaporation of spray jets has significant effects on the gas-solids mixing near the jet nozzle regions, including non-uniform solids concentration dilution, gas/solids temperature reduction, and gas/solids velocity acceleration. Furthermore, the jet structure is altered by the change of solids loading, jet mass flow rate and initial droplet size distribution. These interactions of gas, solids and evaporating droplets dominate the process efficiency and product quality. There is an urgent need for exploring fundamental mechanisms of the multi-phase interactions with heat and mass transfer as there are few reported studies on this topic.

This study is aimed at better understanding the phase interactions and microstructures of concurrent evaporating spray jets in gas-solids pipe flows. A study that combined experiments, analytical modeling and numerical simulation has been carried out to explore the unique characteristics of phase mixing and spray evaporation. A continuously circulating gas-solids suspension flow apparatus has been constructed, and a concentric liquid nitrogen spray jet was concurrently introduced into the fully developed gas-solids flow. The spray structure was investigated based on both laser-assisted flow visualization and temperature measurements along the axis using a thermocouple array. In order to interpret the experimental findings and go beyond the experiment limits, modeling approaches were developed, including analytical models and full-field

numerical simulations. The analytical model accounts for turbulent phase transfer and interactions between the spray and the ambient flow and successfully reveals basic characteristic phenomena such as the shortening of the spray penetration, evaporation induced temperature reduction and evaporation-induced gas acceleration. The numerical simulation, based on a hybrid Eulerian-Lagrangian method, yields the local phase interactions, evaporation rate, and phase distributions that would otherwise be difficult to determine.

In this study, an innovative and practical method has been developed for demarcation of the dense spray region and the dilute spray region in gas-solids suspensions with strong evaporation. Based on the thermocouple measurements, the dense evaporation length can be clearly determined from a jump in the axial temperature distribution. The proposed thermocouple measurement method can quantitatively determine the dense spray region not only for the cases where optical visualization can be applied but also for sprays in dense gas-solids flows and in dilute gas-solids suspensions with indistinguishable droplets and solids particles. The proposed mechanistic model for thermocouple measurement has successfully interpreted the temperature profiles; the model suggests that the spray region demarcation is characterized by two time scales, namely the collision contact time between a droplet and the thermocouple τ_c and the time interval between two adjacent droplet collisions on the thermocouple τ_{dd}.

In this work, a systematic investigation is carried out for the shortening effect of solids loading on the spray evaporation length. The evaporation length is found to decrease monotonically and asymptotically when the solids concentration is increased. Within the range of this study, a solids volumetric loading of 1.0% leads to shortening of

the total evaporation length by 50%, compared to that of the solids-free case, whereas the dense region length is shortened by nearly 70%. Due to the asymptotic nature, within the range of this investigation, the most sensitive range of shortening effect of solids loading occurs within 0.5%, whereas the shortening effect becomes relatively insensitive beyond this point. This indicates that the spray structure in a dense gas-solids suspension should be very similar to that in a dilute suspension flow.

The numerical simulation reveals a strong non-uniformity in phase distributions. It shows that a dense solids layer exists around the jet boundary, which affects the heat and mass transfer between the spray region and its surrounding flows. Another interesting finding is the existence of similarity in gas velocity profile in the main spray region. The dimensionless velocity distributions are not only similar but also match the Schlichting formula or "the Law of 3/2" of single-phase jets. It appears that the similarity model for a one-phase jet may be extended to three-phase jets with strong droplet evaporation.

CONCURRENT EVAPORATING SPRAY JETS IN DILUTE GAS-SOLID PIPE FLOWS

by

Xiaohua Wang

A Dissertation
Submitted to the Faculty of
New Jersey Institute of Technology
in Partial Fulfillment of the Requirements for the Degree of
Doctor of Philosophy in Mechanical Engineering

Department of Mechanical Engineering

May 2002

APPROVAL PAGE

CONCURRENT EVAPORATING SPRAY JETS IN DILUTE GAS-SOLID PIPE FLOWS

Xiaohua Wang

5-1-02

Dr. Chao Zhu, Dissertation Advisor — Date
Assistant Professor of Mechanical Engineering, NJIT

4-24-2002

Dr. Rajesh Ahluwalia, Dissertation Co-Advisor — Date
Senior Engineer, Argonne National Laboratory, Argonne, IL

5/2/02

Dr. Nadine Aubry, Committee Member — Date
Chairman and Professor of Mechanical Engineering, NJIT

5/3/02

Dr. Rajesh Dave, Committee Member — Date
Professor of Mechanical Engineering, NJIT

4/24/2002

Dr. Teh C. Ho, Committee Member — Date
Senior Research Associate, ExxonMobil R&D Corporation, Annandale, NJ

BIOGRAPHICAL SKETCH

Author: Xiaohua Wang

Degree: Doctor of Philosophy

Date: May 2002

Date of Birth:

Place of Birth:

Undergraduate and Graduate Education:

- Doctor of Philosophy in Mechanical Engineering,
  New Jersey Institute of Technology, Newark, NJ, 2002
- Master of Engineering in Fluid Mechanics,
  Tsinghua University, Beijing, P. R. China, 1996
- Bachelor of Engineering in Engineering Mechanics,
  Tsinghua University, Beijing, P. R. China, 1993

Major: Mechanical Engineering

Presentations and Publications

X. Wang and C. Zhu, "Concentric Evaporating Spray Jets in Dilute Gas-Solid Pipe Flows," Submitted to *Powder Technology*, 2002.

C. Zhu, G. Liu, X. Wang, and L.-S. Fan, "A Parametric Model for Evaporating Liquid Jets in Gas-Solid Flow," Accepted by *International Journal of Multiphase Flow*, 2001.

L.-S. Fan, R. Lau, C. Zhu, K. Vuong, W. Warsito, X. Wang, G. Liu, "Evaporative Liquid Jets In Gas-Liquid-Solid Flow System," *Chemical Engineering Science*, 56, 5871-5891, 2001.

C. Zhu, X. Wang, G. Liu, and L.-S. Fan, "A Similarity Model Of Evaporating Liquid Spray Jets in Concurrent Gas-solid Flows," *Powder Technology*, 119, 292-297, 2001.

C. Zhu, X. Wang and L.-S. Fan, "Effect of Solids Concentration on Evaporative Liquid Jets in Gas-Solid Flows," *Powder Technology*, 111, 79-82, 2000.

C. Zhu, X. Wang and G. Liu, "Numerical Simulation of Coaxial Evaporating Spray in Nozzle Region of Circulating Fluidized Reactor," To be presented on *ASME 2002 FED Summer Meeting*, July 14-18, 2002, Montreal, Quebec, Canada.

C. Zhu, G. Liu and X. Wang, "Oblique Evaporating Sprays in Gas-Solid Suspensions," To be presented on *ASME 2002 FED Summer Meeting*, July 14-18, 2002, Montreal, Quebec, Canada.

C. Zhu, X. Wang and G. Liu, "Effect of Particle Loading on Liquid Nitrogen Jet Mixing in a FCC Riser," *CFB7: 7th International Conference on Circulating Fluidized Beds,* May 5-8, 2002, Niagara Falls, Canada, 881-888.

C. Zhu, G. Liu and X. Wang, "Evaporative Cross-flow Jets in Gas-Solid Suspension Flows," *4th International Conference on Multiphase Flow ICMF'2001*, No. 117, New Orleans, LA, U.S.A., May 27-June 1, 2001.

C. Zhu, X. Wang and G. Liu, "Evaporative Liquid Jets in Concurrent Gas-Solid Pipe Flows," *Proceeding of NHTC'00 34th National Heat Transfer Conference*, NHTC2000-12143, Pittsburgh, Pennsylvania, August 20-22, 2000.

X. Wang, G. Liu and C. Zhu, "Experimental Study of Evaporative Liquid Jets in Vertical Gas-solid Pipe Flows," *AIChE 2000 Spring National Meeting*, No.18b, Atlanta, GA, March5~9, 2000.

C. Zhu, G. Liu and X. Wang, "Heat and Mass Transfer in Ultrasonic Enhanced Membrane Distillation," *AIChE 2000 Spring National Meeting*, No.18e, Atlanta, GA, March5~9, 2000.

This dissertation is dedicated to my wife, Xiaofen and my son, Andy.

ACKNOWLEDGMENT

I wish to express my sincere appreciation to my advisors, Dr. Chao Zhu and Dr. Rajesh Dave, for their remarkable guidance, constant supervision, friendship and moral support throughout this research. Without their guidance, it would have been impossible for me to finish this program so smoothly. Special thanks are given to Dr. Teh C. Ho, Dr. Nadine Aubry, Dr. Rajesh Dave for their active participation in my dissertation committee. I'm also thankful to Dr. L.-S. Fan at Ohio State University for his valuable suggestions and kind assistance during these years.

I acknowledge the supports from Department of Mechanical Engineering, New Jersey Institute of Technology for TA scholarship, ExxonMobil R&D Incorporation and Petroleum Research Fund for the research funding. Hongqing Xu, who was a visiting professor at NJIT in 1999, deserves many thanks for his great help in the laser visualization system setup. I would especially like to thank Dr. Susan Picologlou for the reading and correcting my dissertation thoroughly and carefully. I appreciate the friendship and cooperation of Dr. Guangliang Liu, Dr. Jianjun Luo, Tong Lee and all of my research group colleagues during this study.

I would like to express my endless gratitude to my parents, Shichao Wang and Yigen Du, who have always supported my academic pursuit and helped me in every possible way. I also would like to give the thanks to my brothers and sisters for their selfless dedication and generous support. Last, I want to thank my wife, Xiaofen Fu, and my son, Andy Wang, for their love and encouragement throughout these years.

TABLE OF CONTENTS

TABLE OF CONTENTS
(Continued)

TABLE OF CONTENTS
(Continued)

Chapter **Page**

TABLE OF CONTENTS
(Continued)

Chapter **Page**

LIST OF TABLES

LIST OF FIGURES

LIST OF FIGURES
(Continued)

LIST OF FIGURES
(Continued)

Figure **Page**

LIST OF SYMBOLS

Symbols	Meaning
A	area
Ae	aspiration efficiency
Ar	Archimedes number [$= d_s^3 \rho_g (\rho_s - \rho_g) g / \mu_f^2$]
C	specific heat
C_{D0}	standard drag force coefficient
C_D^*	effective drag force coefficient
d	diameter
D	pipe diameter
f	friction factor
g	gravity
h	heat transfer coefficient
H	latent heat or heat transfer
I	momentum transfer
k	thermal conductivity
L	length
m	mass or mixture
M	mass flow rate or molecular weight
$\dot{m}$	Volumetric evaporation rate
n	number density
Nu	Nusselt number
N_u^*	effective Nusselt number

LIST OF SYMBOLS
(Continued)

Symbols	Meaning
p	pressure
Pr	Prandtl number
q	heat flux
R	universal gas constant
r	radial coordinate
Re	Renolds number [$=d_d\rho_g v_{dg}/\mu_g$]
S	stress
S_{tk}	Stokes number [$= v_{st} v_0 /(gd_s)$]
T	temperature
v	velocity or vapor
We	Weber number [$=\rho_d d_d v_d^2/\sigma$]
x	axial coordinate
Y	species mass fraction

Greeks

α	volume fraction
γ	turbulent flutation rate
μ	Viscosity
ρ	density
τ	time
Γ	droplet evaporation rate

LIST OF SYMBOLS
(Continued)

Subscript

0	inlet (at x=0) or free stream
1	central region
a	ambient
c	collision or centerline or core region
d	droplet
e	evaporation
et	entrainment
g	gas or gauge
j	jet
LN	liquid nitrogen
n	nitrogen
o	oxygen
s	solid
t	terminal
tc	thermal couple
w	water

CHAPTER 1

INTRODUCTION

Evaporating liquid spray jets in gas-solids flows appear in many chemical and petrochemical processes. Examples include the condensed mode operation of polyethylene synthesis [Jenkins *et al.*, 1986], the fluid catalytic cracking (FCC) process for petroleum refinery [King, 1992], wet scrubbing systems for pollution control of the suspended particulates, and industrial processes of particle nucleation, agglomeration, and coating [Yang *et al.*, 1993].

A typical cracking FCC unit is shown in Figure 1.1. Heavy oil is injected into the FCC riser with recycle streams in the form of concurrent or oblique feed jets at the base of the feed riser, where the oil is mixed with the hot regenerated catalyst. During the mixing process, heavy oil droplets evaporate immediately, absorbing heat within the unit, whereupon the heavy oil vapor is carried into the reaction section with the hot catalyst particles. The cracking reactions start when the heavy oil droplets contact and are evaporated by the hot catalyst in the riser and continue until the oil vapor is separated from the catalyst in the reactor.

In a polymerization process as illustrated in Figure 1.2, a large amount of heat is generated over a short period of time during the reaction process. For high efficiency, operating temperatures are typically maintained close to the sintering temperature of the monomer to maintain process efficiency. Under these conditions, particle agglomeration, hot spot formation, and clogging of the gas distributor can occur, which lead to frequent shutdowns and require extensive cleaning of the reactor. In order to relieve the reactor of

the excess heat, an evaporative liquid with a boiling point lower than the operating temperature is injected into the reactor. As in the cracking units, the polymerization reactor is cooled significantly as the evaporating fluid absorbs energy equivalent to its latent heat.

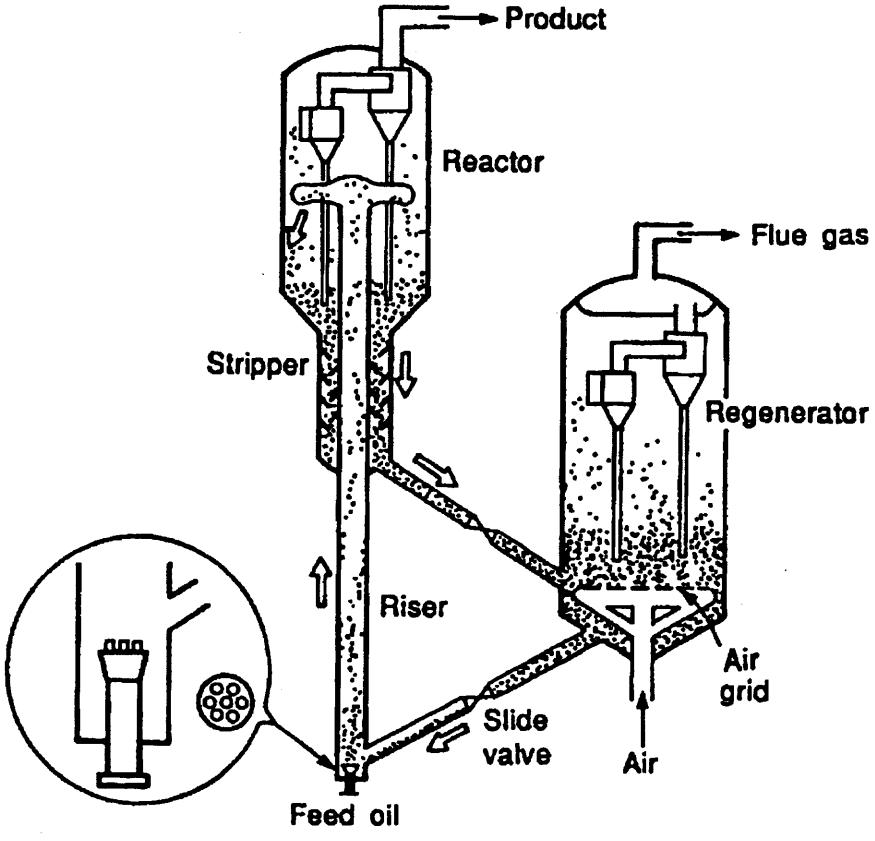

Figure 1.1 Riser cracking FCC unit
(Kunii & Levenspiel, 1991).

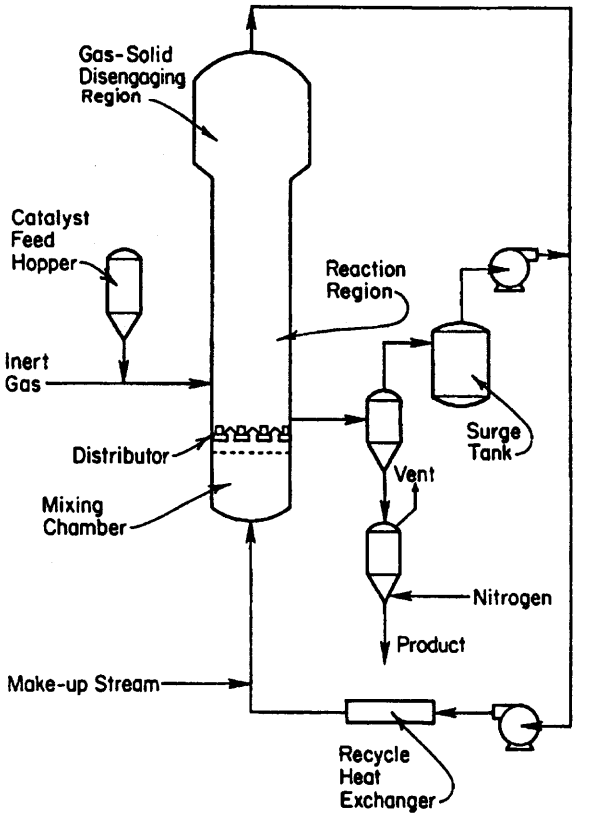

Figure 1.2 Condensed mode of operation for the polymerization process (Jenkins *et al.*, 1986).

Rapid cooling is only one consequence of the introduction of liquid spray jets into a gas-solids system. The resulting sudden expansion also has significant effects on the gas-solids interactions. Typical effects include the reduction of local phase temperature, dilution of the solids concentration, changes in phase velocities, and increase in turbulent intensity and phase collisions. Conversely, the introduction of solid particles represents a large heat sink that promotes evaporation and alters the liquid-solids interactions. The liquid spray evaporation induces a flow-field turbulent modulation and entrainment within the bed. This three-phase interaction behavior further complicates the dynamics.

The bed fluidization behavior, which is severely affected by these localized liquid jet disturbances, deserves a systematic investigation.

Only very limited research in the field of dilute non-isothermal three-phase flows, either numerical or experimental, has been reported so far. The subject of evaporating liquid spray jets in gas-solids flows is multi-disciplinary and also related to multi-phase flows. Closely associated research fields include fluid dynamics of two-phase jets, mixing of two-phase flows, evaporation of liquid droplets, particle-droplet collision, and particle-turbulence modulation. That all these fields are themselves under rapid development and many of them are interacting with other disciplines further complicates the nature of the study. For example, droplet evaporation in a gas-solids flow is much more complex than that in a packed bed of porous particles. Although the effect of particles on droplet/vapor flow should be considered, there is no dynamic coupling between the droplets and the particles. For simplicity, the literature survey on the topic of this research can be roughly separated into four sub-categories, as shown in Figure 1.3. Chapter 2 consists of a thorough review of published works in each field, focusing on progress linked to our main topic: evaporating spray jets in gas-solids flows.

The main objective of this study is to understand the fundamental mechanisms and microstructures of the evaporating liquid spray jets in concurrent gas-solids pipe flows. The emphasis is on the study of droplet evaporation and penetration in a gas-solids suspension. A combined effort of experimental measurements, analytical modeling and full-field numerical simulations has been carried out to investigate characteristics unique to evaporating spray jets in gas-solids pipe flows.

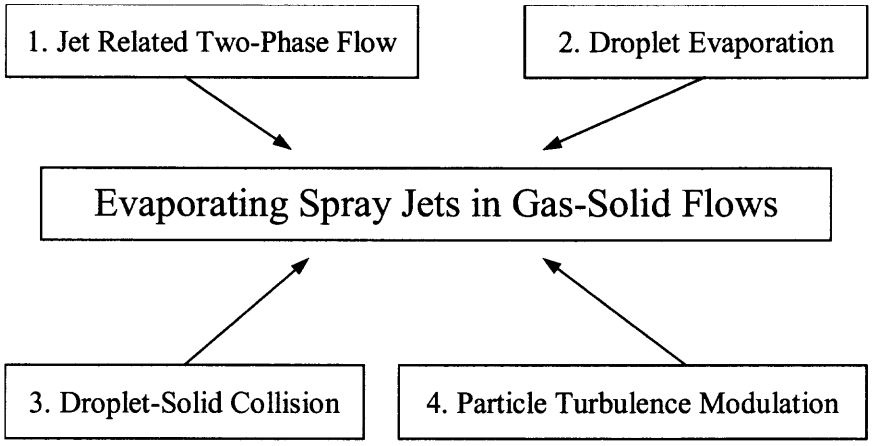

Figure 1.3 Sub-categories related to the thesis topic.

The experimental portion of this study attempts to explore the effects of parameters, such as the gas superficial velocity, solids concentration and liquid/solids loading ratio, on the spray evaporation characteristics. A test loop was set up that operates in a circulating fluidized bed (CFB). Liquid nitrogen was concurrently injected into the gas-solids pipe flow. A laser-assisted visualization system and a thermocouple measurement system were used to determine the spray structure in a gas-solids flow. The experimental investigation provides first-of-its-type data on the characteristics of evaporating spray jets in gas-solids flows. The data are used to explore the physical phenomenon and to validate analytical modeling and numerical simulations.

In the analytical modeling section, a one-dimensional model is formulated to elucidate the phase information of gas, solids, and droplets both in the evaporation region and in the ambient gas-solids flow region. A mechanistic model is also developed to build the linkage between the phase-averaged temperature and the temperature of each phase. The longitude profile of mixture temperature predicted by the analytical model

thus could be used to compare with the experimental measurements to validate the model. Based on the modeling predictions, various parametric effects on general flow characteristics are further investigated.

The numerical study is aimed to better understand the phase interactions and field distributions, which are difficult to study experimentally. The governing equations of gas-solids-liquid flows with strong phase interactions and transfers are developed, in which gas and solids phases are solved by the Eulerian method, while the droplet phase is modeled by the Lagrangian approach. This study particularly focuses on the effects of droplet evaporation on the phase dilution, temperature reduction and phase velocity change in the flow field. The general jet structure with droplet evaporation also could be revealed from this full field numerical simulation.

CHAPTER 2

LITERATURE SURVEY

As shown in Figure 1.3, the topic of evaporating spray jets in gas-solids flows overlaps several cross-linked fields, such as jet related two-phase flows, droplet evaporation, droplet-solids collision, and particle turbulence modulation. Following is a summary of literature survey in each respective field.

2.1 Jet Related Two-Phase Flow

Studies on the concurrent jet related gas-solids flows have been extensively reported over the past few decades. These studies are mainly focused on the effect of solids loading on the jet entrainment. Field (1963) measured the gas entrainment by an air-solids jet using Ricou and Spalding's (1961) direct measurement technique and found that the entrainment can be enhanced, suppressed, or unchanged depending on the size of the particles. Tatterson *et al.* (1987) studied a gas-solids free jet and found the particle effects on jet entrainment depends on the ratio of particle-stopping distance to nozzle diameter. In the presence of particles, gas entrainment increases for ratios less than 3; it decreases for ratios between 3 and 65, while no particle effect is found for ratios greater than 65. Tsuji *et al.* (1988) performed an experimental study of the air jet laden with coarse solids. They attributed the jet mixing to significant particle diffusion. Subramanian and associates (1982a, 1982b, 1984a, 1984b, 1985) studied concentric air jet mixing in a gas-solids suspension flow and calculated the jet entrainment from assumed distributions of phase velocities, particle concentration and phase temperatures. Measurements on

velocity distributions or entrainment velocities of phases of two-phase jets or of single-phase jets into two-phase flows have also been conducted [Memmot & Smoot, 1978; Subramanian & Raman, 1983; Filla *et al.,* 1983]. When a flow is turbulent, the addition of particles can either enhance or reduce the flow turbulence, affecting the transport behavior of both particles and fluid phases [Hinze, 1971; Gore & Crowe, 1989].

Many studies on an evaporative spray jet in a particle-free environment have been reported. These studies are typically focused on the droplet generation, evaporation and droplet-droplet interactions. Peter *et al.* (1994) experimentally investigated the flashing and shattering phenomena of superheated liquid jets injected into a flashing chamber. It was shown that a flashing liquid jet could either shatter or remain in the form of an irregular continuous column after being released from the nozzle. Exponential temperature distributions of the liquid jet along the axial direction were correlated. Bazile and Stepowski (1994) used dying visualization and image technique to study the atomization and vaporization dynamics of liquid methanol in a burning spray jet. Local vaporization dynamics was observed and reduction in droplet diameter was correlated. Silverman and Sirignano (1994) studied the effect of multi-droplet interactions on evaporation and droplet motion of a dense spray in a hot gas environment. Gavalses *et al.* (1996) used the phase Doppler method to evaluate the effect of droplet collisions on spray mixing. Kouremenous *et al.* (1995) developed a model to illustrate the phase change process of evaporation, in which the fuel spray is divided into three regimes, namely the sheet portion, the break-up portion, and the droplet portion. Lasheras *et al.* (1998) visualized the break-up and atomization of a round water jet by a high-speed annular air jet. The specific flux of kinetic energy supplied by the gas to the spray jet was

found to be the primary parameter determining the secondary break-up and coalescence of droplets in the far field.

Many researchers simulated the droplet evaporation and spray dynamics with partial verifications from experimental measurements. Zuev and Lepeshinskii (1995) proposed a mathematical model of a gas-droplet non-isothermal multi-component poly-disperse turbulent jet based on a multi-fluid concept by solving Eulerian governing equations. Chen and Pereira (1995, 1996) applied the Eulerian-Lagrangian stochastic method to the dilute evaporating spray in a co-flowing, turbulent heated air stream. The model showed that the droplet mass fluxes persistently accumulate near the centerline region. Sirignano (1999) addressed the spray and droplet behavior in terms of fluid dynamics and transport phenomena with both theoretical and computational studies. Various topics such as isolated droplet vaporization, heating and acceleration, multi-component liquid droplet, droplet-droplet and droplet-wall collisions, droplet interactions with turbulence and vortical structures, and other computational issues and applications need to be considered.

2.2 Droplet Evaporation

Several evaporation models of a single droplet have been widely used, such as the d^2 law, the infinite conductivity model, the limited conduction model, and the vortex model. Aggarwal *et al.* (1984) examined the effect of different models on the evaporation of a single-component droplet in a transient one-dimensional flow of air-fuel droplet mixture. It was shown that both the d^2 law and the infinite conductivity model are not adequate to predict the evaporation behavior in the convective environment. He recommended the

spherically symmetric conduction model for low Reynolds numbers and the simplified vortex model for high Reynolds numbers. With multi-component droplets, additional analysis of the liquid-phase mass diffusion is necessary for the prediction rates of each component [Aggarwal *et al.*, 1991; Hallett, 2000]. The effect of turbulent flow on the droplet evaporation rate has also been extensively investigated [e.g., Gakkhar & Ppakash, 1990; Michaeledes & Li, 1992; Haywood *et al.*, 1994]. The results showed that the turbulence enhancement elements could be advantageously used to improve the phase change process. Gemmen *et al.* (1990) and Sujith *et al.* (1996) studied the effect of acoustic fields on droplet evaporation rate by using both experimental and numerical approaches. The oscillating convection motion was found to greatly enhance the droplet evaporation rate.

Vaporization of a droplet in a spray is often affected by the interaction with its neighboring droplets [Chiang & Kleinstreuer, 1992; Silverman & Sirignano, 1994]. The droplet interactions may strongly affect various transport coefficients of the droplets, such as drag coefficient, Nusselt number and Sherwood number. Silverman and Sirignano (1994) developed a dense spray model to study the multi-droplet interactions on evaporation and motion of a dense spray in a hot gaseous environment. Sornek *et al.* (2000) and Reveillon and Vervisch (2000) respectively studied the effect of turbulence on vaporization, mixing, and combustion of liquid-fuel sprays with droplet interactions. It was shown that the turbulence produces more uniform spatial distribution of droplets and reduces the inter-droplet interactions, which hampers droplet evaporation. Spray evaporation may also be strongly affected by the droplet-vortex interactions, especially in turbulent jets with large flow entrainment and separations [Park *et al.*, 1996; Zuo &

Bulck, 1998]. Blake (1996) investigated the coupling effects between a downward spray and a rising saturated buoyant jet prior to impact on a heated surface.

A few studies of droplet evaporation in a gas-solids flow have been reported, in which many additional important factors control the droplet evaporation phenomena. Harpole (1980) and Lage and Range (1993) discussed the effect of thermal radiation on single droplet vaporization. Thermal diffusion was found to be essential to evaporation or combustion of fuel droplets with internal heat sources. Droplet evaporation also affects the droplet-solids collision [Leong *et al.*, 1985], which depends on the heat transfer type, collision time and contacting area. Buchanan (1994) analyzed the heating and vaporization of feed droplets in FCC risers. Considering the vapor diffusion of droplets and the effect of particles, he proposed an empirical correlation of the heat transfer coefficient for a droplet in the FCC riser. For droplets containing small particles, Elperin and Krasovitov (1995) used the quasi-steady approximation to develop an evaporation model, which takes into account effects of compressibility and penetration of a gas-vapor mixture within the porous shell.

2.3 Droplet-Solids Collision

The dynamics of droplet collisions is of considerable importance in the study of spray in gas-solids flows. The collision process generally involves large deformations and rupture of the interface separating or combining the drops. Chen *et al.* (1998a, 1998b) examined the effect of turbulence on droplet collisions by means of direct numerical simulation of turbulence and numerical computation of particle trajectories in a turbulent channel flow. Nobari *et al.* (1996) simulated the head-on collision of two droplets from solving Navier-

Stokes equations. Kitron *et al.* (1990) used the Monte Carlo method to simulate a head-on impingement of two gas-solids jets. Their results suggested that the particle concentration in the impingement region is strongly reduced by the effects of inter-particle collisions. There are many other reports on droplets collisions, including both theoretical studies [e.g., Luo & Svendsen, 1996; Jeelani & Hartland, 1998; Hagesaether *et al.*, 1999] and experimental ones [e.g., Jiang, 1992; Estrade *et al.,* 1999].

Very few literature reports are available on non-isothermal droplet-solids collisions. Nevertheless some fundamental mechanisms could be linked to collisions of droplets with isothermal curved surfaces or with non-isothermal planar surfaces. Levin and Hobbs (1971) used a high-speed camera to examine the isothermal droplet impact on a curved surface. Podvysotsky and Dubrovsky (1986) studied the mass transfer of the collision of droplets with a spherical solid particle and proposed an empirical correlation for a three-component polydispersed flow with coagulation and fragmentation of particles. Dear and Field (1988) experimentally investigated the geometric effect of a curved surface on the propagation of a shock wave in a liquid-solids collision. Dubrovsky *et al.* (1992) studied the isothermal collision of drops with solid particles of different sizes, which demonstrated that the impact of fast moving small drops on large solid particles results in droplet breakup and the formation of polydispersed fragments. Some mechanisms on particle agglomeration or coalescence of droplets by particle collisions have been numerically simulated [Bos & Ooms, 1985; Zinchenko & Davis, 1994]. Bussmann *et al.* (1997) investigated collisions of a single water droplet impacting on an arbitrary surface geometry, revealing a significant effect of surface curvature. Huang and Yao (1999) experimentally investigated the impact of water droplets on isothermal

cylindrical wires. Yao and Cai (1988) studied the impact of droplets on thin rectangular strips at a temperature beyond the Leidenfrost temperature. They showed that the impact includes a combination of splashing and cutting when the droplet size and strip thickness were comparable. Foss *et al.* (1989) proposed a parametric model of collision efficiency for collisions between an evaporating droplet and a non-spherical particle, in which effects of initial particle orientation, aspect ratio and rotational inertia were illustrated. So far, partially due to the lack of reliable experimental results, simple and reliable analytical mechanistic models of inter-particle collisions in a jet flow have not been developed.

2.4 Turbulence Modulation

In a turbulent particulate multi-phase flow, the particles are dispersed through turbulent flow fluctuations. The addition of particles can enhance or reduce the flow turbulence, affecting transport behavior of particle and flow phases. One of the earliest models for turbulence modulation in homogeneous dilute particle-laden flows is Hinze's approach (1971), in which "vortex trapping" of particles is assumed. According to this model, particles should always suppress the flow turbulence, which is true for fine particles but not supported by experimental results for large particles [Lee & Durst, 1982; Tsuji *et al.*, 1988]. One predominant mechanism for the enhancement of turbulence in the presence of large particles is due to wake shedding, i.e., vortex shedding from the particle wake. With a particle Reynolds number less than 110, there is no wake shedding, while, with a value over 400, wake shedding occurs [Achenbach, 1974; Hetsroni, 1989]. This observation suggests that large particles, with a particle Reynolds number over 400, lead to an

enhancement of the turbulence; i.e., the wake shedding by large particles causes energy to be transferred from the average velocity to the fluctuating velocity. Gore and Crowe (1989) proposed a critical ratio (about 0.1) of particle diameter to a characteristic integral length scale of turbulence. The turbulence intensity is enhanced when the ratio is greater than the critical value and is suppressed when the ratio is less than the critical value. This criterion indicates the turbulence is attenuated by small particles, while it is amplified by large particles.

At this stage, complete modeling including all of the preceding mechanisms is not possible because of the complex coupling relationships of the turbulent interactions and the lack of knowledge of turbulence generation. Nevertheless, simple mechanistic modeling accounting for a few of the predominant mechanisms of the modulation of turbulence has been numerically attempted [Parthasarathy & Faeth, 1990; Yuan & Michaelides, 1992; Elghobashi & Truesdell, 1993; McLaughlin, 1994; Yarin & Hetsroni, 1994; Wu & Faeth, 1995]. For evaporative droplet particles, the mechanism is more complex, no literature is available to explain the turbulence modulation, enhancement, or suppression.

2.5 Evaporating Spray Jets in Gas-Solids Flows

Reports on evaporating liquid spray in gas-solid flows have been scarce. Research in this field requires an interactive study of many advanced topics, such as dispersion and mixing of two-phase flows, particle-droplet collision, particle-turbulence modulation, and evaporation of liquid droplets. Preliminary measurements on flow mixing characteristics of evaporating sprays in gas-solids flows became available in the late 90s. In a

preliminary industry-scaled study of liquid nitrogen spray in FCC risers, Skouby (1998) used the sampling probe measurements to investigate the effect of nozzle characteristics on the flow mixing. It was found that the spray mixing is heavily dependent upon the nozzle design. Newton (1998) illustrated a x-ray imaging technique to visualize the flow patterns of a liquid nitrogen spray inside a large-scale fluidized bed, which showed a significant difference between the spray in the open space and the one in a fluidized bed. In an attempt to simulate the hydrodynamic and superheated characteristics of a riser reactor, Gu (1995) investigated the evaporation rate of liquid nitrogen spray in the riser. However, his model underestimated the phase interactions and hence the evaporation rate. Warsito and Fan (2001) developed an electrical capacitance tomography (ECT) system to capture images of an evaporating liquid nitrogen jet into the dense phase gas-solids fluidized bed. Using an image reconstruction algorithm, the cross-sectional images of the multi-phase flow system could be achieved from the measured capacitance values.

Several full-field numerical simulations on crude oil spray in FCC reactors were reported on the hydrodynamic processes of heat transfer, droplet evaporation, and mixing Chang *et al.* (1996, 1998) performed a full-field numerical simulation of oil spray in FCC reactors. The hydrodynamic processes of heat transfer, droplet evaporation, and mixing were investigated. However, in his study, the effects of particle-droplet collisions on droplet evaporation were ignored. Gupta and Rao (2001) investigated the effect of atomization on the performance of a fluid catalytic crack riser reactor by numerical simulation. Most parameters including heat transfer, gas oil vaporization, and catalyst entrainment and catalytic deactivation are considered in this one-dimensional model, while each phase is assumed to be well mixed. Hence, this model couldn't provide the

detailed hydrodynamic mixing process of the evaporative spray in gas-solids flow. Gao *et al.* (2001) established a three-dimensional gas-liquid-solid three-phase model, incorporating thirteen-lump kinetics for residuum cracking reactions. Since the droplet evaporation rate is a strong function of droplet size, the multi-lump method may lead to a large biased error in the estimation of droplet evaporation rate. In these numerical simulations, some significant mechanisms such as phase interactions on phase transfer and collision-dominated droplet evaporation were either ignored or oversimplified. In addition, these numerical simulations were not experimentally validated. A similar approach of solving full-coupling Eulerian equations has also been applied for other gas-solids-droplet flows such as food drying process and bio-reactor applications [Crowe, 1984; Straatsma *et al.,* 1999].

CHAPTER 3

EXPERIMENTAL METHOD

3.1 Introduction

The experimental investigation was concerned with the determination of the spray-jet structure, such as the jet penetration depth and phase temperature, in a gas-solids pipe flow. For the experimental study, a test loop with an operational mode of circulating fluidized bed (CFB) was set up, as shown in Figure 3.1. The liquid nitrogen is used as the jet liquid, and the solids are FCC particles. In this study, both laser-assisted visualization and a temperature measurement system are used. The parametric effects of ambient inlet gas velocity, solids concentration and liquid/solids ratio on the spray jet characteristics were experimentally investigated. In this chapter we will introduce the experimental setup of the gas-solids pipe flow system, spray jet system, and measurement methods.

3.2 Experimental Setup of the Gas-Solids Pipe Flow System

In this part, the circulating fluidized bed loop for establishing a continuous gas-solids suspension flow will be described with the associated methods to determine the experimental operation parameters.

3.2.1 Circulating Fluidized Bed Loop

As shown in Figure 3.1, the major integral parts of the circulating fluidized bed loop include a riser, a cyclone separator, a downcomer, a porous-plate distributor, and a couple of valves for solids flow control. The vertical riser is the main component of the system

and is 2.5 m in height and 2 inches in inner diameter. The fluidizing gas is introduced into the system through the distributor located at the bottom of the riser, whereas the solid particles from the downcomer are recirculated, fed via a control device and carried upward in the riser. The test section is located in the center of the riser, where the solids are nearly fully developed and the liquid nitrogen spray jet is introduced. The test section is made of a transparent acrylic tube, which could withstand temperatures down to –200°C. The particles, separated from the carrying gas by a 6-inch cyclone (PE-06, RSG), are collected in the downcomer and recirculated to the riser.

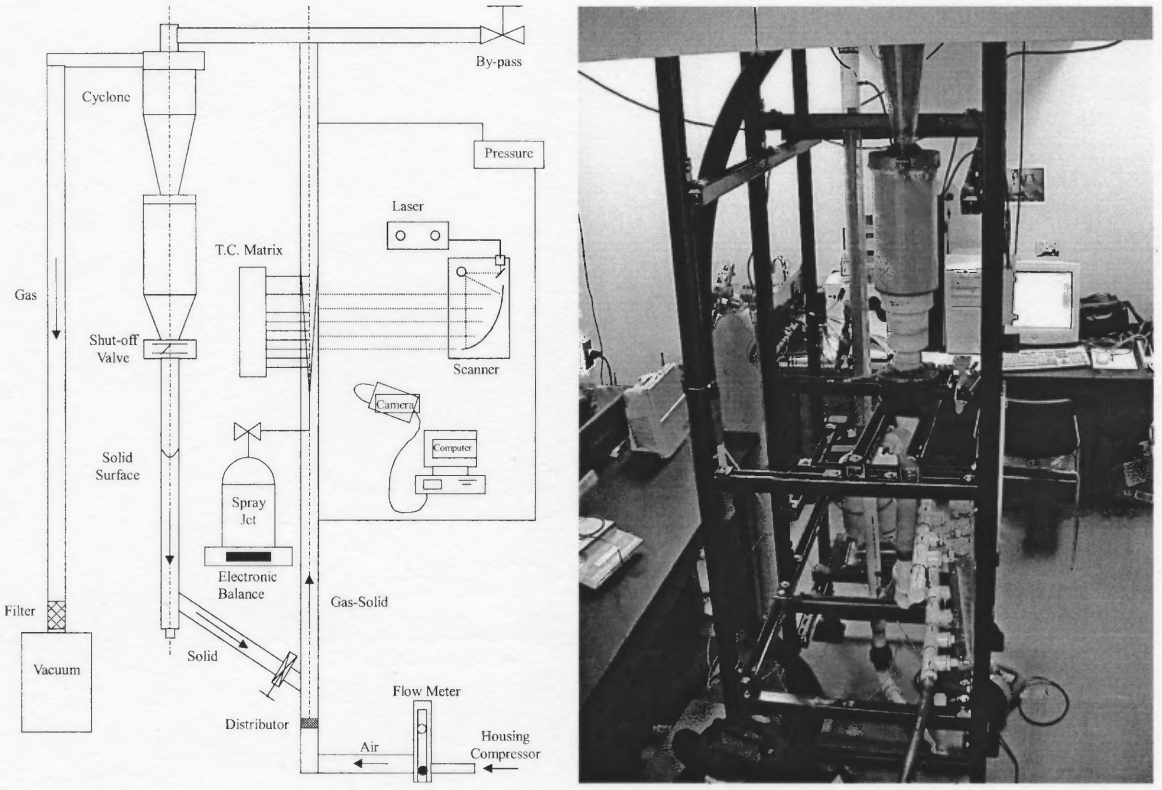

(a) Schematic diagram. (b) Photograph.

Figure 3.1 Experimental and measurement system.

The gas-solids flow system is operated by a combination of a house compressor and an induced fan for better control of the flow and circulation of solids. The air from the house compressor is regulated into a low pressure with a maximum flow rate of 2600 SCFH. The air flow rate in the riser is fully controlled by adjusting the Dwyer flow meter valves. In order to satisfy the minimum velocity required for solids separation in the cycle, an additional air stream is introduced into the loop by the induced fan (QPL625, Shop-Vac) through the by-pass valve, which is located atop of the test section and near the cyclone inlet. The gas from the cyclone exit, a particulate-laden gas, passes through the vacuum filter before it is discharged to the building ventilation hood. Besides easy control of the gas flow rate in the system, the combination of positive-pressure (compressor) and negative-pressure (vacuum) flow operation is also convenient for particle collection and pollution control. Since the pressure inside the loop is kept lower than that of the ambient air, there is no out-leaking particulate pollution.

The solid particles are FCC particles of 70 μm in mean diameter and 1200 kg/m^3 in density. The solids are fed into the gas flow above the distributor, a stainless steel porous disc with an averaged 40-μm pore size and a thickness of 0.062 inch. The high-pressure drop across the distributor leads to a uniform gas flow distribution in the riser. The solids feeding and mixing are illustrated in Figure 3.2, where the distributor is mounted in the PVC tee. In principle, the solids feeding rate could be adjusted by controlling the feed control valve. However, this method may not be effective under certain experimental conditions. For example, at low air humidity, significant electrostatic charges may be generated directly affecting the flow of solids in the downcomer, especially near the feeding valve (metal). Thus, a second air stream with a

small amount of gas is introduced near the feed valve to aerate the solids in the packed bed of the downcomer. In this experimental system, the second gas stream is provided by the nitrogen gas cylinder. In order to reduce static charge buildup in the system, a small amount of quaternary ammonium compound (LAROSTAT®519, PPG/MAZER CHEMICALS) is added with the solids.

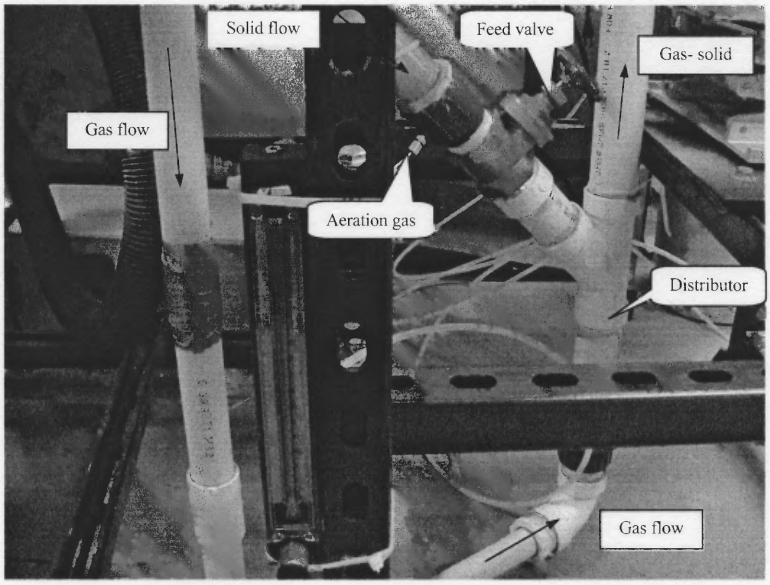

Figure 3.2 Photograph of the solids feeding and mixing parts.

A fully developed gas-solids suspension is obtained in the vertical test section (1.5 m above the distributor), where a concurrent and concentric liquid nitrogen spray is introduced. The spray droplets penetrate into the gas-solids suspension and collide with solids in the test section, then quickly evaporate. Both laser-assisted visualization and a temperature profile measurement are used to study the spray jet structure in the test section. The solids are separated from the gas-solids flow by a 6-inch I.D. cyclone (PE-06, RSG) with a high collection efficiency, as shown in Table 3.1. The solids flow further

down through a butterfly valve, then pass through a feed valve, and are transported to the riser through the solids inlet. The solids feeding rate is up to 10.0 g/s.

Table 3.1 Cyclone Collection Efficiency (Gas Flow Rate100 CFM)

Microns	Collection (%)
75	99.999
45	99.7
30	98.1
20	95.3
10	90.0
5	76.9
2	53.6

3.2.2 Determination of Operation Parameters

The determination of parameters for ambient gas-solids flows was conducted without spray jets injecting into the pipe flow. Three operation parameters, namely, the gas flow rate, the solids mass flow rate, and the pressure drop across the test section, are measured to determine gas and solids velocities and solids concentration in the ambient flows. Air flow rate to the CFB was metered by the Dwyer flow meters of RMC-104 (0~400 SCFH), RMC-106 (0~1000SCFH) and RMC-108 (0~1800SCFH). These flow meters are arranged in parallel, as shown in Figure 3.3, and each flow meter has a needle valve to control the individual gas flow rate. This combination provides an easy way to control and measure the flow rate with both rough and fine adjustment. In this experimental study, the gas flow rate was changed from 400 SCFH to 2100 SCFH, which corresponds to a gas velocity of 1.6 m/s to 5.6 m/s in the 2-inch pipe flow, respectively.

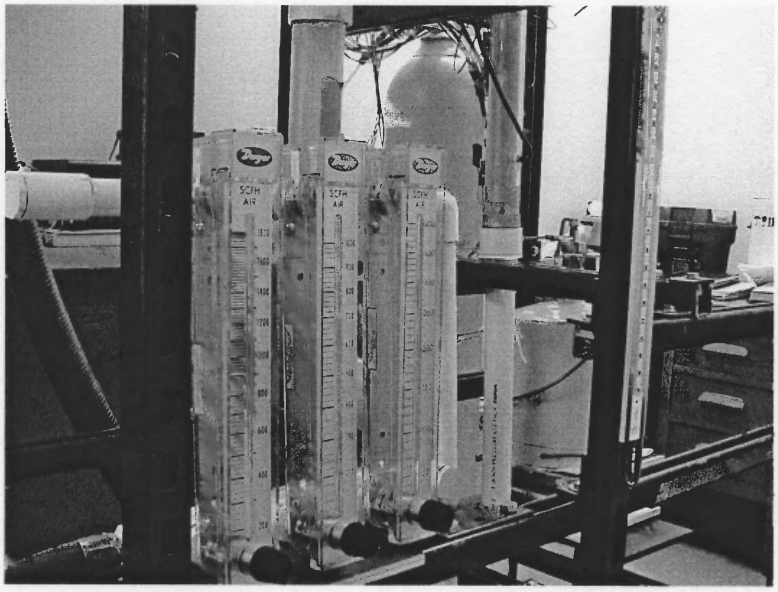

Figure 3.3 Dwyer flow meters for air flow measurement and control.

At present, no accurate method exists for measurement of the solids mass flow rate. In this study, we adopted an approximate method. After the butterfly valve in the downcomer is quickly closed, recycling of the solids phase was stopped, and the solids started to accumulate in the bin collector. A ruler mounted on the outside of the tube measures the surface rising speed of the packed solids. Since the effect of valve closing does not immediately affect the flow of the returning solids, the initial surface rising speed can be used to estimate the overall solids flow rate before the closing. In this estimation, the packing density of solids needs to be estimated and the collapsing effect of solids due to the valve closing needs to be either estimated or ignored.

Some other variables are also monitored during the experiments, for example gas and solids temperature and pressure drop along the test section. The gas and solids temperatures are measured by the thermocouples inserted in the gas inlet and in the

downcomer. The pressure drop along the fully developed bed is detected between two points across the test section wall with one-meter vertical distance. This pressure drop reflects the solids holdup in the riser, which reflects the averaged solids concentration in the riser.

3.2.3 Determination of Phase Velocity and Concentration

Since the solids concentration is very low (less than 1%), the gas velocity is determined from the gas flow rate at the inlet. When the solids movement can be approximated as one-dimensional in the test section, the group solids velocity can be directly measured using the duo-beam cross-correlation method [Zhu *et al.*, 1991]. However, this method will fail when the solids are uniformly distributed at very dilute conditions or when the solids are in a recycling motion at the wall boundary at the relatively dense conditions. Regarding the determination of solids concentration, many approaches are available, for example the Phase-Doppler Anemometry method [Sommerfeld & Qiu, 1995], optical probes [Johnsson & Johnsson, 2001] and capacitance probes [Wiesendorf & Werther, 2000]. In this study, gas/solids velocity and solids concentration under stratified flow conditions are determined from the gas flow rate, bed pressure drop and correlation relationship between gas velocity and solids velocity under dilute conditions. Schematic diagram of stratified gas-solids flow in a vertical pipe is shown in Figure 3.4, where the flow region is divided into a central flow region with dilute gas-solids moving upward and a wall boundary region with sliding bed moving downward.

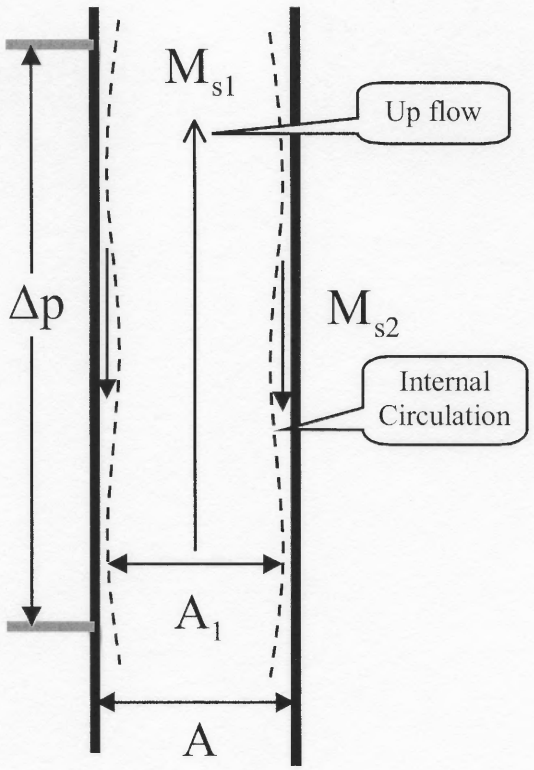

Figure 3.4 Schematic diagram of stratified gas-solids flow in a vertical pipe.

In the central region, the mass flow rate for the gas phase is expressed as:

$$M_{g1} = \rho_g \alpha_{g1} v_{g1} A_1 . \tag{3.1}$$

For the dilute gas-solids flow, the solids velocity is given from the correlation relationship between gas velocity and solids velocity [Klinzing *et al.*, 1989]

$$\frac{v_{s1}}{(gD_1)^{1/2}} = \left[\frac{v_{g1}}{(gD_1)^{1/2}} - \left(\frac{v_t}{(gD_1)^{1/2}} \right)^{0.087} \right] \left(\frac{D_1}{d_s} \right)^{0.031} \left(\frac{\rho_g}{\rho_s} \right)^{0.0321} \left(\frac{1}{2} \right)^{0.0765} . \tag{3.2}$$

Based on the momentum balance, the pressure drop can be estimated by:

$$\frac{dp}{dx} = \rho_g \alpha_{g1} g + \rho_s (1 - \alpha_{g1}) g + f_s \frac{\rho_g v_{s1}^2}{2D_1} (1 - \alpha_{g1}), \tag{3.3}$$

where f_s is the solids friction factor in vertical pneumatic conveying, which could be expressed by [Yang, 1974]:

$$f_s = 0.0206 \frac{1-\alpha_{lg}}{\alpha_{lg}^3} \left[(1-\alpha_{lg}) \frac{Re_t}{Re_s} \right]^{-0.869} . \tag{3.4}$$

Assume that the area of stratified flow is much less than the cross section of pipe flow. Using the actual measured pressure drop, the gas velocity, solids velocity and solids volume fraction could be estimated from Equation (3.1) to Equation (3.3). Furthermore, the internal solids mass flow rate could be calculated by

$$M_{sl} = \rho_s (1-\alpha_{gl}) v_{sl} A_l . \tag{3.5}$$

The difference between the calculated mass flow in the central region and the solids loading from external circulation yields the mass re-entrainment rate (or stratified flow) near the wall:

$$\Delta M = M_{sl} - M_s . \tag{3.6}$$

To validate the above analysis method, measurements of solids flow in the central region are taken from the isokinetic sampling system shown in Figure 3.5. When the gas velocity is low, anisokinetic sampling is required. For anisokinetic sampling, collection aspiration efficiency is defined as the ratio of actual sampling rate and free stream theoretical sampling rate as [Belyaev & Levin, 1974]

$$A_e = \frac{C_s}{C_0} = 1 + \frac{(2 + 0.062 v_s/v_0) S_{tk}}{1 + (2 + 0.062 v_s/v_0) S_{tk}} \left(\frac{v_0}{v_s} - 1 \right), \tag{3.7}$$

where v_0 is free stream velocity; v_s is the sampling velocity. S_{tk} is the solids Stokes number, which is a function of solids terminal velocity and solids diameter:

$$S_{tk} = \frac{v_{st} v_0}{g d_s} . \tag{3.8}$$

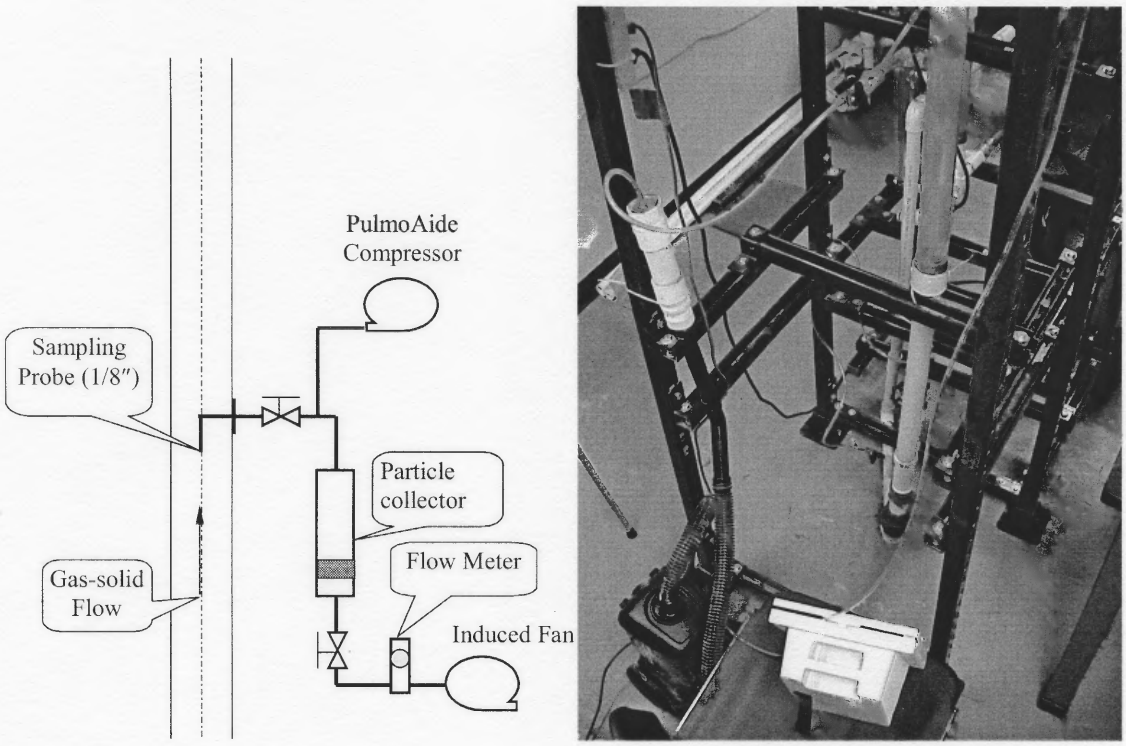

(a) Schematic diagram. (b) Photograph.

Figure 3.5 Isokinetic sampling system.

Table 3.2 Determination of Solids Concentration in Vertical Gas-Solids Pipe Flow (External Solids Loading 12.2 g/s)

Gas	M_{s1}	Sampling Mass Flow			α_{g1}	Velocity (m/s)	
		Analy.	Meas	Corr.		Gas	Solids
900	12.0	3.2	3.17	3.32	.9981	3.61	2.79
800	15.3	3.95	3.50	3.56	.9973	3.21	2.42
700	15.1	3.9	4.16	4.09	.9969	2.81	2.05
600	24.0	6.2	6.75	6.34	.9939	2.42	1.68
500	27.2	6.95	10.0	9.05	.9921	2.02	1.31

Table 3.2 compares the measurements using isokinetic sampling with the analytical predictions. It shows that when the solids concentration is low, the results are comparable. However, when the solids concentration is high, the experimental measurement of solids mass flux exceeds the analytical results. This may be due to the non-uniform axial distribution of solids concentration in the test section.

3.3 Liquid Nitrogen Spray Jet System

In this section, the liquid nitrogen spray system and its calibrations will be described. The system can operate at room temperature with an adjustable jet velocity. Calibration of the system includes determination of the jet mass flow rate, jet velocity and droplet initial size under the different operation conditions.

3.3.1 Evaporating Spray System

A liquid nitrogen spray jet system with a 5-liter dewar (Brymill Cryogenic), as shown in Figure 3.6, is used to generate the evaporating jet spray that is introduced into the gas-solids suspension flow at room temperature. With the aid of partial evaporation via a heat transfer coil, the liquid nitrogen is pressurized in the dewar. Driven by the pressure difference between the dewar and the test section, a liquid nitrogen spray jet can be generated. In this study, the maximum mass flow rate of liquid nitrogen is about 5.0 g/s with a dewar pressure of 12 psi and nozzle opening of 1.5 mm. Due to the effect of heat leakage along the spray tube, a small fraction of liquid nitrogen is pre-vaporized before injection so that the liquid nitrogen spray is actually a liquid-vapor mixture. Calibration

of the spray nozzle will be illustrated in next section, which describes the experimental parameter determination.

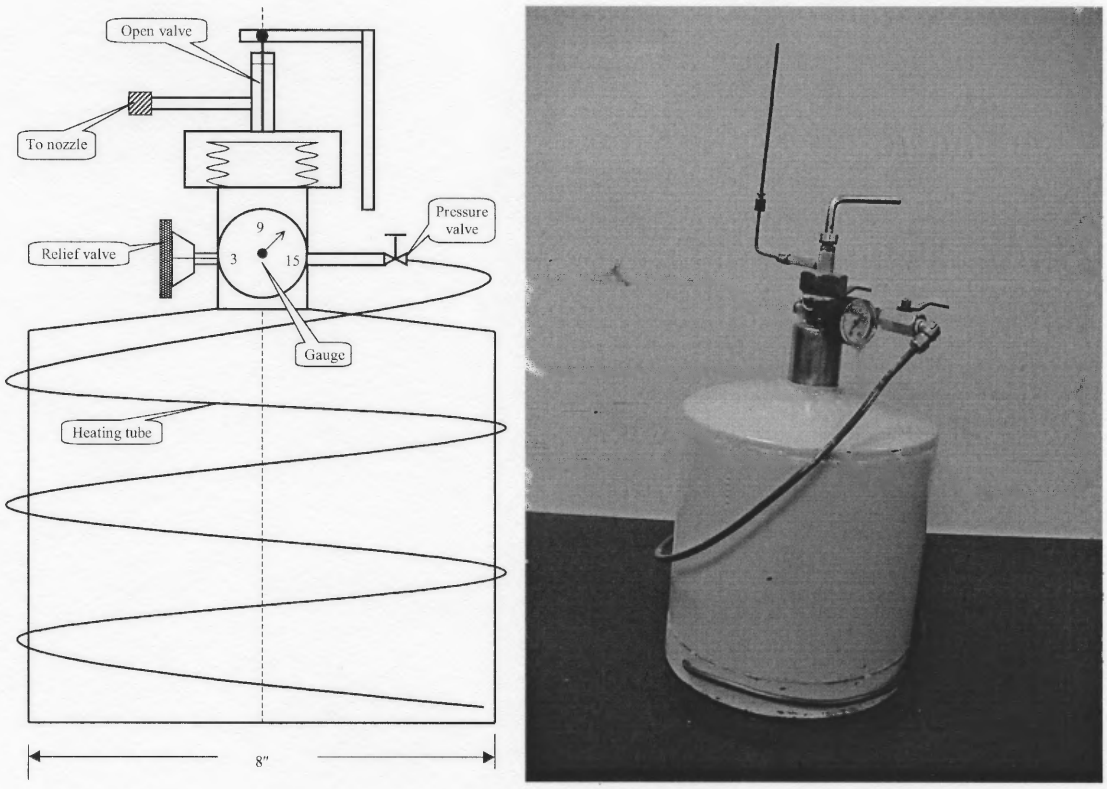

(a) Schematic diagram. (b) Photograph.

Figure 3.6 Spray jet system with 5-liter dewar.

3.3.2 Spray Calibration

Characteristic parameters for the spray jet include the spray mass flow rate, injection velocity of droplets, droplet size, and liquid volumetric fraction at injection. As noted, due to the heat leakage of the spray system, a small fraction of liquid nitrogen in the nozzle tube is pre-vaporized before the injection so that the liquid nitrogen spray is

actually a mixture of vapor-liquid nitrogen. Thus, the mass flow rate of liquid nitrogen and droplet jet velocity calibrations should be separated.

The spray mass flow rate is directly measured by an electronic balance (SV-30, Acculab) with a digital output. This balance has a capacity of 30 kg and a readability of 0.005 kg. The tank is first filled full with liquid nitrogen, then the gas pressure inside the tank is adjusted by controlling the liquid evaporation rate in the heat transfer coil to 10 psi (gauge pressure). By opening the jet valve, the liquid will be pushed out by the pressure difference. Since the jet status depends on the heat transfer on the nozzle tube, a certain waiting period (two to five minutes in this case) is needed before the start of measurements to allow the jet system to reach a heat transfer balance and a stable spray. Figure 3.7 illustrates a history curve of tank weight with liquid nitrogen, in which the initial weight is around 9.4 kg, and all the liquid nitrogen is sprayed out within 25 minutes. The liquid nitrogen flow rate is about 0.15 kg/minute.

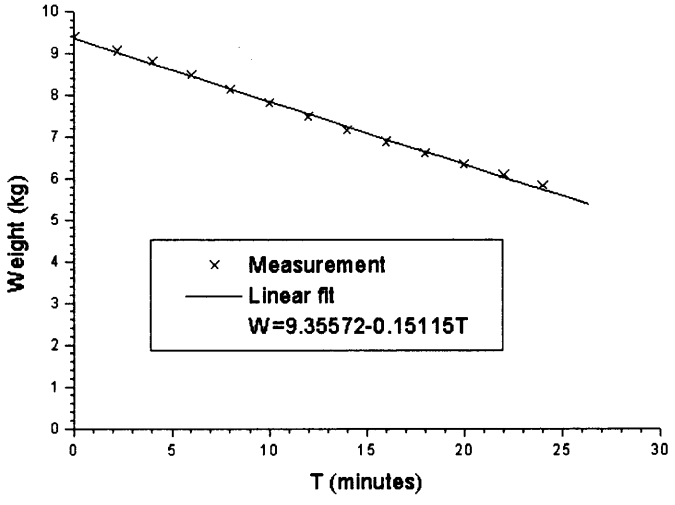

Figure 3.7 Calibration of liquid nitrogen mass flow rate (d_j=0.8 mm, p_g=10.0 psi).

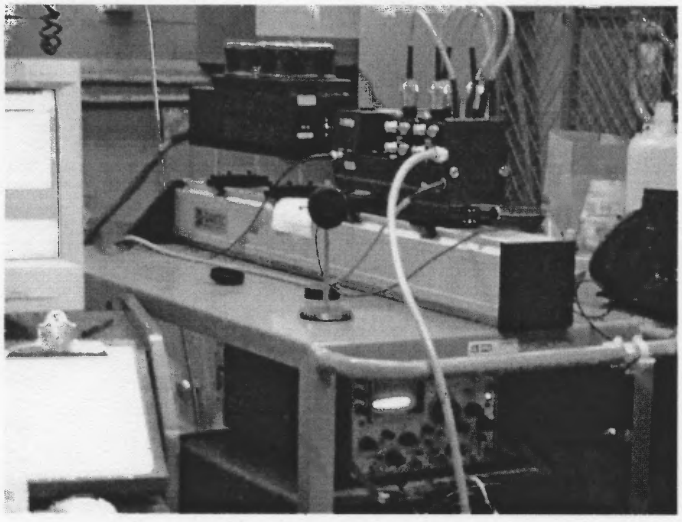

(a) Dantec PDPA system.

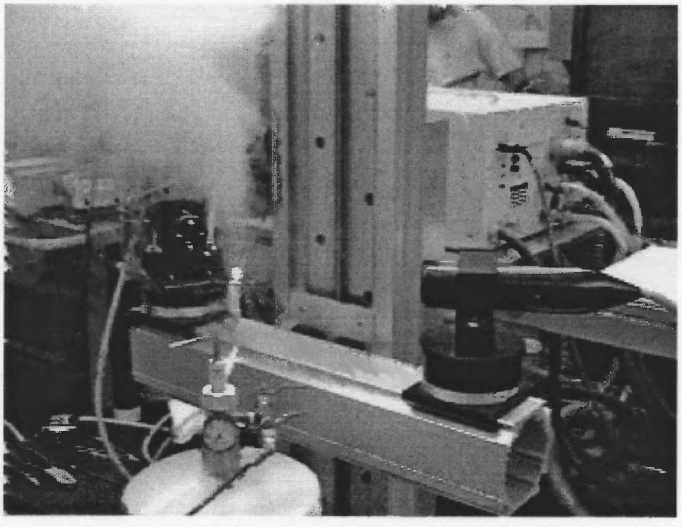

(b) Experiment setup and probes.

Figure 3.8 Spray jet calibration system.

The velocity and size distributions of the liquid nitrogen sprays were calibrated near the nozzle exit using a Phase Doppler Particle Anemometer (PDPA 58N70, Dantec). The PDPA 58N70 system and experimental setup are shown in Figure 3.8. The optical lens is 250 mm. The focus is adjusted in the center of the liquid nitrogen spray, which is about 15 mm over the spray nozzle. Figure 3.9 shows the measurement schematic diagram.

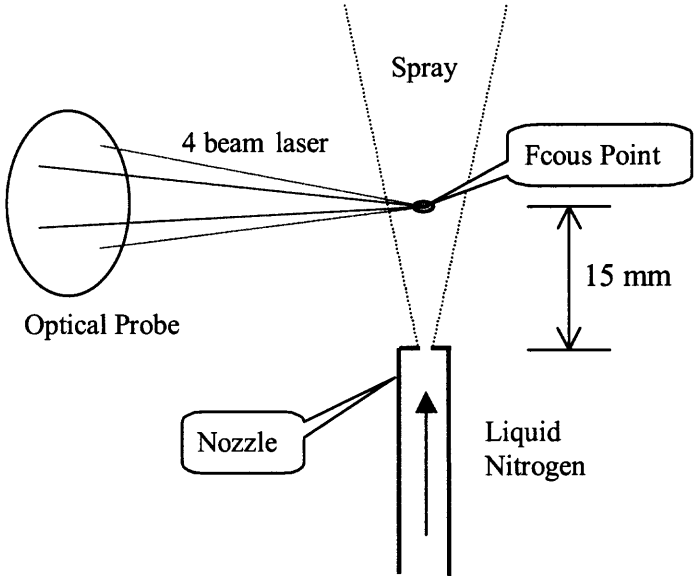

Figure 3.9 Laser Doppler Velocimeter measurement schematic diagram.

The experimental conditions are listed in the Table 3.3. In the measurement of spray velocity, the Laser Doppler Velocimeter (LDV) mode of the PDPA system is used, in which only one optical probe is needed. Figure 3.10 illustrates a typical histogram of the velocity measurement within a sampling period of 20 seconds, which indicates that the velocities are Gaussian distributed. The averaged velocity is 23.48 m/s with 6.0 m/s in

standard deviation for the axial velocity, whereas the mean is 1.15 m/s with 1.6m/s in standard deviation for the radial velocity.

Table 3.3 List of Calibration Conditions

Pressure inside the Tanks	10 Psi
Measurement Point	15 mm above Nozzle
Focus Length	250 mm
Sampling Time	20 Seconds

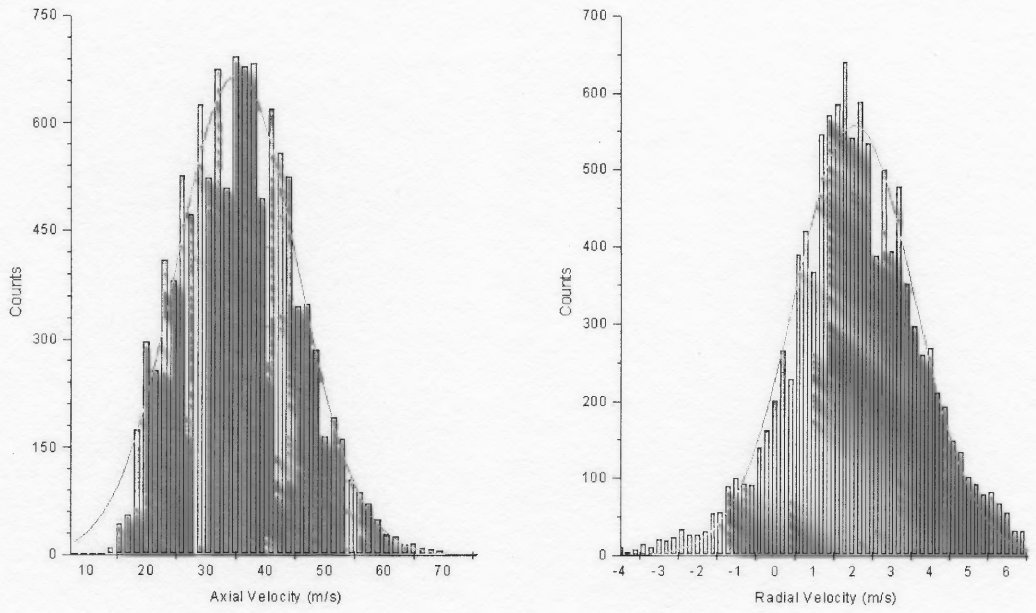

(a) Axial velocity. (b) Radial velocity.

Figure 3.10 Typical velocity measurement results (L6G9).

Table 3.4 lists the velocity calibrations for different nozzles under a tank pressure of 10 psi. The nozzle geometry and dimensions are illustrated in Figure 3.11 and Table

3.5, respectively. The data in Table 3.4 show that the spray velocity depends on the nozzle tube length and nozzle openness. The longer the tube length, the more liquid is pre-evaporated, and consequently the higher the spray velocity. The nozzle with a smaller opening also leads to an increased jet velocity.

Table 3.4 Spray Velocity near the Nozzle Exit

Nozzle	Axial Velocity (m/s)		Radial Velocity (m/s)	
	Mean	σ	Mean	σ
L3G3	37.87	11.85	2.18	1.98
L3G6	25.10	7.30	1.88	1.80
L3G9	23.90	6.775	1.25	1.68
L6G3	39.63	12.23	1.52	2.14
L6G6	37.15	10.0	1.37	1.93
L6G9	35.79	9.66	2.00	1.79
L9G3	47.47	12.25	2.87	1.94
L9G6	36.14	10.80	1.03	1.91
L9G9	32.22	9.44	3.86	1.61

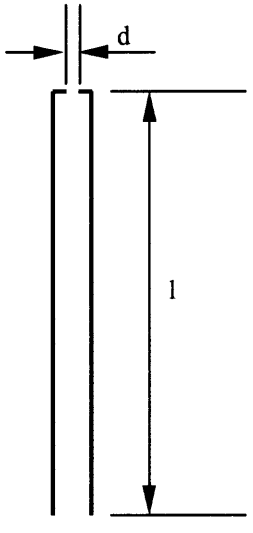

Figure 3.11 Schematic diagram of the nozzle geometry.

Table 3.5 Nozzle Geometry Dimensions

Nozzle Type	Dimensions
L3G3	l: 76.2 mm d: 0.3 mm
L3G6	l: 76.2 mm d: 0.6 mm
L3G9	l: 76.2 mm d: 0.8 mm
L6G3	l: 152.5 mm d: 0.3 mm
L6G6	l: 152.4 mm d: 0.6 mm
L6G9	l: 152.4 mm d: 0.8 mm
L9G3	l: 228.6 mm d: 0.3 mm
L9G6	l: 228.6 mm d: 0.6 mm
L9G9	l: 228.6 mm d: 0.8 mm

Measurement of the droplet size is much more difficult than measurement of the velocity since the PDPA system requires the use of both an optical sender and optical receiver. Figure 3.12 presents a typical droplet size distribution with the use of nozzle L6G9, in which the average size for large droplets is about 90 μm. Due to the current equipment limitation of the PDPA system, the receiver probe could only detect droplets up to 120 μm. A wider range of measurements requires the use of a lens with a larger focal length or laser sheet image analysis. In the numerical simulation and analytical model, an average droplet size of 120~160 μm is assumed, and the effect of droplet size on spray jet structure is discussed.

Assuming non-slip in velocity between vapor and droplets at the nozzle tip, we estimate the vapor volume fraction in the initial vapor-liquid mixture from liquid mass flow rate and droplet velocity by

$$\alpha_g = \frac{1}{\rho_d - \rho_g}\left(\rho_d - \frac{M_j}{\pi r_j^2 v_d}\right). \tag{3.9}$$

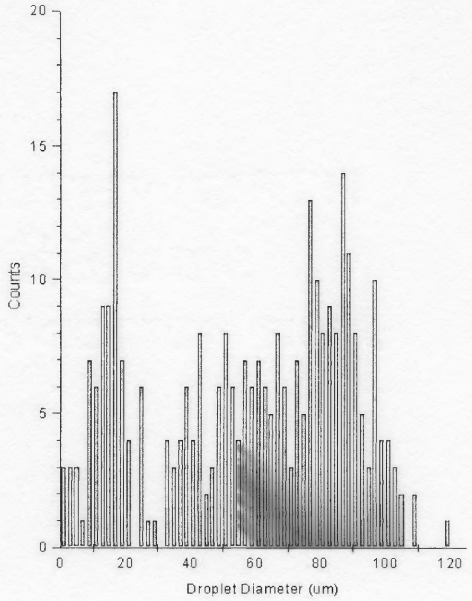

Figure 3.12 Typical droplet size distribution (L6G9).

For example, nozzle L6G9 has an averaged velocity of 35.79 m/s, a mass flow rate of 2.5 g/s and a nozzle size of 0.8 mm in diameter under the tank pressure of 10 psi. The vapor fraction is thus estimated to be 82.6% from Equation (3.9), which corresponds to less than 3% of mass fraction.

3.4 Measurement Methodology

In this experimental study, the major characteristic parameters of interest include jet penetration length and flow pattern. The penetration length is measured using a temperature measurement system with fast response thermal probes, while the flow

pattern is captured by a laser-assisted visualization system. The measurement methods are introduced briefly in the following sections.

3.4.1 Laser-Assisted Visualization

As previously described, the test section is made of a transparent acrylic tube, which provides a window for us to investigate the flow pattern in the nozzle region. The test section is illuminated by the sweeping laser sheet, where the flow pattern images are captured by the digital camera. The laser sheet generation system is shown in Figure 3.13 and Figure 3.14. The laser sheet generation mechanism is explained in the following.

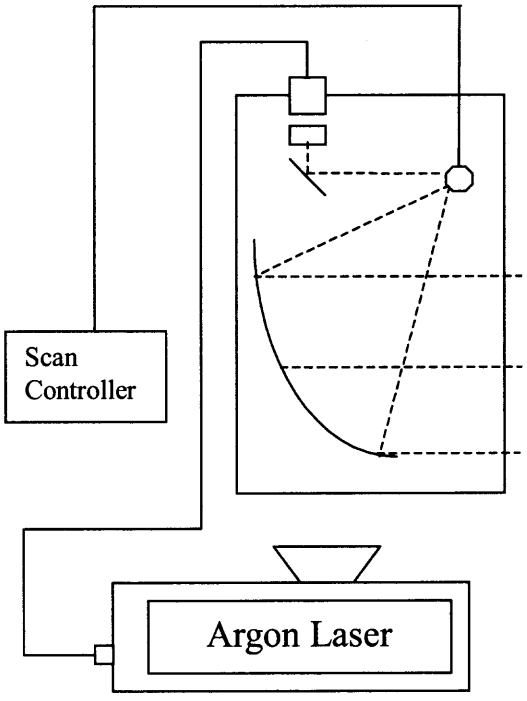

Figure 3.13 Schematic diagram of the laser sheet generation system.

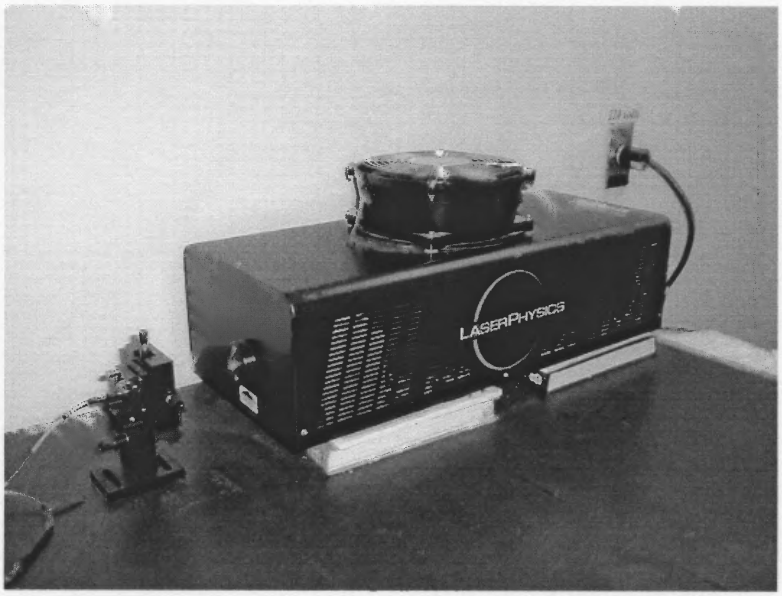

(a) Argon Ion Laser generator and fiberlinker.

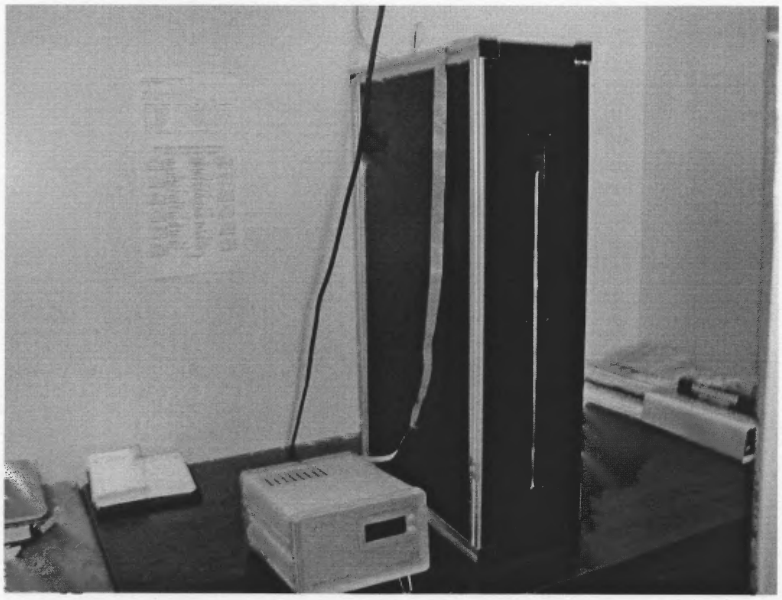

(b) Laser sheet scanner and controller.

Figure 3.14 Photograph of the laser sheet generation system.

First, the laser beam is generated from an argon ion laser (Reliant 1000M, LaserPhysics) with a 3-watt maximum output, then it is sent into a beam-rotating scanner (Optical Flow Systems) by an optical fiber. The scan projects a straight "light" line from the laser beam by reflecting it off a rapidly spinning metal polygon. The scan pattern is 45 degrees in extent and is created by the 8-sided polygon mounted on the shaft of a DC motor. Since the scanner is located in the focus of a parabolic mirror, the final laser beam will be parallel during the sweeping. The laser sheet generated by this rotating scanner has a width of 0.5 m in the vertical direction, which can illuminate the test section meridian plane. The internal motor is powered by a DC power source, and the rotating speed can be adjusted by the scanner controller to match the image exposure time. In this system, the scanning period ranges from 0.5 ms to 12.7 ms.

With the sweeping laser sheet illumination, the spray jet flow pattern near the nozzle region can be visualized, and the images are captured by a CCD camera (ES310, Kodak). The Kodak Megaplus Camera, ES310 is a high-speed, real-time, progressive-scan digital CCD camera with 648 X 484 pixels, imaging from 30 to 85 frames per second. The exposure setting of the camera is from 94 μs to 12 ms in the continuous mode. By adjusting the camera exposure setting and the laser-scanning rate, many different imaging modes can be achieved, such as one frame one exposure, or one frame multi-exposure. Both digital and analog video output are available for the image analysis, which is conducted by the image analysis system (XCAP, EPIX Corporation).

Typical microstructure images of liquid nitrogen jets in air are illustrated in Figure 3.15, which shows that the general structure of evaporative liquid jets can be sectioned into a central core of dense vapor droplets and a surrounding region of dispersed vapor

droplets. Figure 3.15(b) shows a detailed portion of the evaporation region, in which the individual flying droplets and gas entrainment near the jet boundary can be identified.

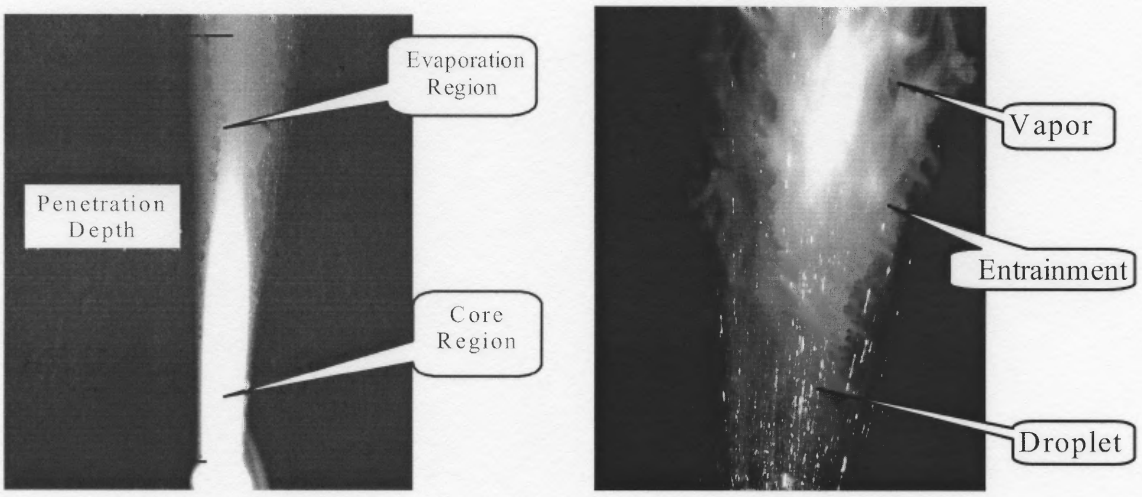

(a) Spray jet evaporation regions. (b) Fully developed evaporation region.

Figure 3.15 Microstructure of liquid nitrogen jet in air.

3.4.2 Temperature Profile Measurement System

A temperature profile measurement system has been set up in the test section to measure the temperature distribution along the spray direction, as shown in Figure 3.16. There are 38 thermocouples distributed along the pipe centerline (see Figure 3.16 and Table 3.6). The thermocouple is OMEGA copper constantan 304SS sheath T type. The sheath diameter is 0.020 inch, and the junction is grounded. The thermocouples are connected to a switchboard; the temperature is displayed in a LCD display.

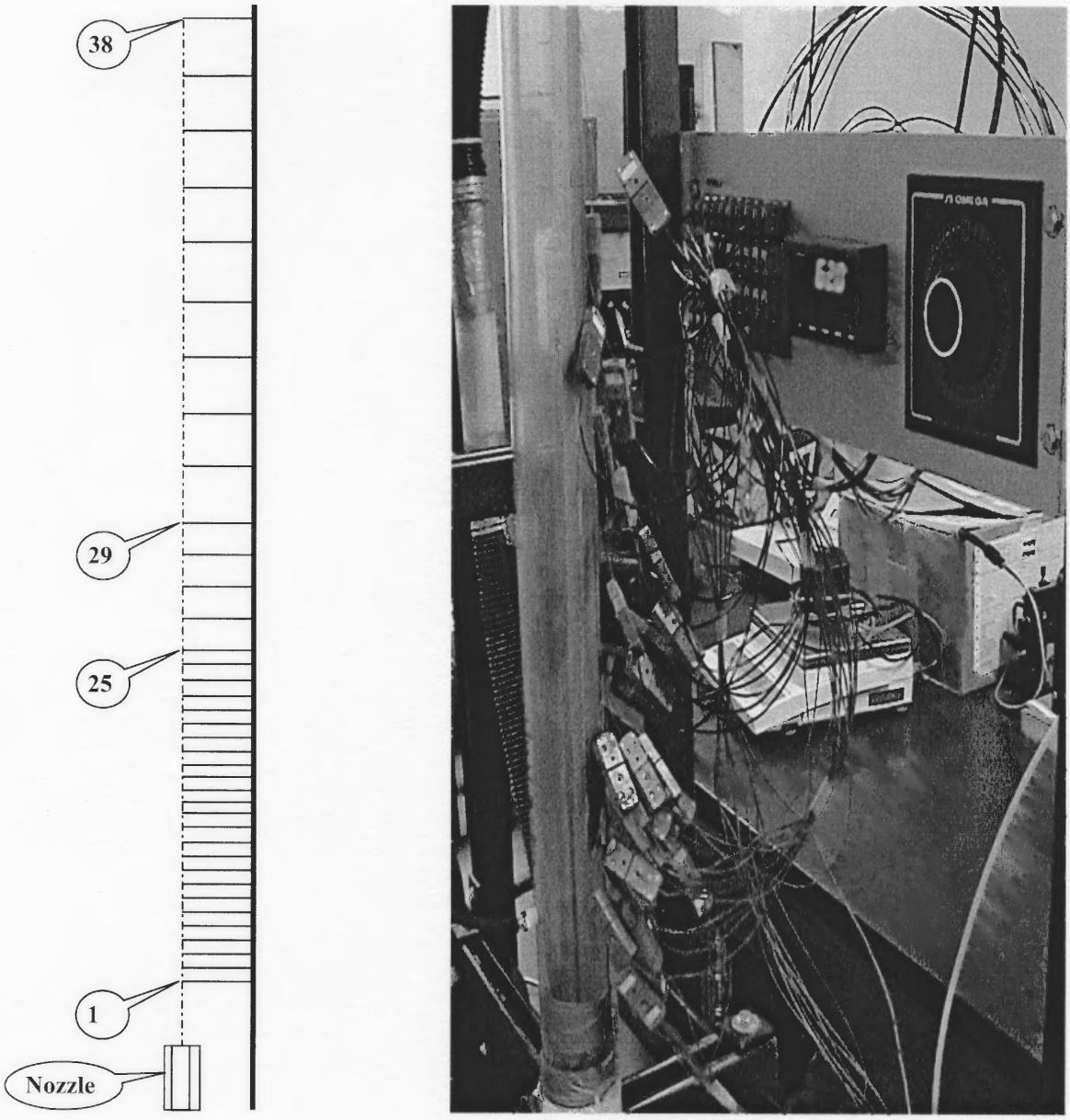

Figure 3.16 Thermocouple distribution in temperature profile measurement system.

Table 3.6 Thermocouple Probes in the Spray Central Line

Probe index	1	25	29	38
Distance from nozzle	0.50″	6.5″	8.5″	17.5″

A typical temperature distribution along the axis is shown in Figure 3.17. When the thermocouple moves from the nozzle tip to A to B to C to D in the spray region in a particle-free pipe flow, as shown in Figure 3.17(a), the temperature profile will have a big temperature jump around point C, as demonstrated in Figure 3.17(b).

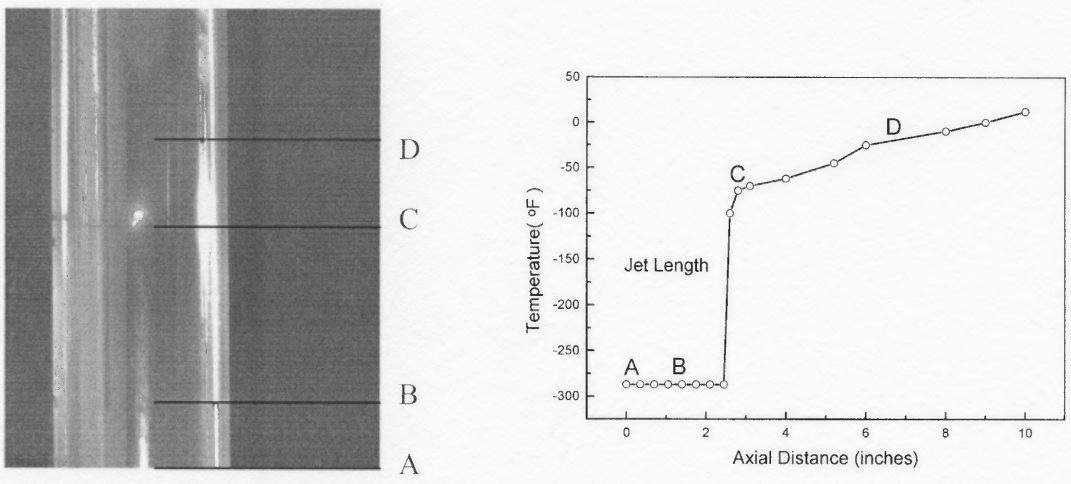

(a) Typical locations (b) Typical axial temperature distribution.

Figure 3.17 Measurement of temperature profile by a thermocouple.

Before this jump point, the temperature measured by the thermocouple is nearly the same as that of the liquid nitrogen. This region is defined as the core evaporation region, which is densely populated with droplets and droplets are always colliding with the thermocouple (see the analytical model). The dilute droplet region is defined as being from the end of the core evaporation region to the point where all the droplets are totally evaporated. The distance between the nozzle tip to the furthest droplet end point is

defined as the spray penetration depth (length). It should be pointed out that this characteristic temperature distribution is valid not only for particle-free flows but is also true for solids-laden flows.

CHAPTER 4

ANALYTICAL MODELING

4.1 Introduction

In this analytical modeling chapter, a one-dimensional model is developed to predict the distributions of velocity, temperature, and concentration of each phase of an evaporating spray jet in a coaxial and concurrent gas-solids pipe flow. Phase transfer and interactions between the spray and the ambient flow, such as entrainment and turbulent transfer across the jet boundary, were delineated in this analytical model. It is realized that the temperature measurement from thermocouples embedded in the spray region represents a phase-weighted temperature of all three phases involved. Hence, in order to interpret the temperature measurements using the analytical results, a mechanistic model for the phase-averaged temperature measured by a thermocouple in the spray region must be further established. The longitude profile of mixture temperature predicted by the analytical model is thus used to compare with the experimental measurements for validation of the model.

Based on the model predictions, various parametric effects on general flow characteristics could be further investigated. In this chapter, the analytical method will be introduced, including the general consideration for the model, governing equations, and the mechanistic interpretation of phase-averaged temperature. The modeling validation and parametric study of ambient flow velocity, solids loading, and spray jet mass flow on both jet structure and temperature profiles will be illustrated in Chapter 6.

4.2 General Consideration

Consider a spray jet evaporating in a concurrent gas-solids pipe flow, as schematically shown in Figure 4.1. In general, the spray boundary expands along the downstream direction and eventually loses its identity with respect to the surrounding flow. Thus, the flow region could be divided into two regions, the spray region, which contains all of the droplets, and the ambient flow region bounded by the spray boundary and the pipe wall.

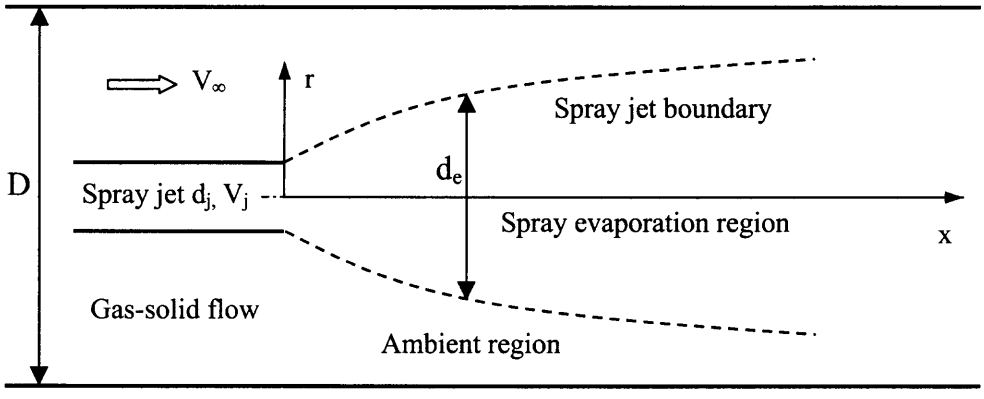

Figure 4.1 Schematic diagram of a concentric evaporating jet in a gas-solids flow.

In this modeling approach, it is assumed the jet belongs to the boundary-layer type, that is, in the jet region, the axial velocity of the jet is at least one order of magnitude higher than the radial component. Thus, only the axial velocity appears in the governing equations. For simplicity, the gas-solids suspension is considered as a special mixture where the local solids are always in thermal equilibrium with the local gas medium, whereas the solids velocity lags behind the local gas velocity. In the upward vertical flow applications, this velocity slip is approximated by the particle terminal velocity. With these approximations, the momentum and energy conservation equations

could be constructed for the gas-solids "mixture" without the requirement of a detailed account of interactions between the gas and the solids. Thus, the complicated gas-solids-droplets interactions may be simplified into a "two-phase" interaction problem, namely, the interaction between the droplet phase and the special gas-solids mixture (with an understanding that this "mixture" now contains gas and solids moving at different velocities). The gas or solids volume fraction in the mixture could be determined from the species equation by a mass balance over the control volume defined in Figure 4.2.

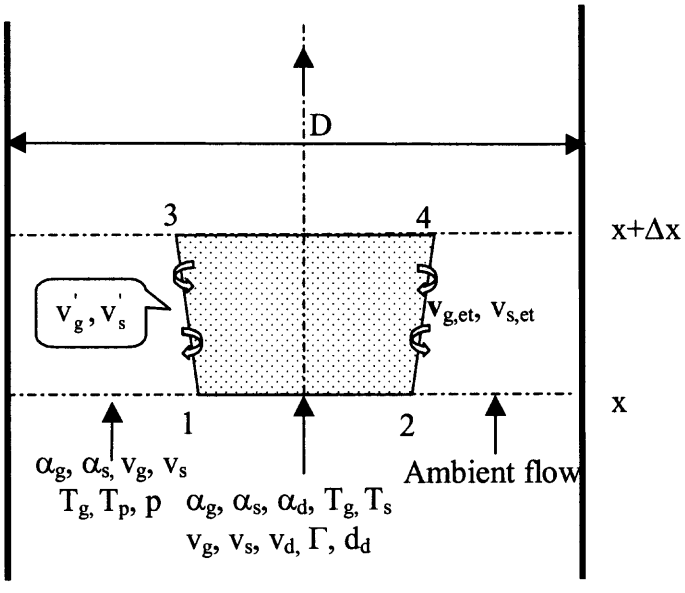

Figure 4.2 Schematic diagram of the control volume of the spray jet.

Due to the axisymmetry of the pipe flow and concentric jet, the following conservation equations of mass, momentum and energy in the spray region and ambient flow region are expressed in the cylindrical coordinates.

4.3 Governing Equations

4.3.1 Gas-Solids Mixture in Spray Region

The mass conservation equations of gas and solids can be obtained, respectively, from the mass balance of each phase over the control volume defined in Figure 4.2 as

$$\frac{d}{dx}(d_e^2\rho_{ge}\alpha_{ge}v_{ge}) = 4d_e\alpha_{ga}\rho_{ga}v_{g,et} + d_e^2 n_d \Gamma \tag{4.1}$$

$$\frac{d}{dx}(d_e^2\rho_s\alpha_{se}v_{se}) = 4d_e\alpha_{sa}\rho_s v_{s,et} \tag{4.2}$$

where the sources are due to the droplet evaporation and jet entrainment from the ambient flows. The droplet evaporation rate, dominated by the local heat transfer from droplet-solids collisions, will be discussed separately in the following section. Equations (4.1) and (4.2) are used to calculate the volume fractions of the gas and solids in the mixture.

Neglecting the pressure change in the spray region, the momentum equation for the mixture is given by:

$$\begin{aligned}\frac{d}{dx}\left[d_e^2(\rho_{ge}\alpha_{ge}v_{ge}^2 + \rho_s\alpha_{se}v_{se}^2)\right] &= 4d_e\left[\alpha_{ga}\rho_{ga}v_{g,et}v_{ga} + \alpha_{sa}\rho_s v_{s,et}v_{sa}\right] \\ &+ 4d_e\left[\gamma_g v_{ga}(\alpha_{ga}\rho_{ga}v_{ga} - \alpha_{ge}\rho_{ge}v_{ge}) + \rho_s\gamma_s v_{sa}(\alpha_{sa}v_{sa} - \alpha_{se}v_{se})\right], \\ &+ d_e^2 n_d\left(\frac{1}{8}C_D^*\left|v_{d,ge}\right|v_{d,ge}\pi d_d^2 + \Gamma v_d\right)\end{aligned} \tag{4.3}$$

where the first term on the right-hand side stands for the contribution of gas-solids entrainment, and the second term denotes the turbulent momentum transfer of gas and particles from the ambient flow to the spray region. The last item is related to the drag forces between the droplets and the gas-solids mixture (the relative velocity is characterized by the velocity difference between the droplets and the gas), and the evaporation-induced momentum transfer to the control volume. Equation (4.3) indicates a fact that, among the interactions between the spray and the ambient flow, the entrainment

of gas-solids mixture by the jet and jet-induced turbulent transfer crossing the boundary plays the dominant role in the momentum and energy exchange between the spray jets and ambient flows.

Similarly, the energy balance equation for the gas-solids mixture in the spray region is be given by:

$$\begin{aligned}\frac{d}{dx}\left[d_e^2(\rho_{ge}\alpha_{ge}v_{ge}C_{pg}T_{ge}+\rho_s\alpha_{se}v_{se}C_sT_{se})\right]&=4d_e\left[\alpha_{ga}\rho_{ga}v_{g,et}C_{pg}T_{ga}+\alpha_{sa}\rho_sv_{s,et}C_sT_{sa}\right]\\&+4d_e\left[\gamma_gv_{ga}C_{pg}(\alpha_{ga}\rho_{ga}T_{ga}-\alpha_{ge}\rho_{ge}T_{ge})+\gamma_gv_{sa}C_s\rho_s(\alpha_{sa}T_{sa}-\alpha_{se}T_{se})\right],\\&+d_e^2n_d(C_{pg}T_d\Gamma-q_t)\end{aligned}\quad (4.4)$$

Once again the sources reflect the contributions from the entrainment of the gas-solids mixture, turbulent heat transfer across the jet boundary, and energy exchange between the droplets and the gas-solids mixture.

4.3.2 Droplet Phase in the Spray Region

The mass balance of droplets in the spray region yields:

$$\frac{d}{dx}(d_e^2\rho_d\alpha_dv_d)=-d_e^2n_d\Gamma, \quad (4.5)$$

where the source term is due to the droplet evaporation.

Neglecting the pressure change in the spray region, the momentum conservation equation is given by

$$\frac{d}{dx}(d_e^2\rho_d\alpha_dv_d^2)=-d_e^2n_d(v_d\Gamma+\frac{1}{8}C_D^*\left|v_{d,ge}\right|v_{d,ge}\pi d_d^2), \quad (4.6)$$

where the source terms represent the interactions due to the evaporation-induced momentum transfer and drag forces between the droplets and the gas-solids mixture.

An energy balance of droplets becomes trivia, and the droplet temperature is assumed to be equal to the wet-bulb temperature in the spray region. Since the evaporation is controlled by the heat transfer between the droplets and the gas-solids mixture, the evaporation rate of a single droplet can be expressed by

$$\Gamma = \frac{q}{H} = \frac{Nu^* k_g}{H}(\pi d_d)(T_{ge} - T_d), \tag{4.7}$$

where the determination of the heat transfer coefficient will be discussed later. From the droplet evaporation rate, the change of droplet radius along the axial direction can be easily determined by

$$\frac{d}{dx}(d_d) = \frac{\Gamma}{2\pi\pi_d^2 \rho_d v_d}. \tag{4.8}$$

4.3.3 Gas-Solids Mixture in Ambient Flow Region

Since all phase transfers occur within a confined space (bounded by the pipe wall), with the droplet evaporation, the ambient temperature of the gas-solids mixture reduces along the downstream direction whereas the ambient gas velocity may increase. According to Giorges *et al.* (2001), the turbulent heat and mass transfer may be assumed to be proportional only to the ambient gas velocity. Hence the mass conservation of gas in the ambient flow region is expressed by

$$\frac{d}{dx}\left[(D^2 - d_e^2)\rho_{ga}\alpha_{ga}v_{ga}\right] = -4d_e\alpha_{ga}\rho_{ga}v_{g,et}. \tag{4.9}$$

Similarly, the mass conservation of solids is established by

$$\frac{d}{dx}\left[(D^2 - d_e^2)\rho_s\alpha_{sa}v_{sa}\right] = -4d_e\alpha_{sa}\rho_s v_{s,et}, \tag{4.10}$$

where the turbulent fluctuation intensities of gas and solids depend on the gas-solids mixing and fluidized bed characteristics. In this study, these turbulent fluctuation intensities are assumed to be 10%.

The momentum and energy conservation equations for the gas-solids mixture in the ambient flow region are obtained, respectively, as

$$\frac{d}{dx}\left[(D^2-d_e^2)(\rho_{ga}\alpha_{ga}v_{ga}^2+\rho_s\alpha_{sa}v_{sa}^2+p)\right]=-4d_e\left(\alpha_{ga}\rho_{ga}v_{g,et}v_{ga}+\alpha_{sa}\rho_s v_{s,et}v_{sa}\right) \\ -4d_e\left[\gamma_g v_{ga}(\alpha_{ga}\rho_{ga}v_{ga}-\alpha_{se}\rho_{ge}v_{se})+\gamma_s v_{sa}\rho_s(\alpha_{sa}v_{sa}-\alpha_{se}v_{se})\right] \tag{4.11}$$

and

$$\frac{d}{dx}\left[(D^2-d_e^2)(\rho_{ga}\alpha_{ga}v_{ga}C_{pg}T_{ga}+\rho_s\alpha_{sa}v_{sa}C_sT_{sa})\right]=-4d_e\gamma_s v_{sa}C_s\rho_s(\alpha_{sa}T_{sa}-\alpha_{se}T_{se}) \\ -4d_e\gamma_g v_{ga}C_{pg}(\alpha_{ga}\rho_{ga}T_{ga}-\alpha_{ge}\rho_{ge}T_{ge})-4d_e\left[\alpha_{ga}\rho_{ga}v_{g,et}C_{pg}T_{ga}+\alpha_{sa}\rho_s v_{s,et}C_sT_{sa}\right] \tag{4.12}$$

4.3.4 Normalization Conditions

All phase volume fractions in both the spray region and the ambient region must be subjected to the normalization conditions as:

$$\alpha_{ge}+\alpha_{se}+\alpha_d=1.0 \tag{4.13}$$

$$\alpha_{ga}+\alpha_{sa}=1.0\ . \tag{4.14}$$

4.3.5 Interactions between Droplets and the Gas-Solids Mixture

A detailed account of interaction terms between the droplets and the gas-solids mixture in the above governing equations would require a deep understanding of many detailed mechanisms of phase interactions that are still far beyond reach currently. Hence, in this

section, the Buchanan's approach [Buchanan, 1994] is adopted to roughly estimate the coupled heat transfer and evaporation rate based on some overall account of phase interactions. Due to the large temperature difference between the liquid nitrogen and the ambient gas-solids flow (at room temperature), by ignoring the porous and curvature effects, it may be reasonable to assume that the solids temperature is always beyond the Leidenfrost temperature so that there is no direct contact between droplet and particles during a droplet-solids collision (Leidenfrost collision). It is further assumed that there is no droplet breakup and no droplet coalescence. The presence of solids in the gas phase decreases the effective thickness of the thermal boundary layer around the droplet while increasing the drag force coefficient of the gas to a droplet.

The effective heat transfer coefficient can be obtained from the effective Nusselt number, which is determined by [Dwyer, 1989]

$$Nu^* = \frac{2 + 0.6 Re_d^{*0.5} Pr^{0.333}}{\left[1 + \frac{C_{pg}(T_{ge} - T_d)}{H}\right]^{0.7}}, \tag{4.15}$$

where the relative Reynolds number of droplets in a gas-solids mixture is defined by

$$Re_d^* = \frac{(\rho_s \alpha_{se} + \rho_{ge} \alpha_{ge})(v_d - v_{ge}) d_d}{\mu_g}. \tag{4.16}$$

Equation (4.15) indicates that the heat transfer coefficient of the ambient gas-solids mixture to a droplet is decreased when there is a substantial evaporation from the droplet, while the increase in solids loading enhances the heat transfer between the droplet and the gas-solids mixture. In the current study, the local volumetric percentage of solids (solids loading) is less than 1%. With a d_p of 120 μm and a slip velocity of 1 m/s, based on Equation (4.16), the relative droplet Reynolds number is calculated as 80.

However, for a droplet in a solids-free flow, the relative droplet Reynolds number will be about 1.0 under the same conditions. Also, the effective heat transfer coefficient will be changed from 2.4 to 8.0.

The droplet effective drag coefficient, C_D^*, can be estimated based on an empirical equation proposed by Mostoufi and Chaouki (1999)

$$C_D^* = C_{D0}\,\alpha_{ge}^{-\beta}, \tag{4.17}$$

where C_{D0} is the standard drag force coefficient for a sphere in particle-free flow and the exponent β is expressed by:

$$\beta = 3.02 Ar_s^{0.22} Re_{dt}^{0.33} \left(\frac{d_d}{d_s}\right)^{0.40}. \tag{4.18}$$

As shown in Equation (4.17), the droplet effective drag coefficient is a function of droplet Reynolds number (based on droplet terminal velocity), solids volumetric concentration in the ambient flow, and the physical properties of the droplet and the surrounding particles. Dependence of the effective drag coefficient to Re_d is represented by C_{D0}. Hence, the correction factor depends on the voidage, solids Archimedes number, droplet terminal Reynolds number, and the diameter ratio of the droplet and the surrounding solids.

4.3.6 Jet Entrainment

In a jet flow, the mass and momentum transfers occur as a result of flow entrainment induced by the jet. For a gas-liquid jet into an unbounded concurrent gas flow, the jet boundary expansion can be formulated according to Abramovich (1963) as:

$$\frac{d}{dx}(d_e) = 0.11 \frac{\left(1+\frac{\rho_\infty}{\rho_j}\right)\left(1-\frac{v_\infty}{v_j}\right)}{1+\frac{\rho_\infty}{\rho_j}\frac{v_\infty}{v_j}}. \tag{4.19}$$

The gas entrainment velocity can thus be derived from the above equation as:

$$v_{et} = 0.055 \frac{\left(1+\frac{\rho_\infty}{\rho_j}\right)}{\left(1+\frac{\rho_\infty}{\rho_j}\frac{v_\infty}{v_j}\right)\left(1+\frac{\rho_\infty}{\rho_j}(1-\frac{v_\infty}{v_j})\right)}(v_j - v_\infty). \tag{4.20}$$

In the current study, the above equation is extended into the cases of spray jets in gas-solids flows, in which the ambient phase density in Equation (4.20) needs to be modified to that of the gas-solids mixture. In addition, according to Ricou and Spalding (1961), the entrainment rate can be significantly reduced, whereas the jet boundary is further expanded due to gas phase expansion by combustion or evaporation. Based on the gas expansion rate due to evaporation, the rough estimation in our study is that nearly 50% entrainment is lost compared to that without evaporation. With these considerations, Equation (4.20) is modified as

$$v_{g,et} = v_{s,et} = 0.0275 \frac{\left(1+\frac{\rho_a}{\rho_e}\right)}{\left(1+\frac{\rho_a}{\rho_e}\frac{v_{ga}}{v_{ge}}\right)\left(1+\frac{\rho_a}{\rho_e}(1-\frac{v_{ga}}{v_{ge}})\right)}(v_{ge} - v_{ga}), \tag{4.21}$$

where

$$\rho_a = \rho_{ga}\alpha_{ga} + \rho_s\alpha_{sa} \tag{4.22}$$

$$\rho_e = \rho_{ge}\alpha_{ge} + \rho_s\alpha_{se} + \rho_d\alpha_d. \tag{4.23}$$

In summary, Equations (4.1) to (4.14) constitute a complete set of governing equations for local phase variables, such as temperature, velocity, phase holdup, and evaporation rate. However, the detailed formulation of phase interaction terms in these governing equations still needs to be established in order to solve these equations. Among the key phase interactions, the jet entrainment can be estimated from Equation (4.21), whereas the effective heat transfer coefficients and drag force coefficients are calculated from Equation (4.15) and Equation (4.17), respectively.

4.4 Boundary Conditions

The boundary conditions in this analytical model include the inlet phase distributions both in the spray region and ambient flow region, such as velocity, volume fraction, and temperature. Table 4.1 lists the inlet conditions. The modeling prediction calculation will be terminated if one of the following criteria is met, 1) the evaporation diameter reaches 90% of the whole pipe diameter, or 2) the droplet diameter is less than 5 μm. Based on the assumptions of terminal velocity difference between the solids and gas phase both in the spray region and ambient flow region, the inlet solids velocity could be derived from the gas velocity. Thus, it does not need to be provided initially.

Table 4.1 Inlet Conditions for the Analytical Modeling Prediction

Spray Jet	V_{d0}	V_{ge0}	T_{ge0}	α_{de0}	α_{se0}	D_{d0}
Ambient Flow	V_{ga0}	V_{sa0}	T_{ga0}	α_{sa0}		

4.5 Mechanistic Model of Phase-Averaged Temperature

It is realized that the temperature measurement from thermocouples embedded in the spray region represents a phase-weighted temperature of all three phases involved. However, the theoretical modeling proposed above only yields the local temperature of each phase. Hence, in order to interpret the temperature measurements using the analytical results, a model for the phase-averaged temperature measured by a thermocouple in the spray region must be further established.

Consider a thermocouple embedded in a mixture of droplets and gas-solids medium. The thermocouple measures an averaged mixture temperature that depends on the local heat balance of the thermocouple from the turbulent thermal convection, the heat transfer due to droplet collision and evaporation, and the heat transfer due to the solids collisions. The contributions of solids phase on the heat transfer to the thermocouple come from two parts. First, the solids collisions on droplets that are in a collision process with the thermocouple will likely carry away some liquid residue or additional evaporation and hence shorten the droplet contact time and associated heat transfer. Second, the heat transfer due to solids-thermocouple collisions may be included in a combined convective heat transfer of the gas-solids mixture. Assuming that the conductive resistance of the thermocouple is much smaller than the convective resistance (i.e., the Biot number is much less than unity), the lump-heat balance equation for the thermocouple can be established by

$$m_{tc} c \frac{dT_{tc}}{dt} = h_g (A_{tc} - A_c)(T_{ge} - T_{tc}) + h_d A_c (T_d - T_{tc}), \tag{4.24}$$

where the first term represents the convective heat transfer from local gas-solids mixture and the second term stands for the contribution from droplet collisions. The droplet

temperature is constant for all droplets in the entire spray region, whereas the temperature of the gas-solids mixture depends on the thermocouple location in the flow and is calculated by the aforementioned one-dimensional analytical model in Section 4.3. The contact areas and heat transfer coefficients mainly depend on the collision frequency, convective velocity of the gas-solids mixture, and the collision velocity and sizes of the droplets and solids.

Equation (4.24) governs the instantaneous temperature of the thermocouple, which is transient in nature. Direct solving for this equation is not only complicated but also unnecessary in this study since the measurement reading is a steady-state or time-independent temperature measurement of a thermocouple. The steady-state temperature measurement of a thermocouple depends on two time scales, namely, the droplet collision time (τ_c) and the time interval between two consecutive droplet collisions (τ_{dd}). When $\tau_c > \tau_{dd}$, liquid will accumulate on the probe surface, so that the thermocouple temperature will be that of the droplets. On the other hand, when $\tau_c < \tau_{dd}$, the thermocouple temperature will be determined according to a time-averaged heat balance, as described below.

Now the discussion will focus on the situation when $\tau_c < \tau_{dd}$. A microscopic heat transfer period between two consecutive droplet collisions contains a period of heat transfer with droplet collision and a period without droplet collision. Ignoring the initial effect of the measurement, the microscopic heat transfer becomes periodic. In this case, the overall heat transfer to the thermocouple sensor during a periodic cycle is balanced, which yields

$$\int_0^{\tau_c} h_g(A_{tc} - A_c)(T_{ge} - T_{tc})\,dt + \int_0^{\tau_c} h_d A_c(T_d - T_{tc})\,dt + \int_{\tau_c}^{\tau_{dd}} h_g A_{tc}(T_{ge} - T_{tc})\,dt = 0. \quad (4.25)$$

Within the range of this investigation, the response time of the thermocouple is at least two orders-of-magnitude longer than the characteristic time interval between two consecutive collisions of droplets. Hence, in a steady-state temperature measurement, the thermocouple temperature fluctuation due to the micro-scaled periodic heat transfer is very small compared to the averaged temperature. Therefore, the steady-state temperature can be estimated from Equation (4.25) as

$$T_{tc} = \frac{T_{ge}\int_0^{\tau_c} h_g(A_{tc} - A_c)\,dt + T_d\int_0^{\tau_c} h_d A_c\,dt + T_{ge}\int_{\tau_c}^{\tau_{dd}} h_g A_{tc}\,dt}{\int_0^{\tau_c} h_g(A_{tc} - A_c)\,dt + \int_0^{\tau_c} h_d A_c\,dt + \int_{\tau_c}^{\tau_{dd}} h_g A_{tc}\,dt} \,. \tag{4.26}$$

The time interval between two consecutive droplet-thermocouple collisions can be calculated from

$$\tau_{dd} = \frac{1.0}{(n_d)^{1/3} v_d} \,. \tag{4.27}$$

In this study of the thermocouple measurements in the dilute spray region where $\tau_c < \tau_{dd}$, the collisions between the liquid nitrogen droplets and the thermocouple belong to Leidenfrost collisions. Since the size of thermocouple sensor is much larger than the colliding droplets, the collision time may be estimated from equations for Leidenfrost collisions of droplets with flat surfaces. Based on the experimental measurements of water droplet collisions with a flat surface over Leidenfrost temperature, Hatta *et al.* (1997) proposed an equation for the contact time:

$$\tau_c = 0.27 We^{0.46} \frac{d_d}{v_d} + 1.25 We^{0.37} \frac{d_d}{v_d} \,, \tag{4.28}$$

where the first term is the time of the spreading period, the second is the time of recoiling period, and We is the Weber number. The maximum collision area between the colliding droplet and thermocouple can also be estimated by [Hatta *et al.*, 1997]

$$A_c = \frac{1}{4}\pi d_d^{\,2}(1.0 + 0.093We^{0.74})^2 . \tag{4.29}$$

In order to apply Equation (4.28) to the analysis of liquid nitrogen droplet collision, two modifications need to be introduced. First, the equation must be modified for evaporating liquids other than water. The effect of material properties of evaporating liquid on the contact time can be obtained from a parametric model of Leidenfrost collisions [Liu & Zhu, 2001]

$$\tau_c \propto \rho_d \rho_g \left(\frac{k_g (T_s - T_d)}{H} \right)^{-2} , \tag{4.30}$$

where the material properties should be evaluated based on the film temperature. The other modification concerns the collision-induced droplet breakup. When We is high (say, larger than 80), droplets will break up upon collision [Wachters & Westerling, 1996]. For droplet-thermocouple collisions, the typical We is about 125, which is based on a droplet diameter of 120 μm and a relative velocity of 5 m/s. With the droplet breakup, the recoiling time should be calculated based on the daughter droplet size. Assuming a binary breakup with equal sized daughter droplets, the recoiling time in Equation (4.28) will be reduced by a factor of 0.73. Hence, the contact time for a Leidenfrost collision of a liquid nitrogen droplet with a high We can be estimated, based on Eq. (4.28) and the two modifications, by

$$\tau_{c,LN2} = \frac{(\rho_d \rho_g)_{LN_2} \left(\frac{K(T_s - T_d)}{L} \right)^2_w}{(\rho_d \rho_g)_w \left(\frac{K(T_s - T_d)}{L} \right)^2_{LN_2}} \left\{ 0.27 We^{0.46} \frac{d_d}{v_d} + 0.91 We^{0.37} \frac{d_d}{v_d} \right\} . \qquad (4.31)$$

As mentioned before, the solids-droplets collision affects the droplet-thermocouple collision and associated heat transfer. Considering this effect, the impacting droplet diameter in Equation (4.31) is modified by [Dabros & Van de Ven, 1994]

$$d_d = d_{d0}(1-f)^{\frac{\tau_{dd}}{3\tau_c}}, \qquad (4.32)$$

where d_{d0} is the original droplet size before the solids collision; f is the mass reduction fraction due to solids-droplet collision during the droplet-thermocouple collision process, and τ_{dd} is the time interval between two consecutive collisions of solids on the droplet that is colliding with the thermocouple.

CHAPTER 5

NUMERICAL SIMULATION

5.1 Introduction

Numerical simulation is an important tool to provide a full-field flow description of the spray mixing and evaporation in a gas-solids flow. In this study, a hybrid Eulerian-Lagrangian method has been applied to numerically simulate a concurrent liquid nitrogen spray in a gas-solids pipe flow. The model takes into account the phase interactions with droplet evaporation among gas, liquid, and solids phases. This study particularly focuses on the effects of solids concentration on spray evaporation and mixing, as well as the effects of droplet evaporation on temperature reduction and dilution of solids concentration. As a part of the modeling validation process, the penetration depth of a liquid nitrogen spray jet in a gas-solids pipe flow from numerical calculations is compared with the our experimental results and those predicted by the analytical modeling. In this chapter, we will introduce the numerical simulation methodology; governing equations for each phase of gas, solids and droplets; intrinsic correlations; and initial and boundary conditions.

5.2 Numerical Simulation Methodology

The chief objective of the numerical simulation is to better understand the phase interactions that are difficult to examine experimentally. For the study of evaporating spray jets in gas-solids flows, different modeling approaches could be selected from the reported literature. One is the continuum multi-fluid method in which each phase of gas,

solids or droplets is a pseudo-continuum and the governing equations are solved simultaneously [Crowe, 1984; Chang *et al.*, 1996, 1998; Straatsma *et al.*, 1999]. However, in cases where particles are poly-dispersed and undergoing a phase change along their paths, it is difficult to define the phase and phase interactions that are size sensitive in the continuum approach. In such circumstances, the particles may be treated by the multi-lump method [Lottes *et al.*, 1993], in which particles are separated into a limited number of lumped groups where the particles in each group are of the same size. For example, in their simulation, Chang *et al.* (1996 & 1998) used a five-lump model for the droplet number density distribution. Since the droplet evaporation rate is a strong function of droplet size, the multi-lump method may lead to a large biased error in the estimation of droplet evaporation rate. The other approach is the probability density function (PDF) method for the droplet phase [Williams, 1958]. However, no studies have been reported on applying the PDF method to account for the droplet-solids interactions, such as collision that is one of the key effects in the study of liquid spray in a gas-solids flow. The hybrid Eulerian-Lagrangian method [Ahluwalia, 1999] is another approach in which gas and solids phases are treated by the Eulerian two-phase continuum method, while the droplets phase is treated by the Lagrangian trajectory method. This approach nevertheless requires a number of iterations on phase coupling between the gas-solids two-phase flow and the droplets phase until all phase interactions are converged. It is noted that, in the numerical studies of gas-solids flows, the Lagrangian method is typically used when the flow is dilute [Kawaguchi *et al*, 1998; Senior & Grace, 1998; Lun, 2000], while the Eulerian method is more often used if the flow is a dense suspension [Sinclair & Jackson, 1989; Joseph *et al.*, 1990].

In this study, the hybrid Eulerian-Lagrangian approach was adopted, namely, the gas-solids suspension flow was calculated using the Eulerian two-fluid model approach, in which the effects of the droplets were coupled through the source terms in the mass, momentum and energy governing equations of each phase. The evaporating spray on the other hand is treated using the deterministic Lagrangian trajectory approach, in which the droplets consist of a finite number of trajectory groups. Droplets evaporate along their trajectories and interact with the surrounding gas-solids suspension along their paths. While the droplet evaporation and trajectory affect the gas-solids flow by the phase interactions, such as the drag forces and droplet-solids collisions, the gas-solids flow field in turn affects the droplet evaporation and its trajectory. By iterations between these two interacting approaches, a final solution of the three-phase flow is obtained once a convergence is achieved.

5.3 Eulerian Approach for the Gas/Solids Phase

In the calculation of gas-solids flows, it is assumed that the solids are mono-dispersed without attrition. The gas phase is a mixture of air and nitrogen , where the components in air are assumed to be nitrogen and oxygen only for the simplification. In this study, the modeling of the gas-solids flow is based on the MFIX code that was originally developed by Morgantown Energy Technology Center [Syamlal *et al.*, 1994; Syamlal, 1995].

5.3.1 Conservation of Mass

The continuity equations for the gas and solids phase are given by

$$\frac{\partial}{\partial t}\left(\alpha_g \rho_g\right) + \nabla \cdot \left(\alpha_g \rho_g \vec{v}_g\right) = \dot{m} \tag{5.1}$$

$$\frac{\partial}{\partial t}(\alpha_s \rho_s) + \nabla \cdot (\alpha_s \rho_s \vec{v}_s) = 0. \tag{5.2}$$

The first term on the left in Equations (5.1) and (5.2) accounts for the rate of mass accumulation per unit volume, and the second term is the net rate of convective mass flux. The term $\dot{m}$ on right of Equation (5.1) is contributed for the gas-vapor mixture accumulation in mass from the droplet evaporation per unit volume.

The air-vapor mixture is modeled as a gas obeying the ideal gas law, which is expressed by

$$\rho_g = \frac{p_g M_w}{R T_g}, \tag{5.3}$$

where T_g is the air-vapor mixture, which can be solved by the energy equation.

5.3.2 Conservation of Momentum

Consider the interactions between droplets with gas and solids, the momentum balance equations for the gas and solids phase could be expressed by

$$\frac{\partial}{\partial t}(\alpha_g \rho_g \vec{v}_g) + \nabla \cdot (\alpha_g \rho_g \vec{v}_g \vec{v}_g) = \nabla \cdot \overline{\overline{S}}_g + \alpha_g \rho_g \vec{g} - \vec{I}_{gs} - \vec{I}_{gd} + \dot{m} \vec{v}_d \tag{5.4}$$

$$\frac{\partial}{\partial t}(\alpha_s \rho_s \vec{v}_s) + \nabla \cdot (\alpha_s \rho_s \vec{v}_s \vec{v}_s) = \nabla \cdot \overline{\overline{S}}_s + \alpha_s \rho_s \vec{g} + \vec{I}_{gs} - \vec{I}_{sd}, \tag{5.5}$$

where $\overline{\overline{S}}_g$ and $\overline{\overline{S}}_s$ are the gas and solids phase stress tensor, respectively. $\vec{I}_{gs}$ is the momentum transfer between the gas and solids phase. The source terms also include contributions not only from the vapor generation, $\dot{m}\vec{v}_d$, but also from the momentum transfer, $\vec{I}_{gd}$ and $\vec{I}_{sd}$, between droplets with gas and solids. The interactions between droplets and gas/solids will be discussed in Section 5.5.

5.3.3 Conservation of Internal Energy

The internal energy balance for the gas phase is written in terms of the gas temperature:

$$\alpha_g \rho_g C_{pg}\left(\frac{\partial T_g}{\partial t}+\vec{v}_g\cdot\nabla T_g\right)=-\nabla\cdot\vec{q}_g-H_{gs}-H_{gd}+\dot{m}C_{pg}T_d, \tag{5.6}$$

where $\vec{q}_g$ is the gas-phase conductive heat flux, H_{gs} and H_{gd} describe gas-solids and gas-droplets inter-phase heat transfer. The last source term in Equation (5.6) accounts for the energy contribution by the droplet evaporation.

The thermal energy balance for the solids phase is given by

$$\alpha_s \rho_s C_{ps}\left(\frac{\partial T_s}{\partial t}+\vec{v}_s\cdot\nabla T_s\right)=-\nabla\cdot\vec{q}_s+H_{gs}-H_{sd}, \tag{5.7}$$

where $\vec{q}_s$ is the solids-phase conductive heat flux, and H_{sd} expresses the energy transfer between droplets and solids due to the droplets-solids collision.

5.3.4 Conservation of Species

The species conservation equation for the nitrogen component in the air-vapor mixture is

$$\frac{\partial}{\partial t}(\alpha_g \rho_g Y_n)+\nabla\cdot\left(\alpha_g \rho_g Y_n \vec{v}_g\right)=\dot{m}, \tag{5.8}$$

where Y_n is the mass fraction of nitrogen and the source term for the nitrogen species is contributed from the liquid nitrogen spray evaporation.

Equation (5.8) considers the accumulation, convection, and evaporation but neglects the diffusive flux. For the oxygen species, the mass fraction can be calculated by the species normalization equation:

$$Y_n + Y_o = 1.0\ . \tag{5.9}$$

The above governing Equations (5.1) to (5.9) could be solved theoretically if all the items on the right side in the equations are defined. The interactions between droplets and the gas/solids phase will be given in the next section. The solids-solids momentum transfer is solved by the granular stress equation based on kinetic theory and friction flow theory [Syamlal, 1995].

5.3.5 Turbulence Model

In a turbulent particulate multi-phase flow, the particles are dispersed through turbulent flow fluctuations. The addition of particles can enhance or reduce the flow turbulence, affecting transport behavior of both particle and flow phases. With evaporating droplets, the turbulence transport mechanism becomes more complicated. So far no literature is available to explain the three-phase turbulence modulation or two-phase turbulence with evaporations. Based on the nozzle diameter and jet velocity, the spray jet flow has a typical Reynolds number of 30,000, which means the turbulent effect should be accounted for in this phase-mixing process. In this study, a simple Prandtl mixing-length model (PMLM) was used, in which the effective fluid viscosity was modified by the characteristic turbulence length scale.

5.4 Lagrangian Approach for Droplet Phase

In this study, the droplet phase field is calculated by tracking the droplets throughout the computational domain using the Lagrangian approach. The initial distributions of droplet size and velocity in the spray could be given according the given experimental probability density function to obtain an adequate number of discrete droplets, each of which represents a set of droplets having the same size and initial conditions. To simplify the numerical simulation, it is assumed that no droplet breakup and coalescence happen during the droplet evaporation and in the droplet penetration trajectories. However, indirect interactions among droplets are included as source terms in the gas-solids field simulation, which provides the gas/solids phase distribution of temperature, velocity and concentration.

5.4.1 Droplets Trajectories

When a droplet moves in a gas-solids flow, the forces acting on it include gravitational, gas/solids drag force, and droplet-solids collision force. To predict the droplet trajectory, one has to know these governing forces. However, there is little information available to illustrate the droplet-solids collision efficiency and momentum and heat transfer among collisions. In this model, the effective drag force for a droplet in a gas-solids flow is experienced from a particle in a fluidized bed, which will be discussed in Section 5.4.3. Then the equations of motion for each of the droplets can be written as,

$$m_{di}\frac{d\vec{v}_{di}}{dt}=\frac{1}{2}C_{di}^{*}\left|\vec{v}_{gdi}\right|\vec{v}_{gdi}\pi r_{di}^{2}+m_{di}\vec{g}, \tag{5.10}$$

where $\vec{v}_{di}$ is the instantaneous droplet velocity. C_{di}^{*} is the effective drag force coefficient for a droplet in a gas-solids media, which is based on the local relative velocity between gas and the droplet, $\vec{v}_{gdi}$, and will be discussed in Section 5.4.3.

The deterministic droplet trajectories are obtained by integrating the available velocities:

$$\frac{d\vec{x}_{di}}{dt} = \vec{v}_{di}. \tag{5.11}$$

5.4.2 Droplet Evaporation Model

Actually, the droplet evaporation will also affect droplet trajectory. Droplet evaporation will reduce droplet size and change the suspension flow field, including particle concentration, phase temperature, and phase velocities. At the same time, particle addition in the flow will also change droplet evaporation, then droplet trajectory.

Assuming that the droplet evaporation rate depends only on the vapor concentration distribution along the radial direction from the droplet surface, we have the droplet evaporation equation as [Aggarwal *et al.*, 1984]

$$\Gamma = -4\pi\pi\rho D_d \ln\left(\frac{y_v(r_\infty)-1}{y_v(r_d)-1}\right), \tag{5.12}$$

where

$$y_v(r_d) = \frac{W_v}{W_v + W_m\left[p/(p_v(T_d)-1\right]}. \tag{5.13}$$

Equation (5.13) indicates that the surface vapor mass fraction is related to the surface temperature T_d [Chen & Pereira, 1995], a quantity obtainable from solving the heat transfer equation of a droplet as follows.

The total thermal energy required for droplet evaporation and for droplet heat-up is based on the heat transfer from the gas/solids flow. For small droplets where the Biot number is much less than unity, the heat balance of a droplet can be expressed from the lumped thermal capacity model:

$$m_d C_d \frac{dT_d}{dt} = \pi D_d Nu^* k_g (T_g - T_d) - H\dot{m}, \tag{5.14}$$

where Nu* is the effective Nusselt number for a droplet in a gas-solids mixture, which will be given in Section 5.4.3.

It should be pointed out that, while the droplet evaporation rate depends on the vapor diffusion, the vapor concentration on the droplet surface relies on the droplet surface temperature, which is controlled by the heat balance on the droplet. When the temperature of droplet is much less than the vapor saturation temperature, the evaporation rate is diffusion controlled, since the concentration difference across the boundary layer is small as compared to a rather large temperature difference. In this case, the heat transferred to the droplet is used for both droplet heat-up and droplet evaporation. Once T_d is approaching the vapor saturation temperature, the droplet evaporation rate becomes heat transfer dominated. Now all the heat transferred from the gas-solids flow is used for droplet evaporation.

5.4.3 Interactions between Droplets and the Gas-Solids Phase

In the heat transfer between the droplets and the gas-solids flow, droplet-solids collision plays a very important or even dominant role. Unfortunately, there is little information available to explain the detailed collision mechanisms. Many factors may affect the collision-induced heat transfer, such as collision frequency, duration of contact per collision, and heat transfer rate during contact. When a particle approaches an evaporating droplet, it is probably in contact only for a very short period, during which there is rapid heat transfer, and after which it is pushed away by the vapor generated at the droplet surface. Based on analysis of the interactions between droplets with gas-solids mixture in Chapter 4, the averaged heat and momentum exchange for a droplet with a gas-solids mixture may be estimated by Equations (4.15) and (4.17), which are used in Equation (5.10) and Equation (5.14), respectively.

However, in the numerical simulation of gas-solids flow, the momentum balance and energy balance are established, respectively, for the gas phase and solids phase. Then we need to know the amount of drag force exerted on the droplet from gas and collision contribution from droplet-particle interaction. For the gas phase, the drag force exerted on the droplets should be corrected by the gas fraction in the flow:

$$C_{D,g} = \alpha_g C_{D0}, \tag{5.15}$$

where C_{D0} is standard drag coefficient. This equation assumes the particle is fine enough to follow the gas flow. The correction reflects the particle volume contribution in the drag force.

The heat transferred to the droplet by the gas phase can be calculated as

$$q_g = \alpha_g \pi D_d N_u^* k_g (T_g - T_d), \tag{5.16}$$

where α_g is the gas phase volume fraction in the gas-solids mixture around the droplet. The correction for the heat transfer coefficient accounts for the deduction of the convective heat transfer by the space occupied by particle in the shell around a droplet.

From Equation (5.15) and Equation (5.16), we can determine the momentum and energy transfer between a droplet and the gas phase. While from Equation (4.15) and Equation (4.17), the drag force and heat transfer between a droplet and the gas/solids mixture can be calculated. Then, we can determine the sources in the solids phase simulation.

5.5 Initial and Boundary Conditions

A schematic diagram of the concentric evaporating jet in a gas-solids pipe flow is shown in Figure 4.1, where the inlet flow could be separated into the jet region and ambient gas-solids flow region. In the jet flow, the fluid is the droplet-vapor mixture with low temperature, while the ambient gas-solids flow has a higher temperature as the environment with uniform solids concentration. However, numerical simulation is performed by the iterations between the Eulerian approach for the gas/solids phase and the Lagrangian approach for the droplet phase, in which the suspension flow is given by the gas-solids simulation. The initial conditions only need to be declared for the gas-solids simulation, while the boundary conditions should be given for both gas-solids flow and droplet phase calculation.

5.5.1 Initial Conditions

The initial values of all field variables for the gas and solids phase must be specified for the entire computational domain, including gas volume fraction; gas pressure; temperature for both gas and solids; velocity for both gas and solids; and species mass fraction for nitrogen and oxygen. The initial conditions need to be accurate enough to allow convergence. The initial conditions can also be given by a pre-calculated numerical simulation result. For example, the initial velocity distribution is given by a calculation with a specified inlet velocity. For the droplet trajectory calculation, the suspension gas-solids flow is given by the two-fluid Eulerian approach. No initial conditions are required, and the computational domain is also given by the gas-solids suspension flow.

5.5.2 Inlet Boundary Conditions

An inflow boundary condition should be specified at the inlet position, where all the field variables need to be specified. In this study, the inflow includes the inlet jet flow and concurrent gas-solids flow, which are specified in the jet region and inlet gas-ambient flow region, respectively. The gas and solids phase inflow conditions are given in the gas-solids flow simulation section, while the droplet inflow conditions are given in the droplet trajectory starting positions.

The inflow boundary conditions for gas-solids in the jet region are given by

$$\begin{cases} V_{gi} = V_{gj} \\ T_{gi} = T_{gj} \\ \alpha_{gi} = 1.0 \\ Y_n = 1.0 \end{cases}, \tag{5.17}$$

where V_{gj} and T_{gj} are the initial jet velocity and the temperature of vapor in the vapor-droplet mixture, respectively. In this study, the initial gas jet velocity is assumed to have the same velocity as the droplets, which is calibrated by the LDV method. The initial vapor may have the same temperature as the droplet saturation temperature at standard air pressure. However, near the nozzle region, the entrainment and fluctuation is very severe. In this study, we specified a vapor temperature of 150 K, which is higher than the droplet temperature. Since the initial solids volume fraction is zero in the jet region, the solids velocity and solids temperature are not required. The only component in the gas phase in the jet flow is nitrogen, a unit species mass fraction is given as the initial jet condition.

The inflow boundary conditions for the gas-solids phase in the jet ambient flow are given by

$$\begin{cases} V_{gi} = V_{ga0} \\ V_{si} = V_{sa0} \\ T_{gi} = T_{ga0} \\ T_{si} = T_{sa0} \\ \alpha_{gi} = \alpha_{ga0} \\ Y_n = 0.7 \end{cases}, \tag{5.18}$$

where both velocity and temperature of gas and solids phase should be given since the initial gas volume fraction is not unity. Also, the initial nitrogen species mass fraction is given as 0.7.

As discussed before, the evaporating spray is treated using the Lagrangian trajectory approach, in which the droplets consist of a finite number of trajectory groups. Each droplet initially starts out with a known position, velocity, size and temperature, which are dependent on the spray jet system characteristics. So, the inflow conditions for

the droplet trajectory calculation include the distribution of droplet size, velocity, and number density. In this study, a uniform droplet and uniform number density distribution is given in the nozzle region.

5.5.3 Outlet Boundary Conditions

In this study, the pressure at the outflow boundary is assumed to be constant. In the gas-solids flow simulation, it is given as

$$P_g\big|_{exit} = P_{stat} = 1.01e^5. \tag{5.19}$$

5.6 Numerical Solution Procedure

In this study, the gas-solids suspension flow was simulated using the Eulerian two-fluid model. The source terms appearing in the mass, momentum, and energy equations represent the interactions between droplets and the gas/solids phase. In all the calculations performed within the droplet evaporation and trajectory model, the distributions of velocity, temperature, and concentration of gas and solids are given as a function of the spatial position at an instance of time. This snapshot of the continuum fields is obtained from the gas-solids flow simulation and is fixed during the calculation of droplet trajectories. The overall source terms for the gas-solids simulation are accumulated, which include the vapor mass, drag force on gas and solids phase, and heat transfer from the gas and solids phase. The average droplet temperature in each control volume is also needed to estimate the source term for the gas phase energy equation due to droplet evaporation.

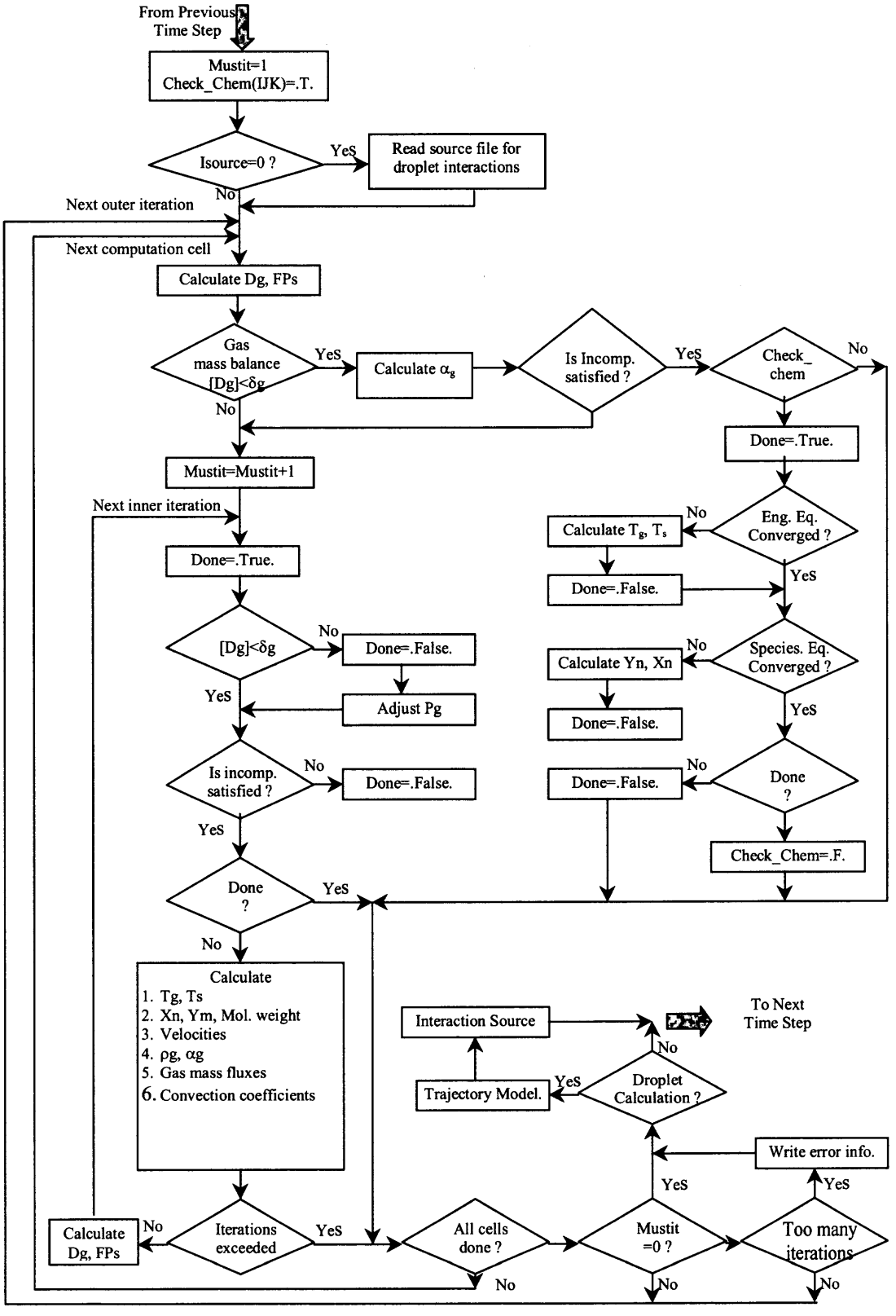

Figure 5.1 Flow chart of the numerical simulation procedure.

The solution procedure for the evaporating spray jet in gas-solids flows was performed by the Multiphase Flow with Interphase eXchange (MFIX) code and droplet evaporation mode code, which was self-developed with Argonne National Laboratory. The flow chart of the solution procedure is shown as Figure 5.1, where the droplet trajectory model is called with a time interval defined by the user. At the beginning of each time step, all the explicit quantities are calculated. Then the difference equations are solved sequentially within the iteration loops. The cells are visited one at a time starting from the

cell with the lowest index and going to the cell with largest index. Convergence is said to occur when all the discretized equations are satisfied simultaneously in all the cells without having to make adjustments in any of the cells.

The solution starts with a guessed pressure field. Initially the gas continuity equation is checked to see if it is satisfied. If not, the pressure is adjusted using Newton's method. If the energy or the species balance equations need to be solved, they are solved for temperature and species mass fractions. The fluid density is updated. The coupled fluid and solids momentum equations are solved for the velocity components. The solids continuity equations are then solved for the solids volume fraction. The gas volume fraction is then calculated by subtracting the solids volume fraction from one.

The above steps complete one pass of the inner iteration for a cell. The inner iterations are continued until the fluid continuity equation is satisfied or the number of inner iterations exceeds a specified limit, which is defined as five.

The inner iterations are continued for all the numerical cells to complete one pass of the outer iteration. The outer iterations are continued until the solution reaches the

point at which no further inner iterations are needed, which implies that the existing solution satisfies all the discretized equations simultaneously in all cells. When such a convergence is obtained or when the number of outer iterations exceeds a specified limit, which is defined as 50 in this solution, the calculations proceed to the next time step. If the time interval for the droplet trajectory calculations is reached, the droplet evaporation model will be called, which provides the updated source items representing the interactions between droplets and the gas/solids phase.

5.6.1 Initial Gas-Solids Flow Field

To achieve a convergent multi-phase flow solution with strong interphase exchange, a good initial gas-solids flow is the first step toward success. In this study, the initial gas-solids flow field represents the initial field without the droplet evaporation source terms, while the complex inlet boundary conditions are incorporated near the nozzle region, such as velocity difference, temperature difference, and solids concentration difference between the flow in the nozzle and the ambient gas-solids flow. The typical inlet conditions in the nozzle include a velocity of 30 m/s, temperature of 150K, solids concentration of 0 (solids free). However, the ambient gas-solids inlet flow has a velocity of 3 m/s, environmental temperature of 300K, and a concentration of 0.5%. Combining all these factors often results in divergence of the solution.

In this study, the procedure was separated into many sub-steps. For example, we tried to achieve the gas-solids field with uniform inlet conditions as the first step. This solution represents the flow field with the effect of the other boundary conditions, for example the boundary of the wall. In the next step, we increased the flow velocity in the

nozzle region. The obvious velocity difference between the flow in the nozzle region and the ambient flow quickly changes the distribution of the flow field velocity and concentration. This solution represents a typical two-phase jet flow with the same temperature. Because of the low temperature of liquid nitrogen in the spray jet, the temperature of the vapor is very low compared with that of the ambient flow. Based on same temperature two-phase jet flow, we reduced the temperature of jet, resulting in a solution for a two-phase jet with temperature difference. Finally, the solids concentration condition is released, which represent a low-temperature gas jet inserted into a high-temperature gas-solids media. Some typical results illustrate the effect of solids concentration, jet velocity and temperature on the phase mixing, which will be discussed in Chapter 6.

By the end of the initial gas-solids field simulation, the data file, with a full description of phase distributions of velocity, temperature, and concentration will be outputted for the droplet trajectory calculation.

5.6.2 Droplet Trajectories in Gas-Solids Suspension Flows

As discussed in Section 5.2, the evaporating spray is treated using the Lagrangian trajectory approach, in which the droplets consist of a finite number of trajectory groups. Each droplet starts out with a known position, velocity, size, and temperature, which are dependent on the spray jet system characteristics. The overall droplet position and velocity are updated over the time step, depending on the interactions between the droplet and local gas-solids flow, which is given by the gas-solids flow simulation. The solution

flow chart of the trajectory model is shown as Figure 5.2. The detailed procedure is described in the following.

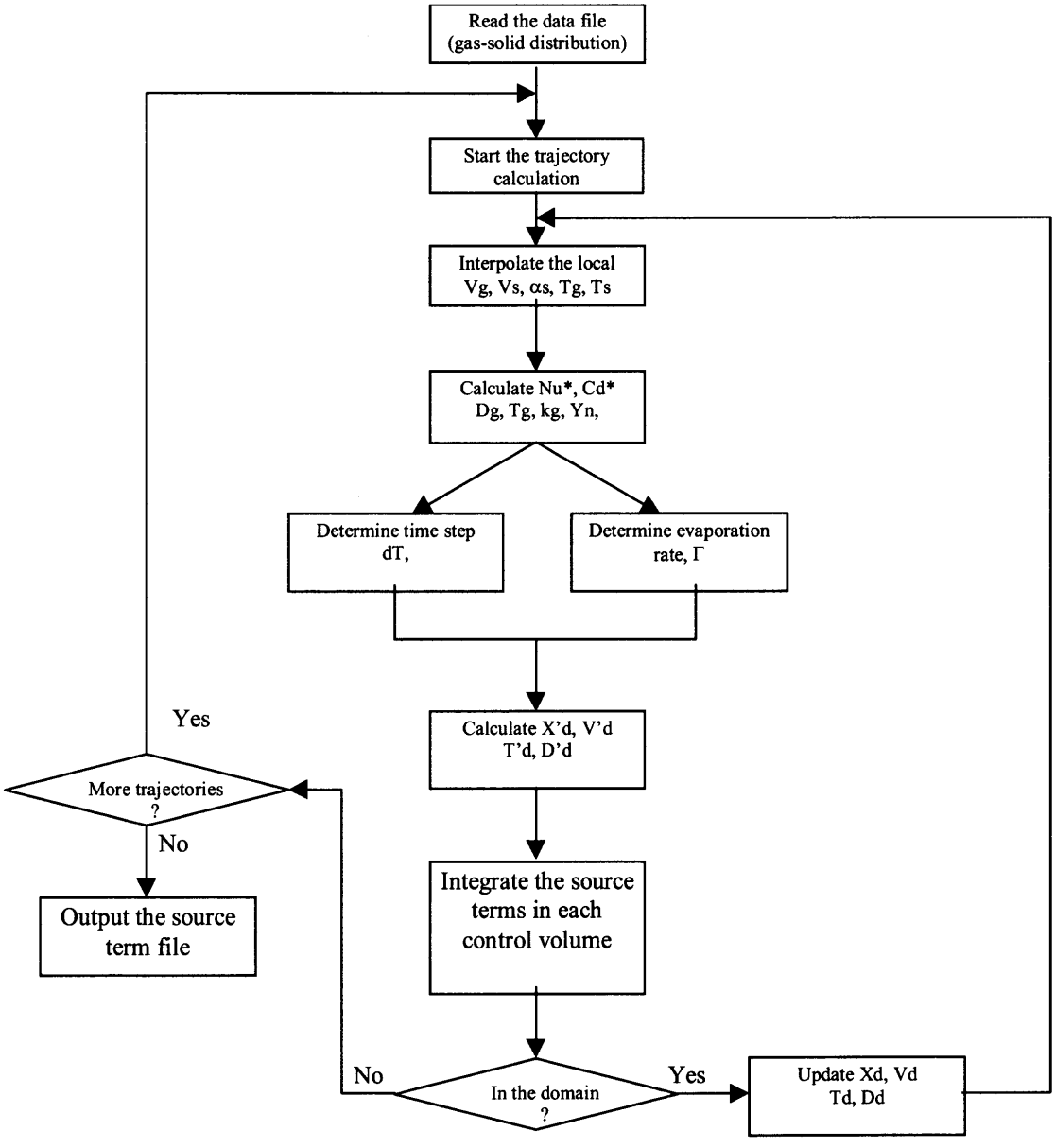

Figure 5.2 Flow chart of droplet trajectory calculations.

The solution starts from a given droplet location, size, and velocity. Based on this location in the calculation domain, the local values in velocity, temperature, and volume fraction of gas and solids can be interpolated. Each integration step along the trajectory starts with an update of thermodynamic and transportation properties of the gas and liquid phases. Then the Nusselt number for heat transfer and drag force coefficient are calculated, taking into consideration the local concentration of the solid particles. The integration time step is estimated from the droplet velocity and grid dimension. A minimum of 10 points is required within one mesh distance. From Eq. (5.11) the new droplet location can be determined from the local droplet velocity and the time step. The droplet velocity, droplet size, and droplet temperature are updated from the droplet mass, momentum, and energy conservation equations. This time integration is continued until the droplet is totally evaporated. In this calculation, this criterion is established as a droplet diameter of less than 5 μm. The entire droplet trajectory calculation is then repeated for a range of different droplet initial conditions representing the nozzle characteristics.

The droplet trajectory model must calculate the source terms for use in the continuum phase calculations. These calculations establish the interactions between droplets and gas and solids phase, respectively, which include the droplet evaporation rate, momentum, and heat transfer. These source terms are volume averaged for the cumulative results over all the trajectory calculations. The updated gas-solids flow fields are used in the next iteration over the droplet trajectory calculations. For reasonable computational speed, the calculation of trajectories cannot be done at every time step

within the gas-solids flow code. Usually, the trajectories are updated every four to eight time intervals depending on the simulation domain and the complexity of the flow field.

5.6.3 Gas-Solids Flow Field with Source Terms

The gas-solids flow field with droplet evaporation is further simulated, incorporating the source terms from the droplet trajectory calculations. The typical effects of droplet evaporation include the dilution of solids concentration, reduction of phase temperature, and change of the phase velocity. Many factors will affect the gas-solids flow field, which depends on the spray jet mass flow rate and droplet evaporation rate. These strong interactions sometimes even affect the calculation convergence, due to the huge amount of vapor generation. As a better solution, the computation is initially performed with a low liquid mass flow rate to avoid the divergence, then with a higher liquid flow rate.

By repeating this procedure, the convergent solutions of gas-solids-droplet flow can be achieved. The interactions among the phases are also realized, which provides an explanation of some of the experimental phenomena and a better understanding of the mixing process of evaporating spray jet in gas-solids flows.

CHAPTER 6

RESULTS AND DISCUSSION

6.1 Experimental Measurement and Analytical Modeling Interpretation

Both analytical and experimental investigations have been performed on hydrodynamic behaviors of axisymmetric concurrent spray jets of liquid nitrogen injected into fully developed gas-solids pipe flows. The experimental measurements are used not only to illustrate the effects of hydrodynamic interaction of the three phases but also to validate our proposed analytical models. The analytical models were developed to understand the hydrodynamic mixing dominated by the comprehensive phase interactions, to provide physical mechanisms for the interpretation of our experimental measurements, and to offer a convenient tool for parametric analysis. Typical comparisons and discussions are based on two groups of studies, namely, (1) jet mixing with a fixed spray rate but variable inlet gas velocities in the absence of solids, and (2) jet mixing with a fixed inlet gas velocity but variable solids volumetric loading at a fixed spray rate or at a fixed spray-to-solids mass ratio. Temperature measurements along the spray axis are used to characterize the spray mixing and to validate the proposed analytical model.

6.1.1 Effect of Inlet Gas Velocity on Jet Mixing without Solids

In this section, effect of gas velocity on jet mixing in the absence of solids will be described. The inlet gas velocity varies from 3.2 m/s to 5.6 m/s, while the spray is fixed with a jet inlet velocity of 30 m/s, an averaged droplet of 120 μm, and a mass flow of 2.7 g/s. Typical temperature profiles of the spray mixture in the particle-free pipe flows are

given in Figure 6.1, which illustrates some unique features of the distribution, such as temperature jump and maximum temperature. Interpretations of these characteristic features are discussed below.

A temperature jump could be clearly identified for all cases of our study, both from measurements and modeling predictions. As shown in Figure 6.1, the measured temperature or the averaged temperature of phase mixture before the jump is nearly the same as the temperature of liquid nitrogen. This phenomenon indicates that the droplet concentration is relatively high before the jump position so that a continuous liquid collision on the thermocouple is ensured. Hence, the length of this constant temperature region before the jump can be used to characterize a densely populated spray core region. There is a noticeable difference in the jump position between the measurements and the modeling results. This is due to the simplification of center-to-center head-on collision used in the modeling assumption, which leads to a somewhat over-estimation of the collision time. Both measurements and modeling results also indicate that the jump position is insensitive to variation in the inlet gas velocity within our investigation range, as shown in Figure 6.1.

Contrary to the intuitive guess of the monotonic increase in temperature profile in the spray region, both measurements and modeling results actually show in Figure 6.1 that peak values exist in those axial temperature profiles at low gas velocities. This phenomenon might be interpreted using the gas temperature profiles shown in Figure 6.2, which are predicted from the analytical modeling. It is noted that the temperature in the ambient gas flow is monotonically decreasing due to the heat absorption from droplet evaporation and limited heat capacity in the bounded pipe flow. The axially reduced gas

temperature, along with the reduced mass entrainment, leads to a reduced heat entrainment along the axis. In the spray region, however, the gas phase is initially pre-evaporated vapor at a temperature close to the liquid temperature. Hence, the initial droplet evaporation rate is low due to the small temperature difference and low heat transfer between the gas and droplets. The rapidly engulfed thermal energy provided by the jet entrainment and turbulent transfer is much more than the energy consumed by the droplet evaporations, which results in a rapid increase in the gas phase temperature. The increased gas temperature, however, enhances the droplet evaporation, which leads to an adverse effect on the increase of gas temperature. A maximum temperature results when the heat provided by the jet entrainment and turbulent transfer just matches that needed for droplet evaporation. Further downstream, the heat transfer from the ambient flow to the spray region is decreased, which approaches a thermal equilibrium for the mixture in the spray region. At a high gas velocity, the strong heat convection from the inlet could provide sufficient heat so that no obvious maximum temperature occurs until the final equilibrium. However, a higher ambient gas velocity causes a reduced velocity difference between the spray jet and ambient flow and hence a reduced entrainment of ambient gas and solids. As a result, the temperature in the spray region may not increase as fast as that at a lower ambient gas velocity, as indicated from the measurements in Figure 6.1. The insufficient modeling description of this temperature lowering effect at high ambient gas velocities indicates that the heat transfer contribution from turbulent fluctuation may be over-estimated for cases of high ambient gas velocity.

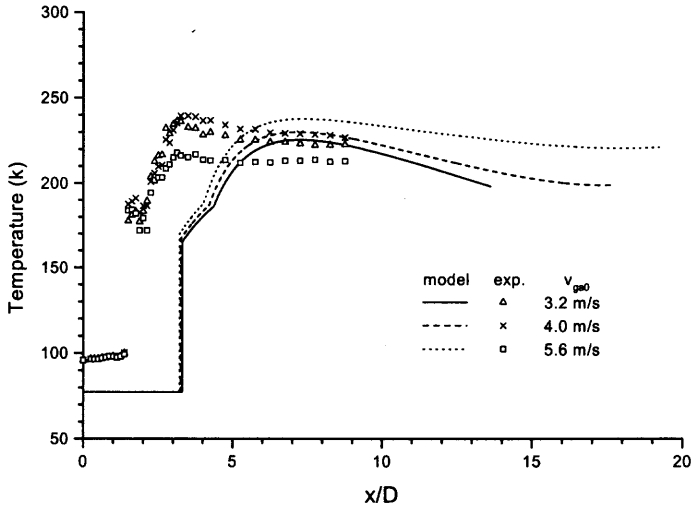

Figure 6.1 Effect of inlet gas velocity on temperature measurement (α_{sa0} =0.0).

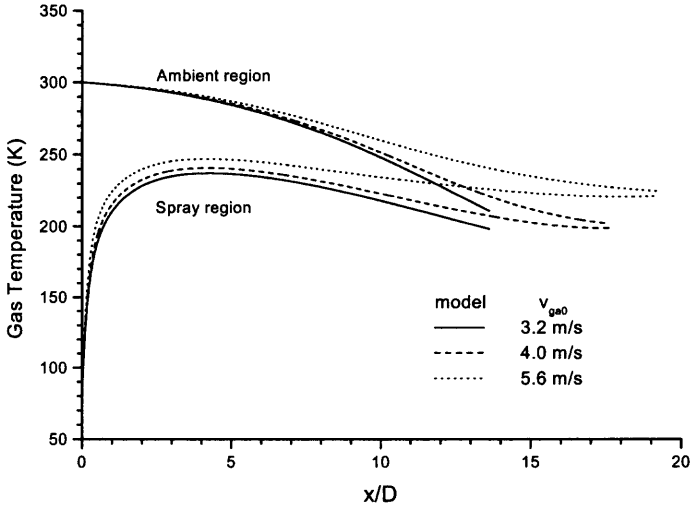

Figure 6.2 Gas temperature distribution in spray and ambient regions (α_{sa0} =0.0).

6.1.2 Effect of Solids Volumetric Loading on Jet Mixing Characteristics

The effects of solids volumetric loading on spray jet mixing were also investigated, and the presence of solids in an ambient flow were found to shorten the spray penetration length. Two groups of experimental studies were performed and compared with the modeling predictions under the same conditions, one was with a fixed gas velocity of 4.0 m/s and the other was at a fixed spray-to-solids mass flow ratio of 0.3. In both cases, the liquid nitrogen spray jet was operated under the same conditions was mentioned.

Typical effects of solids volumetric loading on mixture temperature profiles of the spray in gas-solids pipe flows are illustrated in Figure 6.3(a) for a fixed gas velocity and in Figure 6.3(b) for a fixed solid mass flow rate. A strong drifting effect in the temperature jump position is revealed in both figures as the solids volumetric loading changes. As explained in Section 4.5, the location of the temperature jump is governed by two characteristic time scales in droplet-thermocouple collisions, i.e, the droplet collision time (τ_c) and time interval between two consecutive droplet collisions (τ_{dd}). The axial distributions of both time scales under the conditions of our investigation are given in Figure 6.4, where the junction of the two time scales marks the location of the temperature jump. The increase of solids volumetric loading in the ambient flow enhances the engulfed thermal transfer for droplet evaporation, which not only quickly reduces the droplet size but also dilutes the droplet concentration. Consequently the time interval between two consecutive droplet collisions (τ_{dd}) is prolonged, while, due to the droplet size reduction, the droplet-thermocouple collision time (τ_c) is shortened. As shown in Figure 6.4, as the solids volumetric loading increases, the increase of τ_{dd} and the decrease of τ_c yields a shortening of the spray core penetration length. The ratio of spray

core penetration length to that of the particle-free case (or nearly particle-free case for a fixed spray-to-solids mass flow ratio) is further plotted in Figure 6.5, which clearly shows that the higher the solids volumetric loading, the shorter the spray core penetration.

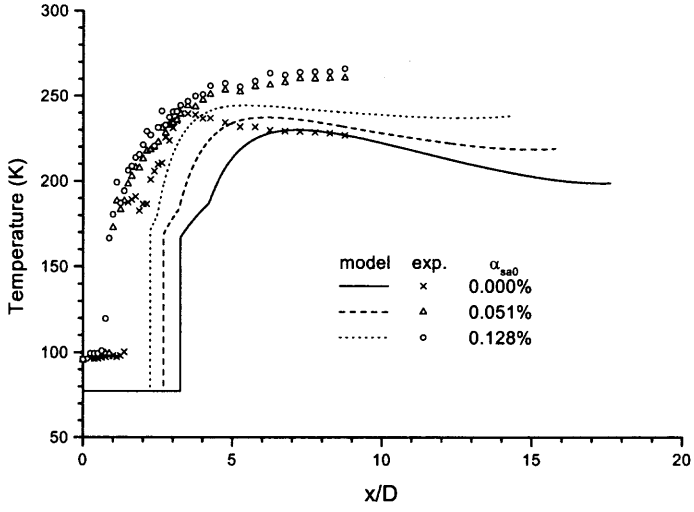

(a) Fixed inlet gas velocity (v_{ga0}=4.0m/s).

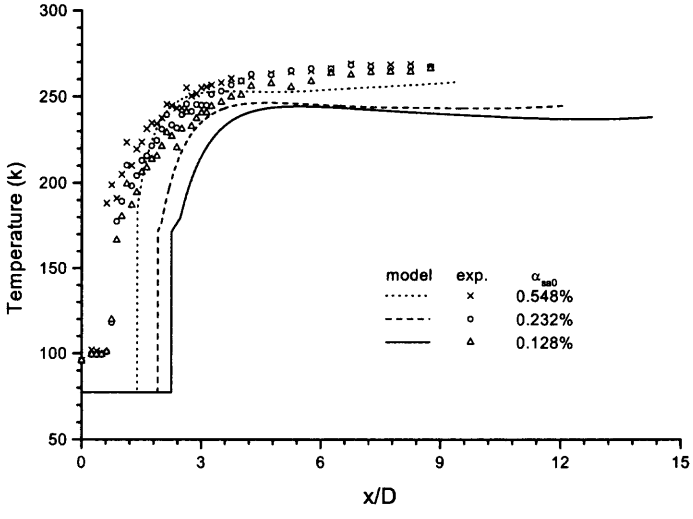

(b) Fixed solids mass flow rate (m_s=10.1g/s).

Figure 6.3 Comparison between experimental measurements and analytical results.

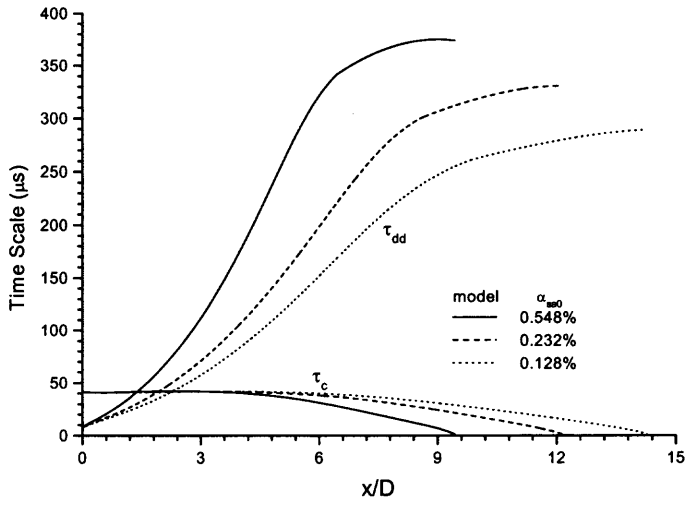

(a) Fixed inlet gas velocity (v_{ga0}=4.0 m/s).

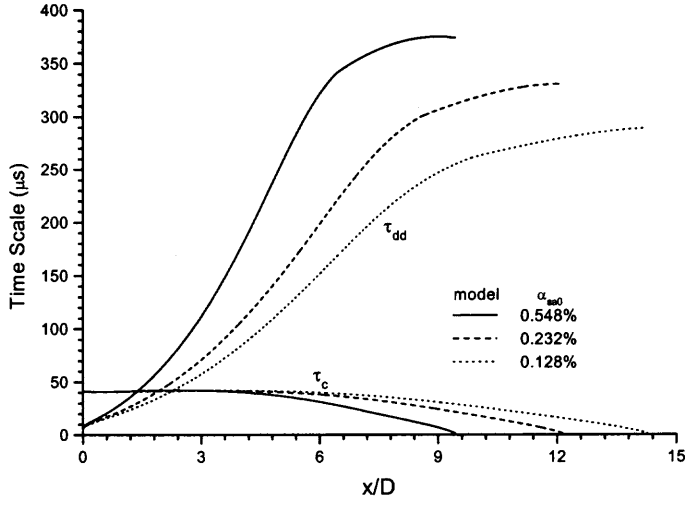

(b) Fixed solids mass flow rate (m_j=10.0g/s).

Figure 6.4 Effect of solids volumetric loading on core region length.

A change in solids volumetric loading in the ambient flow strongly affects not only the overall thermal capacity of the gas-solids mixture but also the heat convection from upstream. In Figure 6.3, as opposed to the temperature distribution of a particle-free flow where a maximum peak occurs, the axial temperature profiles appear to be monotonically and asymptotically increased even with a very dilute loading of solids. Naturally, the higher the solids volumetric loading, the higher the final equilibrium temperature.

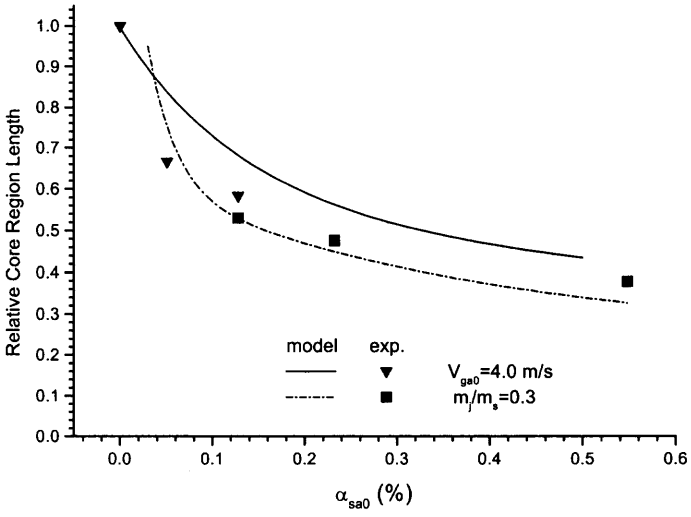

Figure 6.5 Effect of solids volumetric loading on spray core penetration length.

6.1.3 General Hydrodynamic Characteristics

Many unique hydrodynamic features of evaporating spray jets in gas-solids flow are difficult to investigate experimentally and hence have to be understood from mechanistic modeling. Most of these features are spray evaporation induced, such as jet boundary expansion, solids concentration dilution, temperature reduction, and gas velocity acceleration. The following is a discussion of some general hydrodynamic characteristics that are purely based on our analytical model predictions.

Typical gas temperature distributions in the spray and ambient flow regions are given in Figure 6.6, which shows that the gas in the ambient flow is cooled by the spray evaporation while the gas in the core region is heated up due to the strong entrainment and turbulent heat transfer. Figure 6.6(a) shows the effect of solids loading and Figure 6.6(b) illustrates the effect of spray jet mass flow. A comparison between Figure 6.6(a) and Figure 6.2 reveals very similar temperature profiles between the effect of solids loading in gas-solids flows and the effect of gas velocity in particle-free flows under the same spray conditions. This similarity indicates a dominant role of thermal convection on the axial temperature distribution.

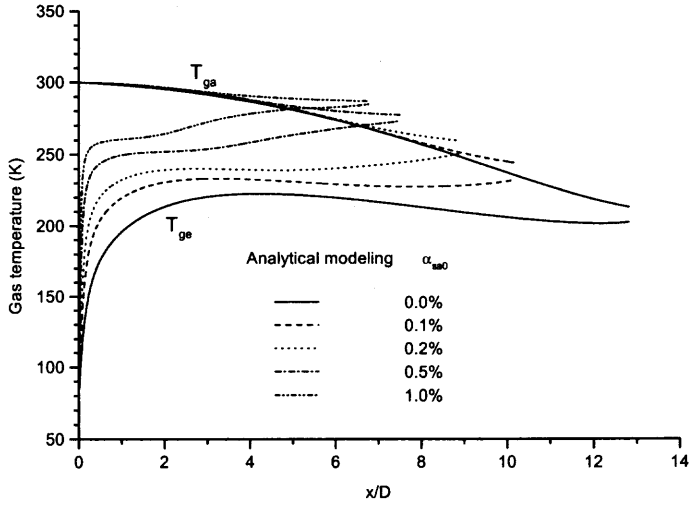

(a) Effect of solids loading (v_{ga0}=4.0 m/s, M_j=2.7 g/s).

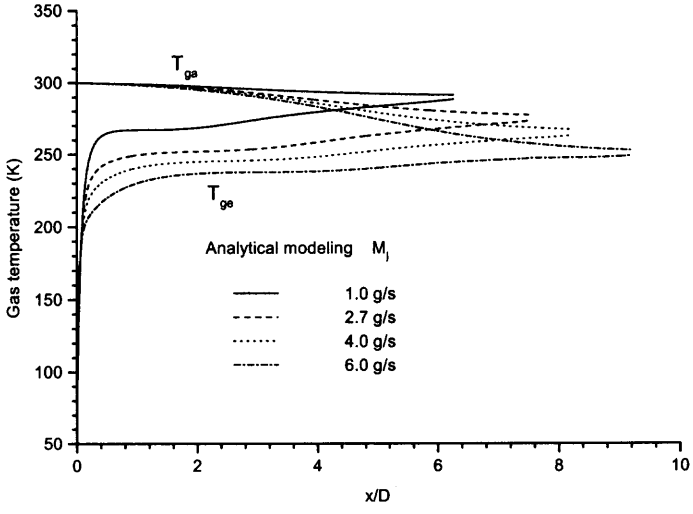

(b) Effect of jet mass flow rate (v_{ga0}=4.0 m/s,α_{sa0}=0.5%).

Figure 6.6 Typical gas temperature distribution.

Typical gas velocity distribution in the ambient region and the droplet velocity distribution in the spray region are illustrated in Figure 6.7, with Figure 6.7(a) showing the effect of solids loading and Figure 6.7(b) showing the effect of spray jet mass flow. Both figures show the gas acceleration in the ambient region, which is mainly due to the evaporation-induced jet boundary expansion as shown in Figure 6.8. Under the flow conditions in Figure 6.8, the final jet boundary expansion or spray region varies from 10% to nearly 50% of the entire pipe cross section. The higher the jet boundary expansion, the more squeezing effect on the ambient gas and hence higher gas acceleration. As indicated in Figure 6.7(a), with a low solids loading, there may exist a slow-down section of the ambient gas, which may be caused by dramatic volumetric contraction from the rapid temperature reduction as shown in Figure 6.6(a). As can be expected, droplet velocities are first exponentially reduced and then slightly accelerated by the gas entrainment and the evaporation-induced gas velocity increase in the spray region. The final balanced phase velocities are reached upon the completion of droplet evaporation and turbulent mixing. Figure 6.7(a) also shows that the higher the ambient solids loading, the shorter the spray penetration.

Figure 6.9 illustrates the typical distribution of the solids volumetric fraction in the spray region. As shown in Figure 6.9, due to the strong solids entrainment, there is a rapid increase in solids concentration near the jet nozzle region. However, the solids concentration is then quickly diluted along the axis due to the excessive vapor generation from droplet evaporation. While the effect of solids loading is strong, as shown in Figure 6.9(a), the effect of spray jet mass flow is fairly weak, as illustrated in Figure 6.9(b).

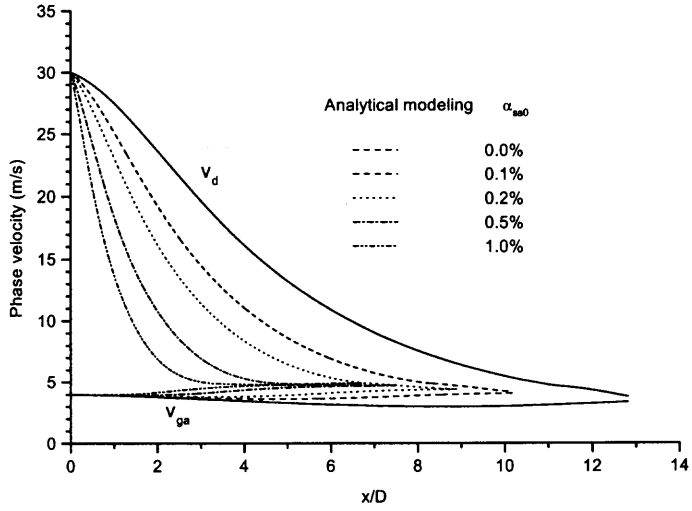

(a) Effect of volumetric solids loading (v_{ga0}=4.0 m/s, M_j=2.7 g/s).

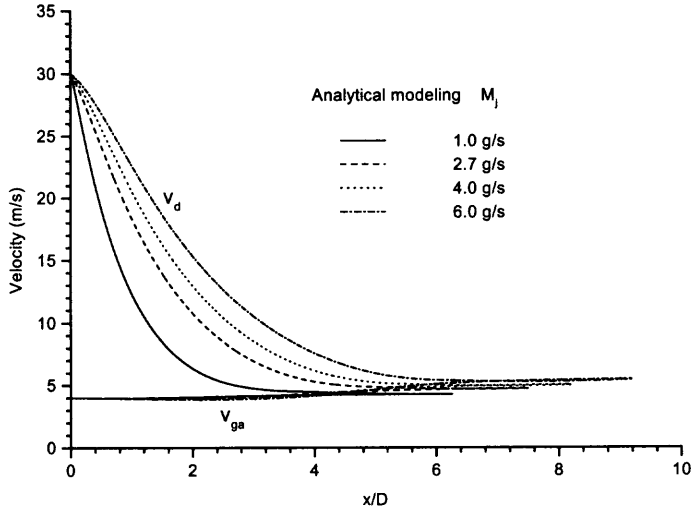

(b) Effect of jet mass flow rate (v_{ga0}=4.0 m/s, α_{sa0}=0.5%).

Figure 6.7 Typical phase velocity distribution.

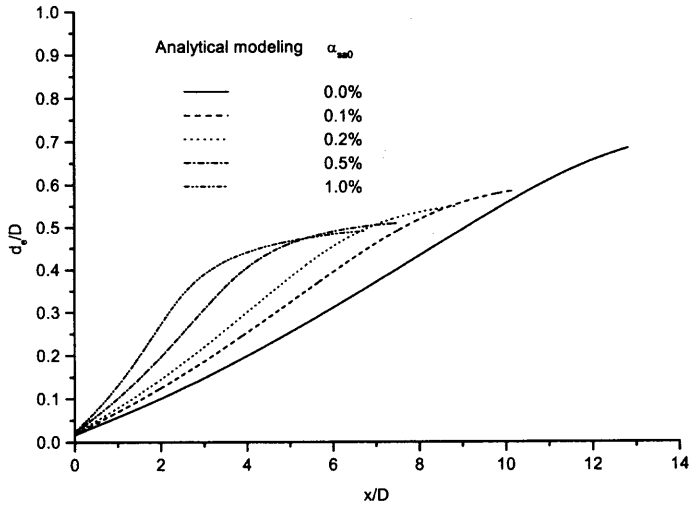

(a) Effect of solids volumetric loading (v_{ga0}=4.0 m/s, m_j=2.7 g/s).

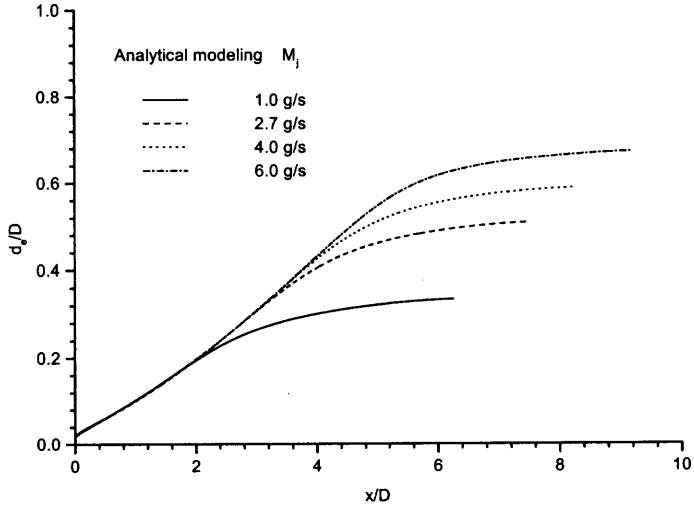

(b) Effect of jet mass flow rate (v_{ga0}=4.0 m/s, α_{sa0}=0.5%).

Figure 6.8 Spray jet boundary expansion.

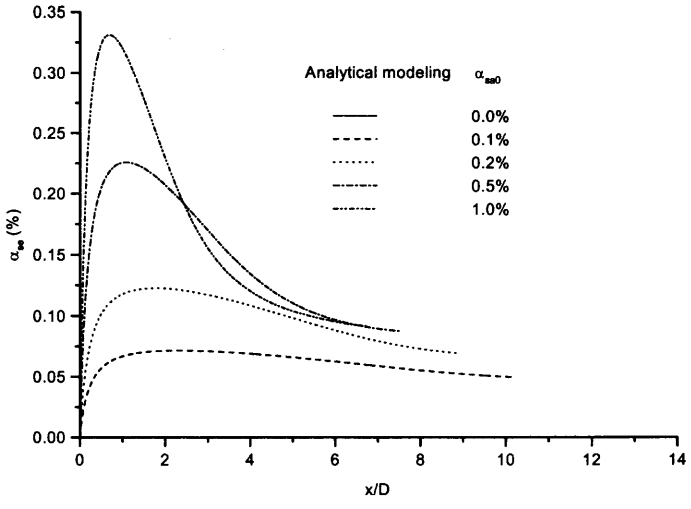

(a) Effect of solids volumetric loading (v_{ga0}=4.0 m/s, m_j=2.7 g/s)

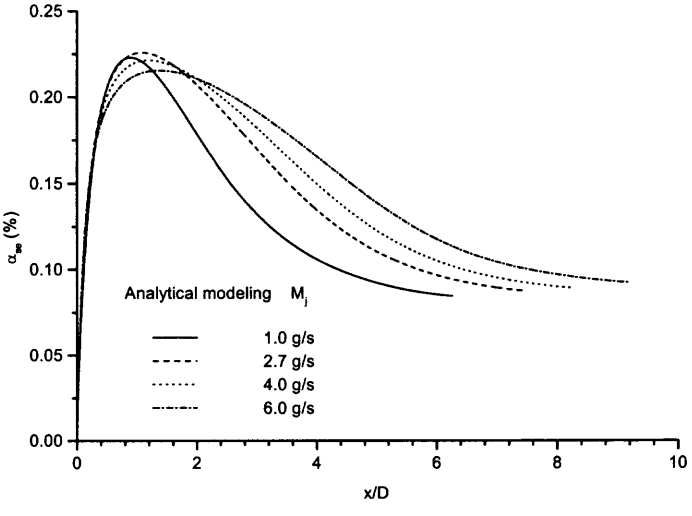

(b) Effect of jet mass flow rate (v_{ga0}=4.0 m/s, α_{sa0}=0.5%).

Figure 6.9 Typical solids volumetric distribution in spray region.

6.2 Numerical Simulation and Interpretation

An example of numerical simulation will be presented here to illustrate the phase mixing process of a concurrent spray jet of liquid nitrogen in a dilute gas-solids pipe flow. The inlet boundary conditions for the calculations are listed in Table 6.1, where the ambient gas-solids pipe flow is at 300 K and 2.4 m/s with 1% solids volume fraction. It is further assumed that there is no slip between gas and solids in the ambient inlet flow and vapor-droplet in the jet flow. Since the droplet phase is calculated using the Lagrangian approach, the volume occupied by droplets is not counted in the jet inlet conditions of the volume fraction in the gas-solids flow simulation.

Table 6.1 Inlet Boundary Conditions

Variable	Ambient	Gas-Solids	Vapor-Droplet Jet		
	Gas	Solids	Gas	Solids	Droplet
Velocity (m/s)	2.42	2.42	30.0	30.0	30.0
Temperature (K)	300.0	300.0	200.0	200.0	77.2
Volume Fraction	0.99	0.01	1.0	0.0	———

The concurrent liquid nitrogen spray is introduced into the gas-solids flow through a straight nozzle located along the centerline of the pipe. The effect of the nozzle wall and the nozzle geometry are also considered. The nozzle opening is set at 4 mm in diameter with a small divergence angle of 2° in the simulation. The medium initial droplet diameter is 120 μm and the mass flow rate of nitrogen spray is about 2.0 g/s. Due to the flow symmetry in concurrent pipe flows, only the flow in the median plane needs

to be simulated. For the convenience of experimental comparison, the computational domain is selected to be 1.0 m by 0.025 m with a uniform grid distribution of 400 × 25.

In order to illustrate the effects of droplet evaporation on the phase mixing and jet structure, the jet without droplets is also simulated under the same gas-solids inlet conditions. The comparisons between them should provide detailed information regarding the contributions of droplets and droplet evaporation in the jet mixing. Effects of droplet evaporation on dilution of solids concentration, reduction of phase temperature and change of phase velocities will be discussed in this section. In addition, the spray evaporation and structure will also be illustrated.

6.2.1 Dilution Effect of Droplet Evaporation

The rapid evaporation of liquid spray in a gas-solids flow has a significant impact on the flow and temperature field of the gas-solids mixture, especially in the evaporation region. Quick droplet evaporation results in an excessive vapor production that is mixed into the surrounding gas stream, which not only changes the local velocities of gas and solids but also produces a dilution of solids concentration as well as a gas/solids phase temperature reduction. Figure 6.10 illustrates the effect of droplet evaporation on solids dilution, where the solids volume fraction is basically what remains besides the gas in the gas-solids mixture excluding droplets. In Figure 6.10, the solids volume fraction in the jet ambient flow has a nearly uniform distribution of 1%. In the jet region, almost no solids exist due to jet expansion and droplet evaporation. One interesting thing indicated by Figure 6.10 is that, due to the jet boundary expansion near the nozzle region, the solids will accumulate near the jet boundary up to 2%, both in the jet without droplets and with 2.0 g/s droplets. This solids buildup near the boundary may be caused by the push-off

effect of solids from the jet region. Figure 6.10 also indicates that the jet without droplets has a much lower ability to expand; it loses its expansion trend near a distance of 50 times of its nozzle diameter. This phenomenon seems reasonable in light of the work by Abramovic, (1963). Compared with the jet without droplets, the jet with 2.0 g/s droplets maintains the trend to expand in the calculation domain, due to the huge vapor generated by droplet evaporation. It reaches its maximum spray jet width at a distance of 0.8 m from the nozzle, where the droplets are completely evaporated.

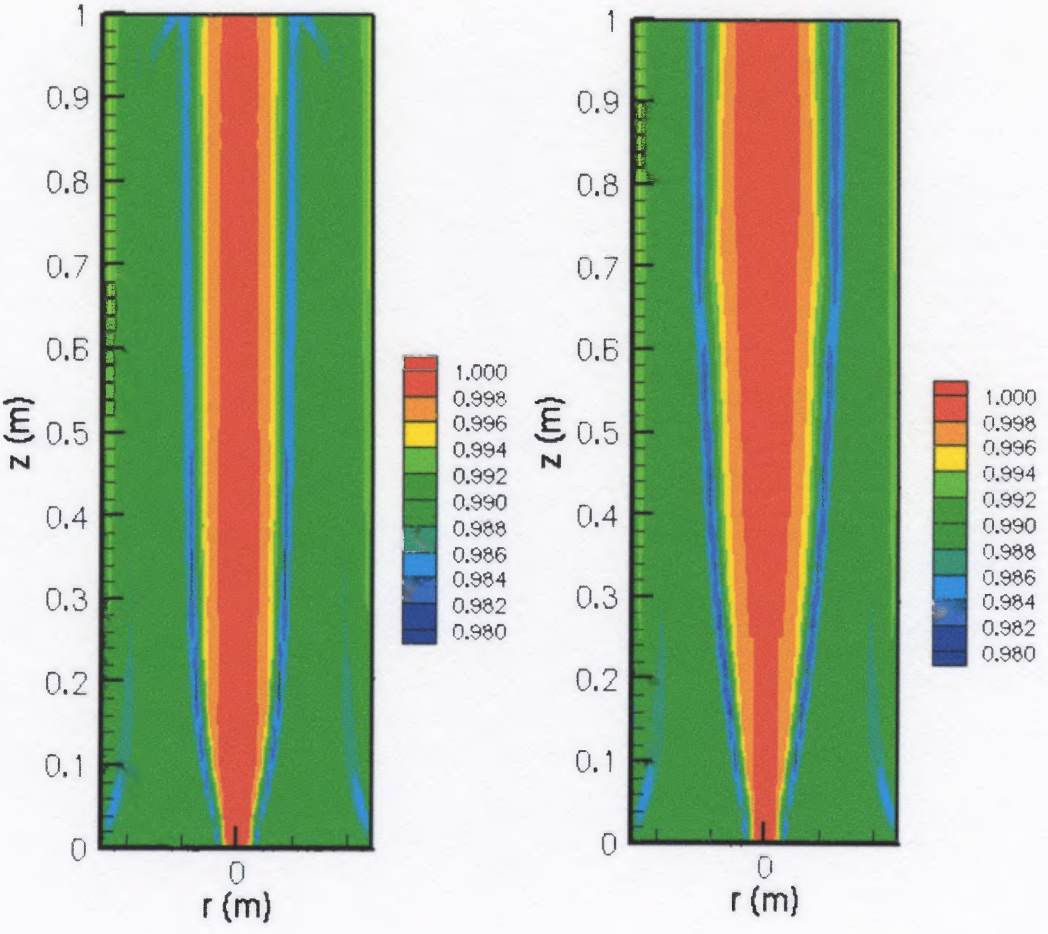

(a) Without droplets (b) With droplets

Figure 6.10 Gas volume fraction distribution.

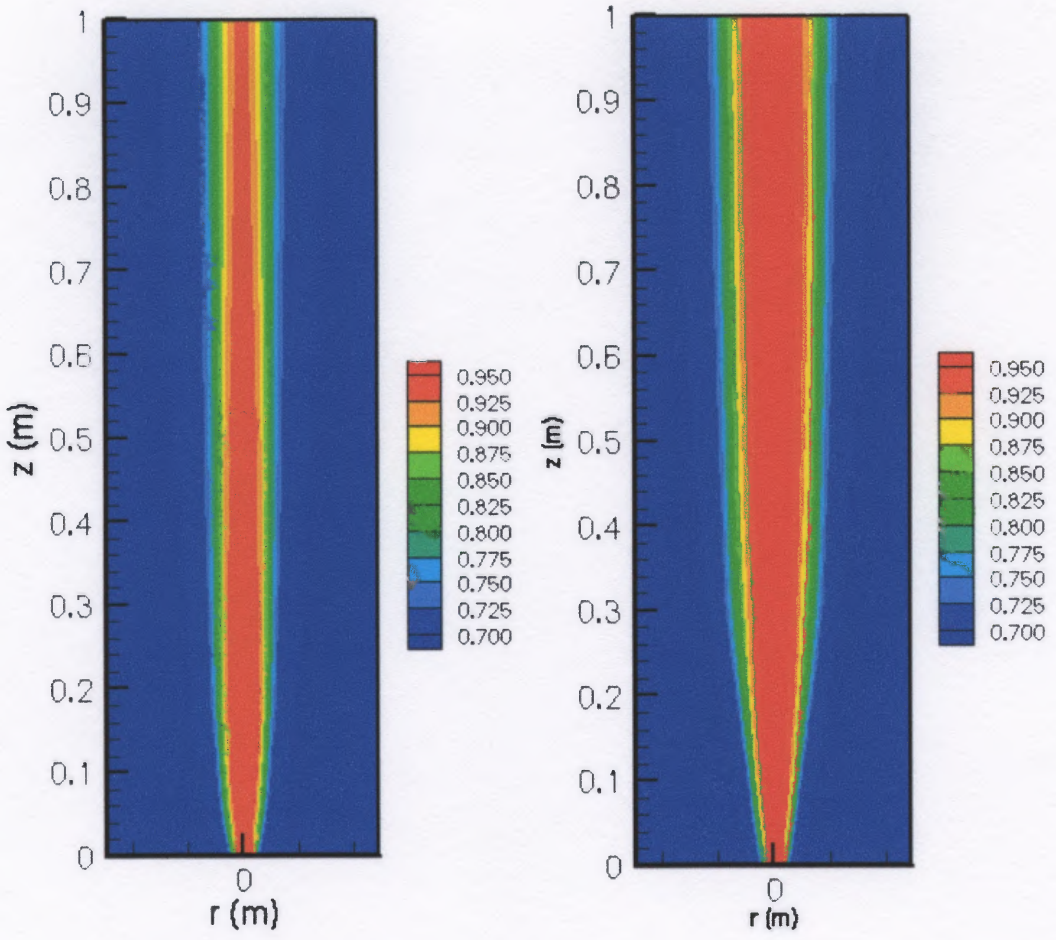

(a) Without droplets (b) With droplets

Figure 6.11 Nitrogen species mass fraction in air-nitrogen mixture.

The droplet evaporation also changes the gaseous concentration distributions in the mixture, as shown in Figure 6.11, which in turn governs the diffusive rate of droplet evaporation. The vapor concentration distribution is also critical to the determination of chemical reactions in fluidized bed reactors. Figure 6.11(a) shows the concentration distribution of nitrogen in the air-vapor mixture for a jet without droplets. It indicates that species concentration has the same trend with the gas volume fraction in the jet expansion section, as shown in Figure 6.10(a). In the ambient flow, the nitrogen concentration has a

uniform distribution of 70% in the air-vapor mixture, whereas in the jet region the nitrogen has a nearly uniform concentration distribution of 100%. Compared with the jet without droplets, the spray jet of 2 g/s has an obvious widened region with high nitrogen concentration in the air-vapor mixture caused by the nitrogen vapor generated by nitrogen droplet evaporation. This vapor is also pushed off with the spray boundary. After the droplets are fully evaporated, the nitrogen concentration will be reduced due to the gas convection.

6.2.2 Effect of Droplet Evaporation on Phase Temperature Reduction

Droplet evaporation in a gas-solids flow also leads to a temperature reduction of the gas and solids due to the absorption of latent heat from the surrounding gas-solids media. The mixing effect of gas-solids at higher temperature and the evaporated nitrogen vapor at lower temperature also contributes to the temperature reduction. Figure 6.12 and Figure 6.13 illustrate the temperature reduction effect of droplet evaporation on gas and solids. Compared with the jet without droplets, Figure 6.12(b) indicates the lowest temperature of gas in the spray region of the jet with 2.0 g/s droplets is 150 K, which is 50 K lower than the lowest gas temperature found in the spray region of jet without droplets, shown by Figure 6.12(a). This lower temperature is caused by droplet evaporation.

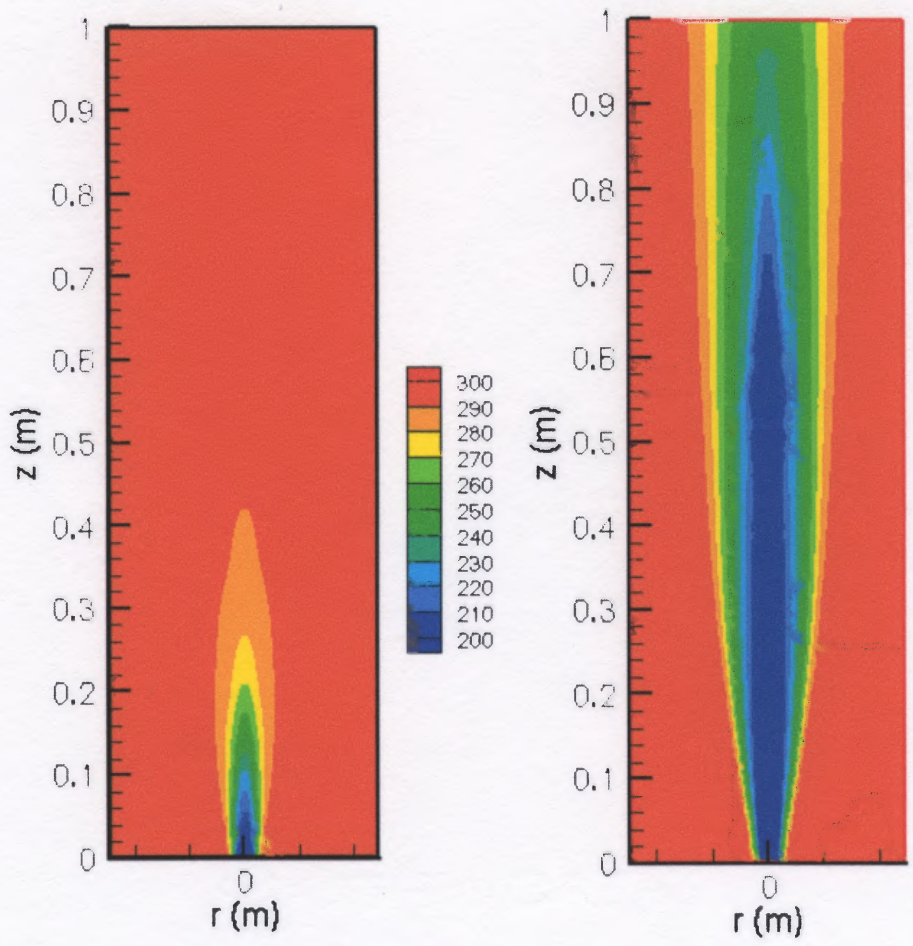

(a) Without droplets (b) With droplets

Figure 6.12 Gas temperature distribution (K).

Figure 6.13 shows the temperature distribution in the flow with and without droplets in the jet. The difference between the lowest solids temperature in the flow region for the two cases indicates the effect of droplet evaporation. In this example, the minimum temperature of the solids is about 250 K for the jet without droplets, whereas it is only 200 K for the jet with droplets. In other words, a temperature reduction of 50 K in

the solids phase results from droplet evaporation. Compared with Figure (6.12), the solids have a much higher temperature than the gas. This is due to the solids having a much higher thermal capacity and lower heat conductivity than the gas.

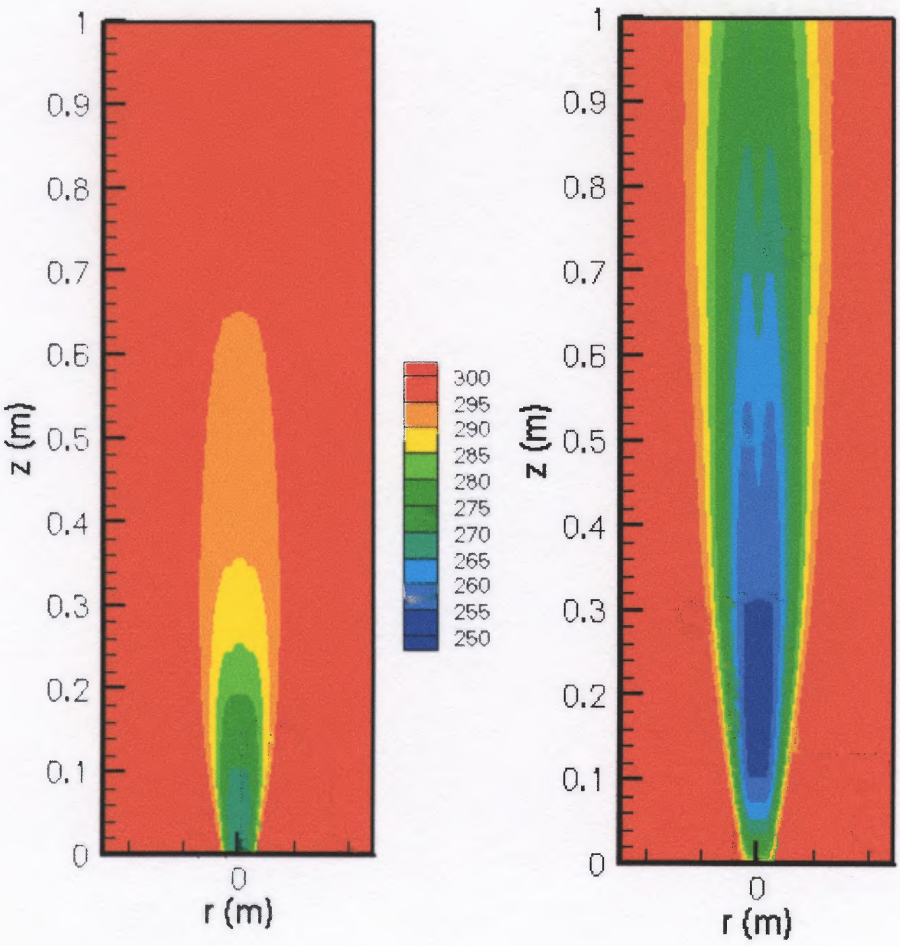

(a) Without droplets (b) With droplets

Figure 6.13 Solids temperature distribution (K).

6.2.3 Effect of Droplet Evaporation on Phase Velocities

Droplet evaporation provides excessive vapor into the gas-solids stream, leading to changes in the velocity of both gas and solids. Figure 6.14 shows the gas velocity distribution with droplet evaporation in the spray. The axial gas velocities are significantly changed by droplet evaporation.

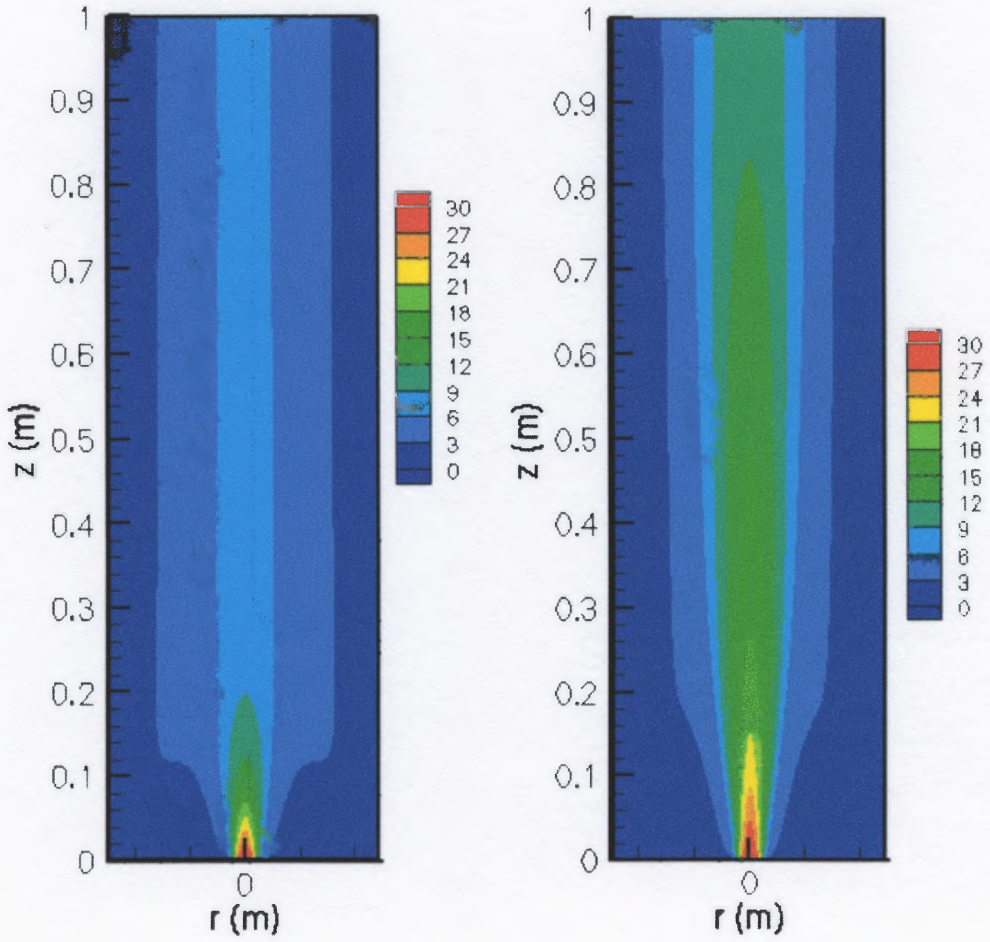

(a) Without droplets. (b) With droplets.

Figure 6.14 Gas axial velocity distribution (m/s).

Figure 6.14(a) indicates that the jet velocity is quickly reduced due to the jet boundary expansion, and jet entrainment of gas and solids. The gas velocity for the jet without droplets decreases from 30 m/s to 10 m/s within 0.12 m from the nozzle exit. However, the spray jet of 2 g/s has a much higher mixture density, even with only 1% volumetric droplets loading. Thus, adding droplets in the jet will increase the jet penetration capability. Figure 6.14(b) illustrates the gas phase velocity in the flow region with a vapor-droplets jet. It indicates that the velocity of gas phase changes from 30 m/s to 10 m/s over a longer distance of 0.8 m, partially due to the droplet evaporation in the spray jet region.

Figure 6.15 further illustrates the phase velocity decrease, due to the jet boundary expansion. As shown in Figure 6.15, the axial gas velocity profiles along the axis are smoothened down with the jet developing. In the jet region, the gas velocity is decreased by the interactions between the jet and the ambient flow, whereas the ambient flow is accelerated. Under the effect of the wall boundary, the gas velocity appears to fit into an exponential distribution. For the jet with droplets and droplet evaporation, the decrease in jet velocity is much slower than that without droplets as shown in Figure 6.16. For example, the gas velocity changed from 30 m/s to 20 m/s, and the distance is about 0.13 m in the case with droplets, while it is 0.06 m for the jet without droplets. The vapor jet merges into the ambient gas-solids flow with an axial distance of 0.2 m, while the vapor-droplet jet has a merging distance of about 0.8 m.

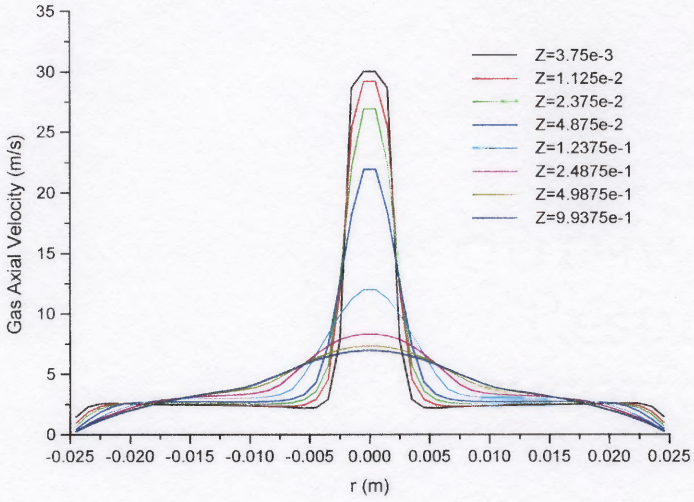

(a) Without droplets.

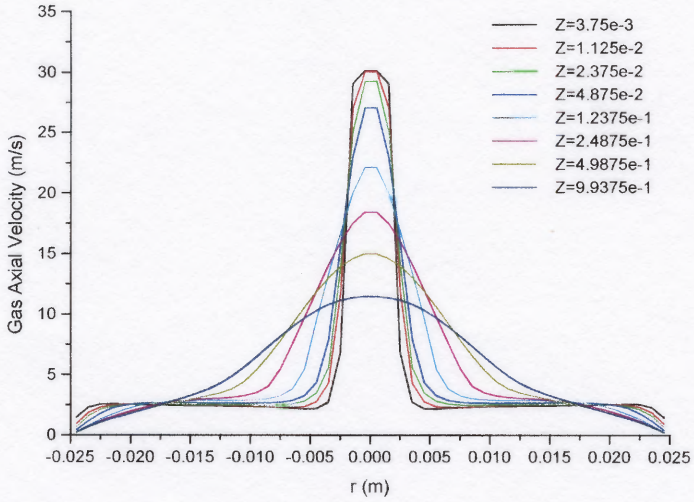

(b) With droplets.

Figure 6.15 Axial velocity profiles along the axis.

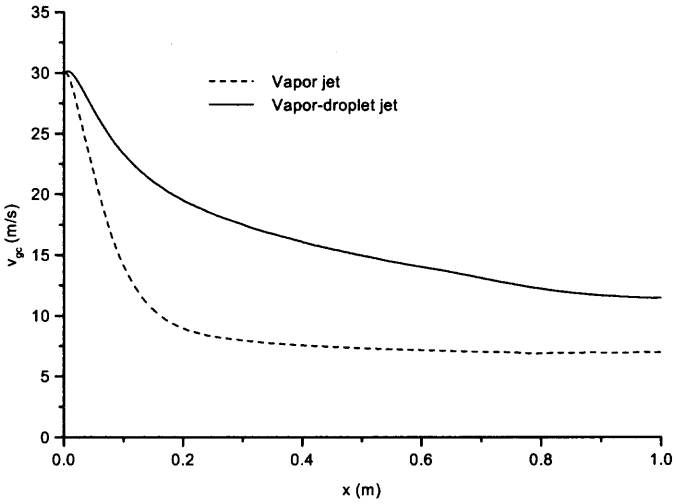

Figure 6.16 Gas velocity along the axis.

Figure 6.17 shows the velocity profiles along the axis using the dimensionless scale, where the jet boundary was determined by the gas velocity profile as shown in Figure 6.15. It revealed that the dimensionless velocity distributions are not only similar but also match the Schlichting formula or "the Law of 3/2" of single-phase jets. Within the range of this study, it appears that the similarity model for one phase jet may be extended into the three-phase jets with strong droplet evaporation.

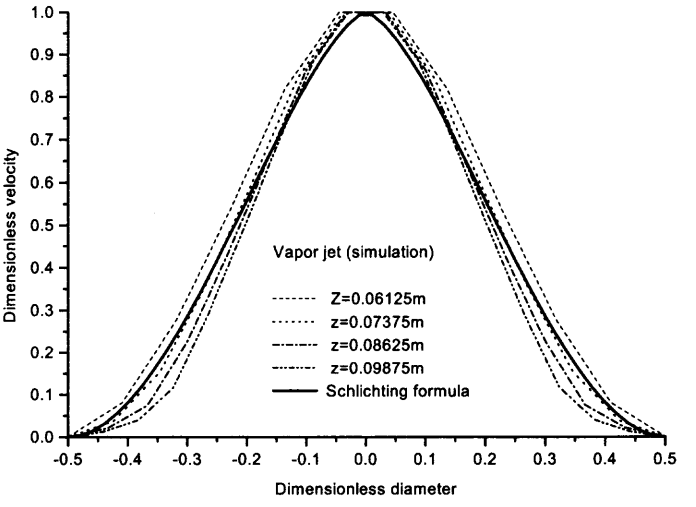

(a) Without droplets

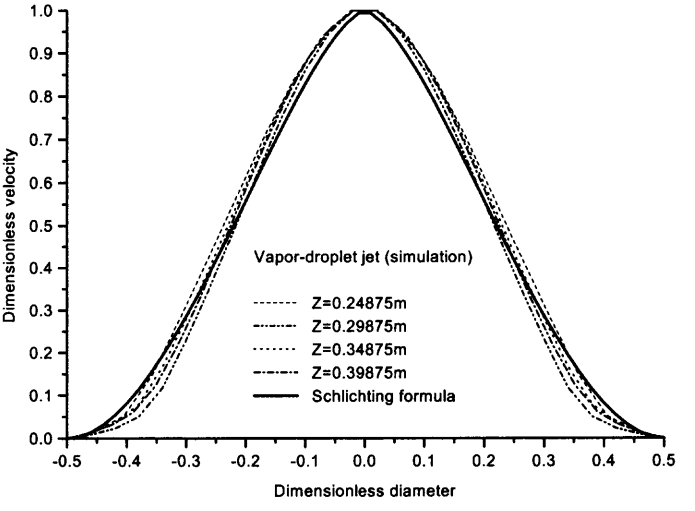

(b) With droplets

Figure 6.17 Similarity velocity profile of the multi-phase jet.

6.2.4 Jet Structure with Droplet Evaporation

The above discussion illustrates that droplet evaporation in a gas-solids flow can strongly affect the hydrodynamic behavior of both gas and solids. The significance of this effect however depends on the droplet evaporation rate that is in turn affected by the solids loading in the gas-solids flow. Figure 6.18 shows the droplet size distribution in the spray region, which defines the evaporation region. From the definition of the spray evaporation length, in this example, the maximum droplet penetration length is about 0.8 m.

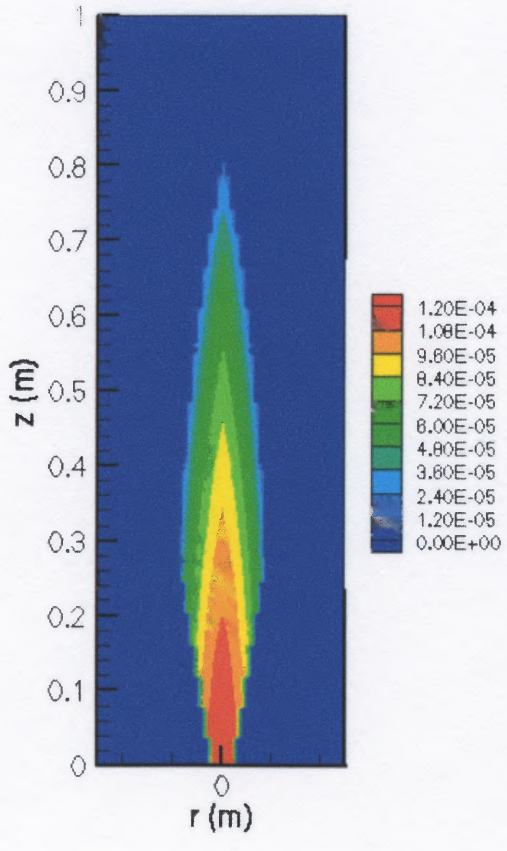

Figure 6.18 Droplet size (m).

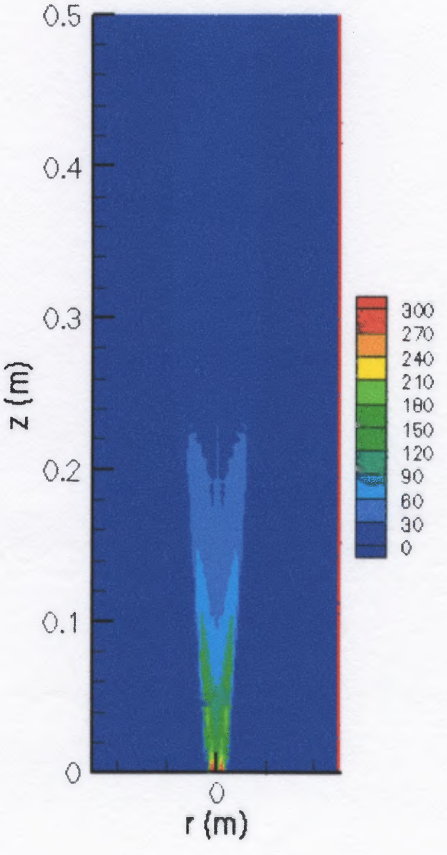

Figure 6.19 Evaporation rate (kg/m^{3}s).

The droplet size distribution depends on droplet evaporation, which is shown in Figure 6.19. As expected, the maximum evaporation rate occurs at the edge of the spray due to the vapor mixing and droplet-solids collision. The maximum droplet evaporation rate occurs at the spray inlet region where the temperature difference between the gas-solids flow and droplets reaches its maximum value. The maximum evaporation rate is about 300 kg/(m^3s) in the flow with 1% solids in the ambient flow.

The spray evaporation region also depends on the droplet velocities in axial and radial directions, as shown in Equation (5.11). With the same droplet size and droplet evaporation rate, droplet could penetrate deeper when the droplets have a higher velocity. Figure 6.20 shows the droplet axial velocity distribution. In this example, droplet has a maximum axial velocity in the inlet region of 30 m/s. With the interactions between droplets with gas and solids, droplet velocity is reduced towards the local velocities of the ambient gas-solid flow. The smaller of the droplet size, the closer the droplet to follow the flow of gas. As shown in Figure 6.20 that droplets gain the radial velocity duo to the droplet evaporation, which means that droplet evaporation will push droplet out of the spray region. The maximum droplet axial velocity happens near the boundary of spray region, where the droplet evaporation rate is the highest as shown in Figure 6.19. In this example, the maximum droplet axial velocity is 0.7 m/s near the nozzle region.

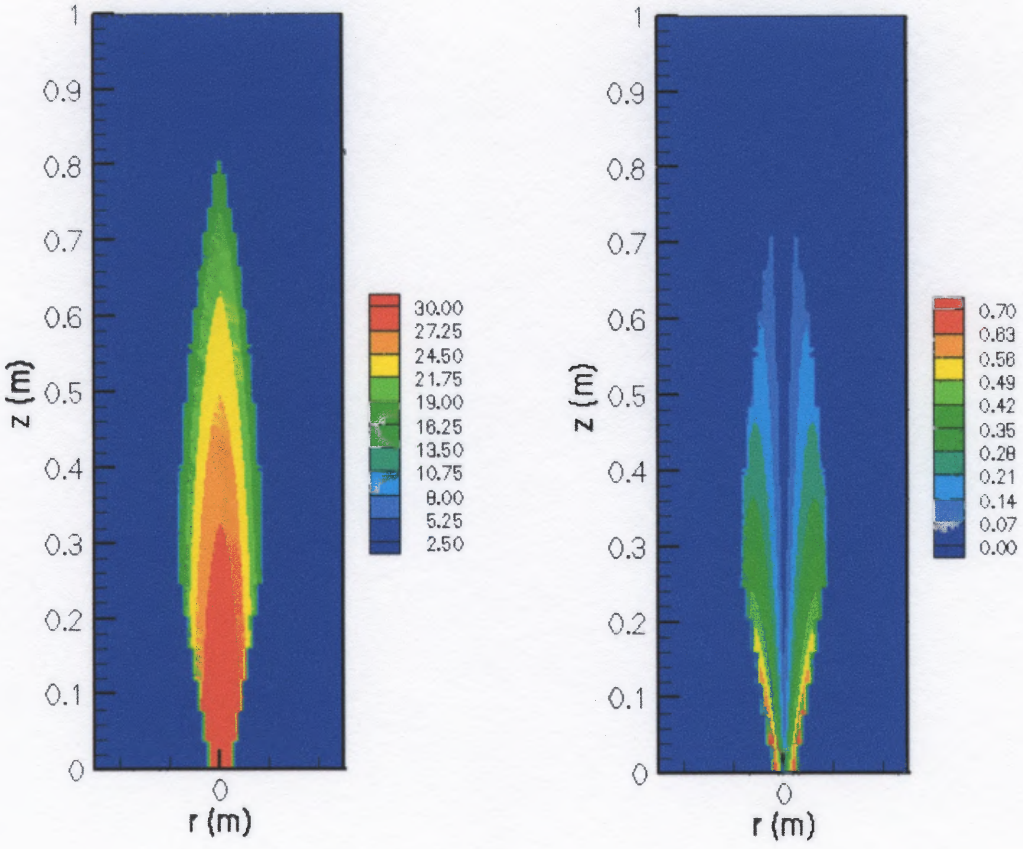

(a) Axial velocity. (b) Radial velocity.

Figure 6.20 Droplet velocity distribution (m/s).

6.3 Parametric Studies on Jet Evaporation Length

Spray jet penetration characteristics are important to many industrial applications, especially for the reaction controlled by mixing between vapor and catalytic particles. As discussed in Section 4.5, the length of the spray core region can be determined by the intersection of the droplet collision time and the time interval between two consecutive droplet collisions. The spray penetration depth, however, is determined by the axial location where the last droplet diminishes.

In this part, a discussion will be given on the parametric effects of ambient inlet solids concentration, inlet ambient flow velocity, jet mass flow rate, and jet initial droplet size distribution on the jet evaporation length. Typical results of spray penetration length, including core evaporation length and spray penetration depth, are investigated by a combined effort of experimental measurements, analytical modeling, and numerical simulations. Since many unique hydrodynamic features of evaporating spray jets in gas-solids flow are difficult to investigate experimentally, they may be revealed from mechanistic modeling and numerical simulations. In order to evaluate the actual droplet-solids mixing region (spray evaporation length), the investigation of the ratio between core evaporation length and spray penetration depth is important. Based on the core evaporation length determined by the thermocouple temperature profile measurement, we can multiply the core evaporation length by the ratio to achieve the whole evaporation length.

6.3.1 Spray Evaporation Length

A typical effect of solids loading on spray evaporation length is illustrated in Figure 6.21 and Figure 6.22. Both experimental and numerical results illustrate that the spray evaporation length is significantly shortened while the spray dispersion is expanded by the addition of solids into the pipe flow. Figure 6.21 provides the direct visualization of the spray contour, whereas Figure 6.22 gives extended information beyond the experimental visualization, such as quantified spray trajectory and spray penetration depth. The simulation conditions for Figure 6.22(b) are listed in Table 6.2.

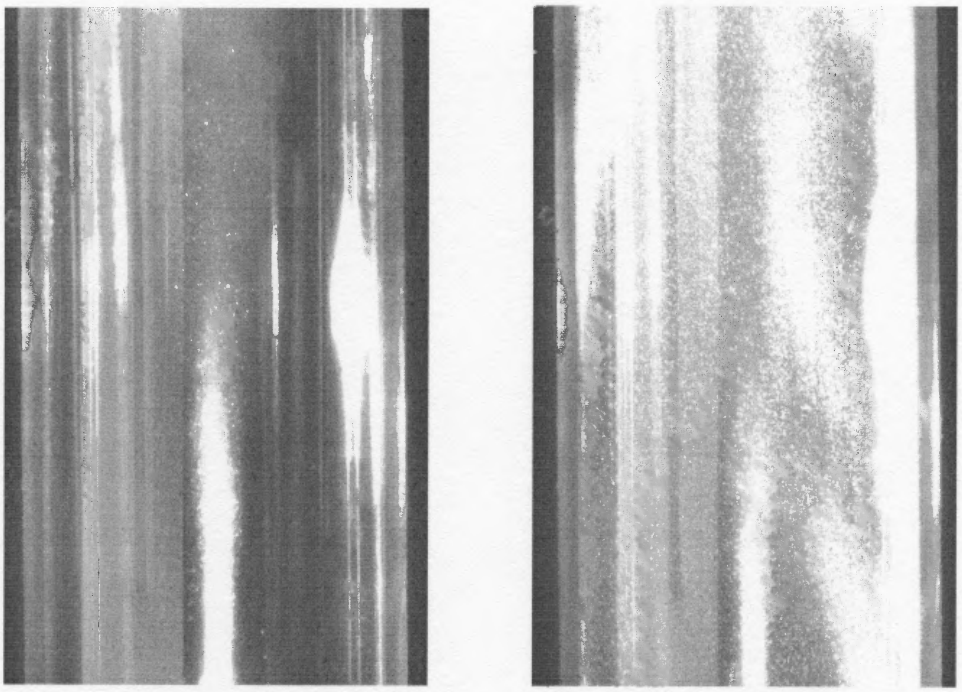

(a) Without solids. (b) With solids.

Figure 6.21 Spray domain by laser-assisted visualization.

Table 6.2 Simulation Conditions for Evaporation Spray in Gas-Solids Flows.

Spray Jet	M_j	V_j	D_{d0}	α_{d0}
Inlet Conditions	2.7 g/s	30 m/s	120μm	21.9%
Ambient Flow	V_{g0}	T_{g0}	V_{s0}	α_{s0}
Inlet Conditions	4.0 m/s	300K	4.0 m/s	0.5%

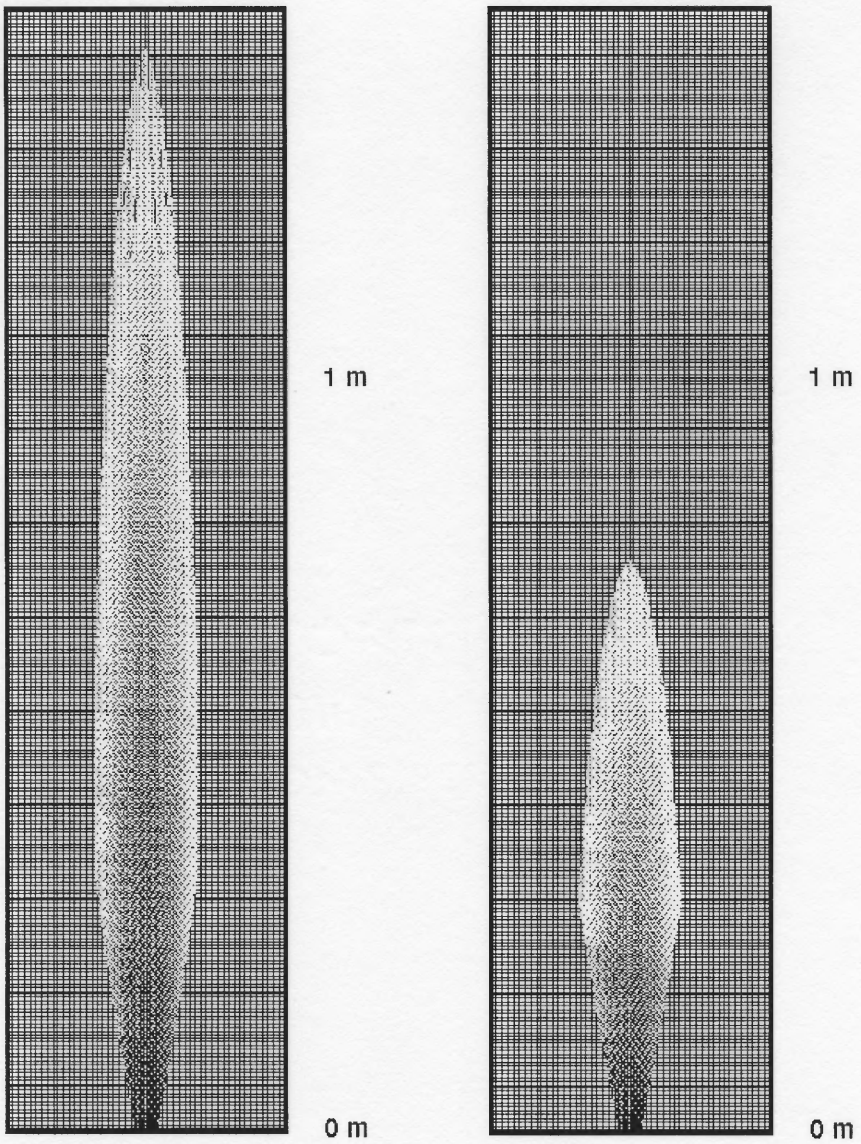

(a) Without solids. (b) With 0.5 % solids loading.

Figure 6.22 Spray domain as determined by calculation.

The parametric effect of solids volumetric concentration on the jet penetration length is shown in Figure 6.23(a), which clearly shows that the jet penetration length significantly decreases with an increase in the solids volumetric concentration. This shortening is due to the much enhanced heat transfer by the droplets-solids collisions and much larger drag force between the droplets and the gas-solids mixture. This effect can also be illustrated in the gas volume fraction and velocity distributions, which are similar to the distributions shown in Figures 6.10 to 6.14. It is noted that while the droplets-solids collisions appear to be the dominating effect on droplet evaporation, the presence of solids in the gas stream also has a significant impact on the heat transfer between the gas and the droplets. This is due to the turbulence modulation and the gas temperature change by the gas-solids heat transfer. In the example of Figure 6.23(a), the jet penetration depth is shortened by up to 48%, from both numerical simulations and analytical modeling predictions, compared with that in particle-free flows. The difference between the two modeling predictions is due to the simplification of analytical modeling into 1-D calculation, which averaged the evaporation depth over all droplets. At the same time, the numerical simulation may underestimate the effect of turbulent heat transfer and turbulent mass transfer between the evaporation region and ambient flows.

In industrial applications, many other parameters, such as jet initial mass flow rate and initial droplet size, will also strongly affect jet penetration length. Their parametric effects are respectively shown in Figure 6.23 (b) and (c). In order to minimize the systematic errors from our modeling approaches, the relative penetration length (i.e., the ratio of penetration length to the referenced one) is used in modeling predictions and numerical simulations. The reference penetration length is calculated under the

conditions listed in Table 6.2. Different from the effect of solids loading, the parametric effects of initial droplet size and jet mass flow rate on spray penetration length appear to be linear relationships within the range of our investigation. An increase in the initial droplet size or jet mass flow rate leads to a similar effect on droplet evaporation, that is, a reduction in droplet evaporation by decreased heat transfer between the droplet and gas-solids ambient flow. For example, increasing the initial droplet size will reduce the specific surface area, thus reducing the heat transfer rate. Increasing the jet mass flow rate will decrease the vapor temperature around the droplet, as shown in Figure 6.6(b), which will reduce the droplet evaporation. As shown in Figure 6.23(b), the change in initial droplet size from 60 μm to 200 μm results in an increase in spray penetration length by 260%. Figure 6.23(c) indicates that the change in penetration length is about 100% when the jet mass flow rate changes from 1.0 g/s to 6.0 g/s.

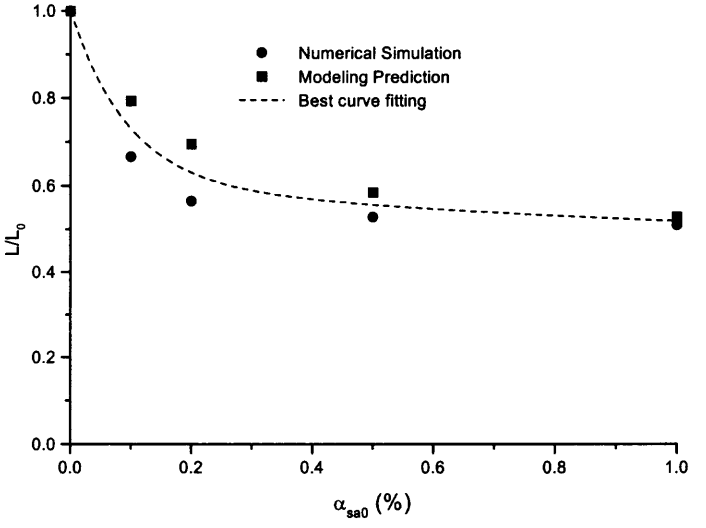

Figure 6.23 Parametric study on spray penetration length (a) Effect of solids loading.

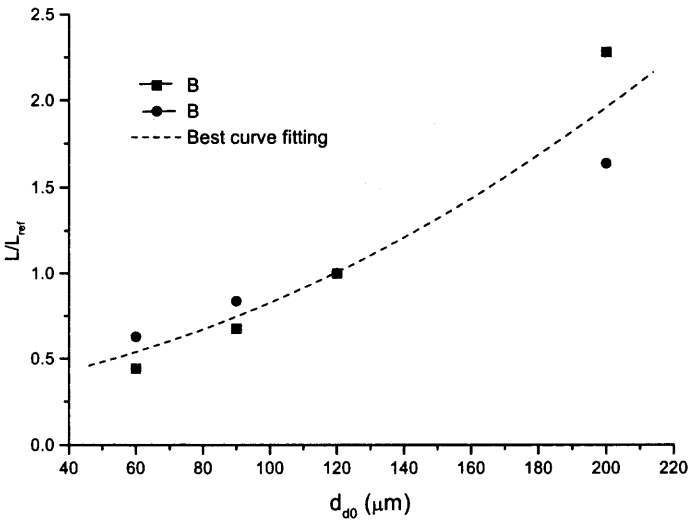

(b) Effect of initial droplet size.

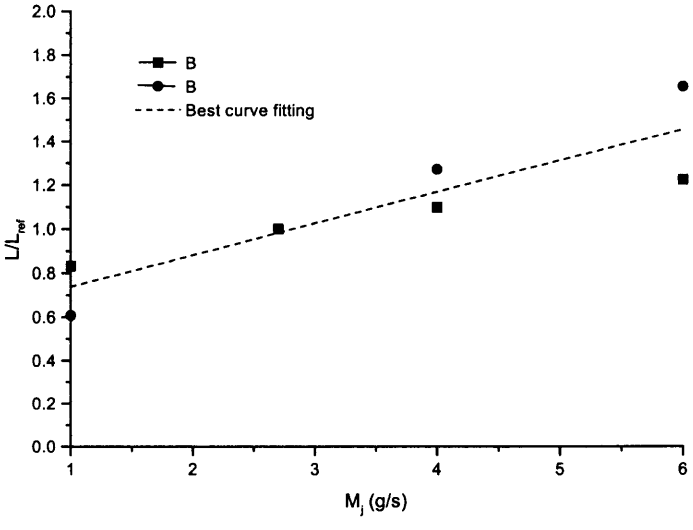

(c) Effect of jet mass flow rate.

Figure 6.23 Parametric study on spray penetration length (b) and (c).

6.3.2 Core Evaporation Length

As discussed in Section 3.4, the core evaporation length of spray could be detected by the thermocouple temperature measurement. In this study, we investigated the parametric effect of solids loading, initial droplet evaporation length, and jet mass flow rate on the core evaporation. The parametric study results are shown in Figure 6.24. Similar to the parametric effect on penetration length, the parametric effect of solids loading on the core evaporation length is significant. As shown in Figure 6.24(a), the core spray evaporation region of spray jet in a 1% solids volumetric loading flow is shortened by up to 70%, compared with that in particle-free flows. The contributions of solids loading on the core evaporation shortening include the effects not only on the spray evaporation rate but also on the phase-averaged temperature measurement by the solids entrained into the evaporation region. The experimental measurement on the spray evaporation length shows good agreement with the analytical modeling, as shown in Figure 6.24(a).

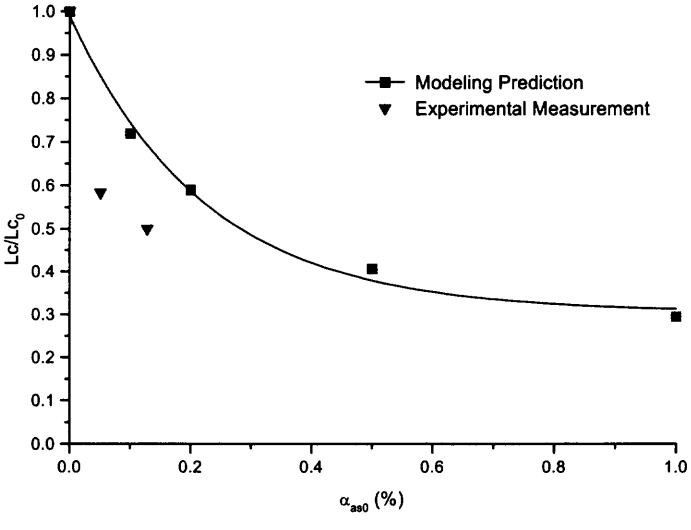

Figure 6.24 Parametric study on core evaporation length (a) Effect of solids loading.

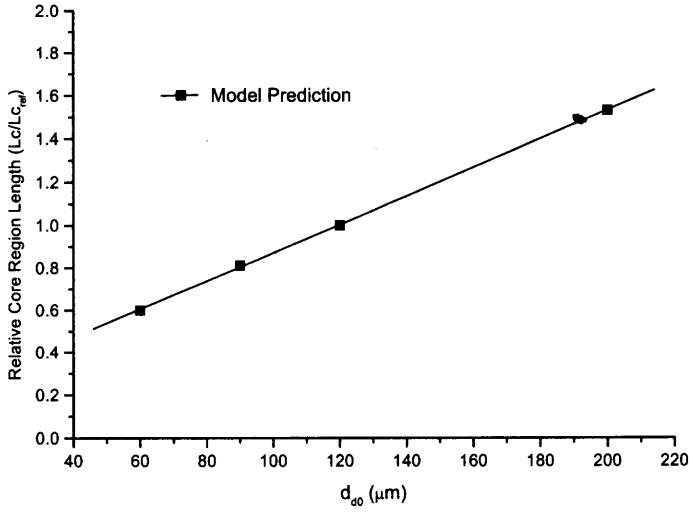

(b) Effect of initial droplet size.

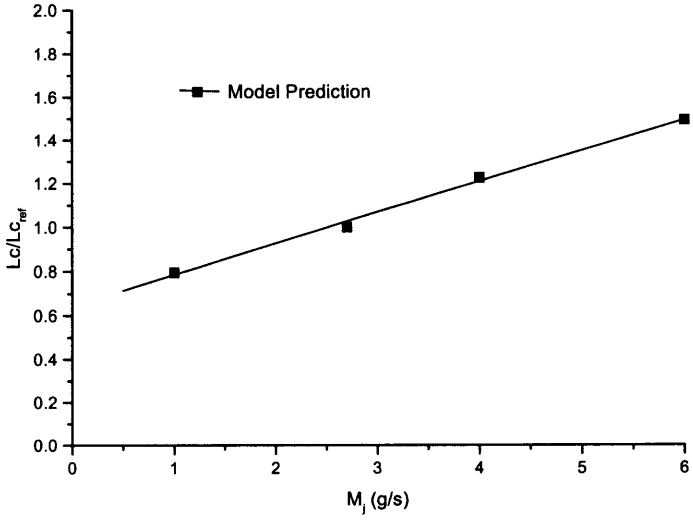

(c) Effect of jet mass flow rate

Figure 6.24 Parametric study on core evaporation length (b) and (c).

Both Figure 6.24(b) and Figure 6.24(c) illustrate a linear relationship between the core evaporation length and initial droplet size and between the core evaporation length and jet mass flow rate. When the initial droplet size changes from 60 μm to 200 μm, the spray core evaporation length is increased by about 155%. While increasing the initial droplet size leads to an increase in the spray penetration depth, it reduces the droplet-solids mixing rate. From the modeling prediction, Figure 6.24(c) illustrates a 90% increase in the core evaporation length as the jet mass flow rate changes from 1 g/s to 6.0 g/s.

6.3.3 Ratio of Core Evaporation and Penetration Length

It is interesting to investigate the ratio of spray core evaporation length (Lc) and penetration length (L) since experimentally only one of these two characteristic lengths can be determined. This parametric study provides an avenue for using experimental measurements of core evaporation length to estimate penetration length.

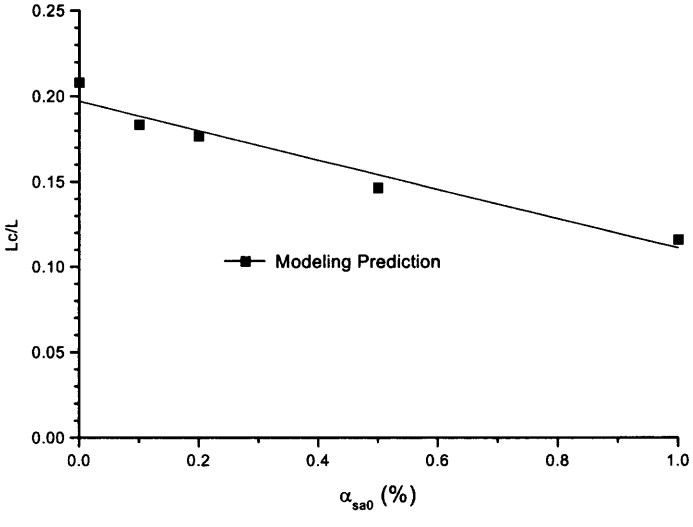

Figure 6.25 Parametric study on the ratio of Lc and L (a) Effect of solids loading.

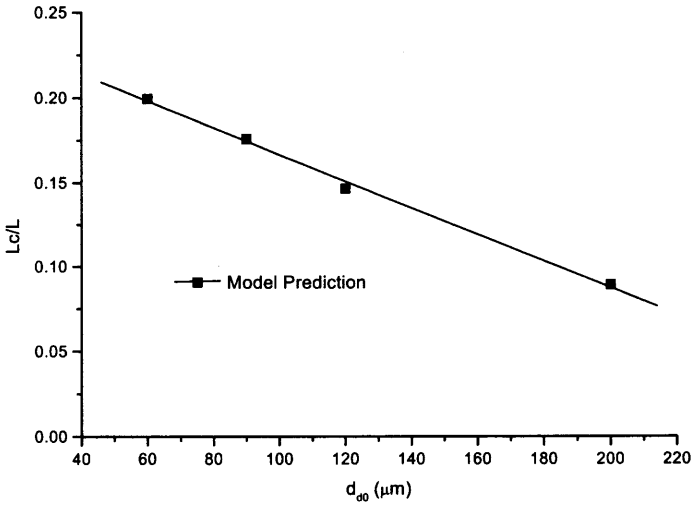

(b) Effect of initial droplet size.

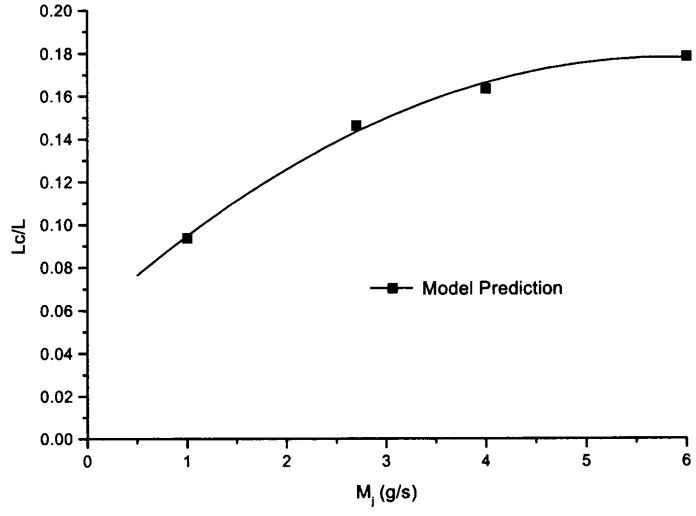

(c) Effect of jet mass flow rate.

Figure 6.25 Parametric study of the ratio of Lc and L (b) and(c).

Figure 6.25 illustrates the parametric effects of solids loading, initial droplet size, and jet mass flow rate on the ratio of Lc/L. The relationship between the ratio of solids loading and initial droplet size is nearly linear, as shown in Figure 6.25(a) and Figure 6.25(b), respectively. When the solids loading is lower than 1.0%, the core region length is within 10% to 20% of the spray penetration length. The higher the solids concentration, the lower the relative length. Figure 6.25(b) shows that the ratio of core evaporation length and spray penetration length is also sensitive to the initial droplet size. When the initial droplet size is changed from 60 μm to 200 μm, the ratio is reduced from 20% to 8%, indicating that the reduced initial droplet size may enhance the droplet mixing in the gas-solids flow. Figure 6.25(c) indicates that the relative length does not follow a linear relationship with the jet mass flow rate. The higher the mass flow rate, the slower the increasing rate in relative length. As the jet mass flow rate changes from 1 g/s to 6 g/s, the ratio of core evaporation and spray penetration length varies from 9 to 16%.

CHAPTER 7

SUMMARY AND CONCLUSIONS

7.1 Research Summary

A systematic study combining experimental measurements, analytical modeling and numerical simulations has been performed to investigate the unique characteristics of phase mixing and spray evaporation of the concurrent evaporating spray jets in dilute gas-solids pipe flows. The experimental work in this study represents the first known effort to determine the spray jet structure by optical visualization and thermocouple-based temperature measurements. The parametric effects of gas velocity, solids loading, and liquid-to-solids ratio on the spray evaporation characteristics have been experimentally explored. These results provide original experimental evidence for better understanding the phase mixing and droplet evaporation process in pipe flow.

In order to interpret the experimental findings and go beyond the experiment limits, modeling approaches have been pursued, including the development of analytical models and numerical simulations. The one-dimensional analytical model is based on the multi-fluid control volume method, in which a spray evaporation region and an ambient gas-solids region are defined for three-phase flow. Turbulent phase transfer and interactions between the spray and the ambient flow are delineated. Characteristic phenomena, such as the shortening of the spray penetration and evaporation-induced temperature reduction and gas acceleration have been explored and interpreted. In the numerical simulation approach, a hybrid Eulerian-Lagrangian method has been applied to investigate a concurrent liquid nitrogen spray jet in a FCC pipe flow, which yielded the local phase interactions and distributions, difficult to study otherwise. The method also

successfully yield the total spray evaporation length as well as similarity laws of phase velocity distributions with strong droplet evaporations.

7.2 Major Research Findings

The phenomenon of evaporating spray jets in a gas-solids pipe flow is very complex and involves many advanced research topics, such as multi-phase jet droplet evaporation, droplet-solids collision-dominated heat and mass transfer, and turbulence modulation by solids loading and droplet evaporation. The following summarizes three major conclusions obtained from this study.

7.2.1 Spray Region Identification

This study developed an innovative and practical method for demarcation of the dense spray region and the dilute spray region with strong evaporation in gas-solids suspensions. Based on the thermocouple measurements, the dense evaporation length can be clearly determined from a temperature jump in the axial temperature distribution. It is noted that the temperature profile measured by a thermocouple in a spray region with strong evaporation has unique characteristics, namely, an isothermal core of the droplet temperature in the densely populated spray region as opposed to a high-temperature distribution in dilute spray region. The sudden jump of temperature can be used to demarcate the interfacial boundary between these two regions. This temperature demarcation method is superior to the conventional optical visualization method that can only be applied to very dilute flows with optically distinguishable droplets and solid particles. The proposed thermocouple measurement method can quantitatively determine

the dense spray region not only for the cases where optical visualization can be applied but also for sprays in dense gas-solids flows and in dilute gas-solids suspensions with indistinguishable droplets and solid particles.

This study also proposed a mechanistic model for the physical interpretation of the temperature jump phenomena in the thermocouple-measured temperature profiles. The model reveals that the spray region demarcation is characterized by two time scales, namely the collision contact time between a droplet and the thermocouple τ_c and the time interval between two adjacent droplet collisions on the thermocouple τ_{dd}. When $\tau_c > \tau_{dd}$, the thermocouple is always in contact with liquid and hence the thermocouple measurement yields a constant temperature close to that of the liquid droplet due to the strong latent heat required for droplet evaporation. This region is thus defined as the dense spray region. When $\tau_c < \tau_{dd}$, the thermocouple is not always in contact with liquid. In this case the thermocouple measurement is a phase-averaged temperature of gas, solids, and droplets, which depends not only on the phase temperature but also on the phase concentration and velocity. Due to the intermittent evaporation and strong turbulent convection of gas and solids, this phase-averaged temperature is significantly higher than that of the droplets. This temperature jump occurs over a very short distance of the measurements. Thus this relatively high-temperature region corresponds to the dilute spray region.

In summary, an innovative measurement method to identify the dense spray region is proposed. Successful interpretation of the physical meaning of the spray regions based on two characteristic time scales is also provided.

7.2.2 Shortening Effect of Solids Loading

In this work, a systematic investigation is carried out for the shortening effect of solids loading on the spray evaporation length by the combined efforts of experimental measurement, analytical modeling, and numerical simulation. For the liquid nitrogen sprays concurrently injected into FCC suspension flows, all three methods illustrate the same trend of the effect of solids loading. It is shown that, the higher the solids concentration, the shorter the spray evaporation length. This shortening effect is true not only for the length of the dense spray region but also for the total spray evaporation length. In addition, the evaporation length is found to decrease monotonically and asymptotically when the solids concentration is increased. Our modeling shows that the jet-induced entrainment is reduced by droplet evaporation. With an increase in solids loading, more solids would be entrained into the spray region, leading to an increase in spray evaporation. However, the increased evaporation in turn would lead to a reduction in the entrainment rate of the solids. Hence, an asymptotic trend of spray evaporation length results with an increase in solids loading.

The parametric study of solids loading on shortening of the spray evaporation length was conducted using the following conditions: ambient gas-solids velocity of 4.0 m/s; ambient gas-solids temperature of 300 K; pipe diameter of 51 mm; spray jet velocity of 30 m/s and spray jet mass flow rate of 2.7 g/s; and nozzle tube diameter of 1.2 mm. The solids volumetric loading varies up to 1%. The study shows that, with a solids loading of 1.0%, the total evaporation length is shortened by 50% compared to that of the solids-free case, whereas the length of the dense region is shortened by nearly 70%. It is shown that the shortening effect of solids loading has more impact on the dense region

than on the total spray region. Due to the asymptotic nature, within the range of this investigation, the most sensitive range of the shortening effect of the solids loading occurs within 0.5%, whereas the shortening effect becomes relatively insensitive beyond this point.

One interesting indication of this study is that, due to the existence of the asymptotic trend, the spray structure in a dense gas-solids suspension may be very similar to that in a dilute suspension flow (say, at a solids loading of 0.5%).

7.2.3 Non-Uniformity of Phase Distributions

In order to investigate the non-uniform phase distributions in the spray region, a numerical simulation was performed, based on a computer program originally developed by Argonne National Laboratory. This study considers special collision modes between evaporating droplets and solids with a temperature above the Leidenfrost temperature. One of the major contributions from this study is the development and implementation of the Leidenfrost collision model into the computational code, which reflects non-direct contact between droplet-solids by the vapor film due to the quick evaporation.

The numerical simulation revealed the strong non-uniformity in phase distributions. Typical simulation conditions include a liquid nitrogen jet of 2.7 g/s, jet velocity of 30 m/s, solids volumetric loading of 1%, and ambient air flow of 4 m/s and room temperature of 300 K. Under these conditions, the maximum temperature difference is about 150 K in the spray region, while the maximum velocity difference is 25 m/s. A strong non-uniform distribution was also illustrated in the solids concentration distribution. Due to the jet expansion and solids inertia, there exists a dense solids layer

around the jet boundary. This high solids concentration layer may strongly affect the heat and mass transfer between the spray region and its surrounding flows. This phenomenon of a dense solids layer may require further experimental exploration and validation.

Another interesting contribution from the numerical simulation is the finding of the existence of similarity in the gas velocity profile in the main spray region. It revealed that dimensionless velocity distributions are not only similar to but also match the Schlichting formula or "the Law of 3/2" of single-phase jets. Within the range of this study, it appears that the similarity model for a one-phase jet may be extended to three-phase jets with strong droplet evaporation.

7.3 Suggested Future Research Topics

Due to the time limit and other restraints, the current study only focused on the methodology development and investigation of solids loading on the shortening of the spray evaporation length. This study undoubtedly opens a wide research area with both high academic value and application significance. Some future research topics are suggested below.

- The measurements should be extended from dilute conditions to dense phase flows. This extension may provide other findings with respect to the spray evaporation rate and solids loading of significant industrial relevance.

- The effect of nozzles should be combined since the atomization process is an integrated part of the entire spray and evaporation process.

- The volumetric effect of droplets on gas-solids flows should be included in the numerical simulation. This effect may be important for the immediate regions near the spray nozzle.

- The current turbulent model is based on the Prandtl mixing length model. A better model (such as the k-ε model) should be used to interpret the phase interactions. A study on turbulence modulation with spray evaporation is also highly recommended.

- The phase interactions and transport due to eccentric collisions between droplets and superheated solids should be investigated, as well as the effect of non-uniform size distributions.

REFERENCES

Abramovich G.N., 1963, "The Theory of Turbulent Jets," M.I.T. Press, Cambridge, MA.

Achenbach E., 1974, "Vortex Shedding from Spheres," *Journal of Fluid Mechanics*, **62**, 209-221.

Aggarwal S.K., Tong A.Y. and Sirignano W. A., 1984, "A Comparison of vaporization Models in Spray Calculations," *AIAA Journal*, **22**, 1448-1457.

Aggarwal S.K., Chen G., Jackson T.A. and Switzer G. L., 1991, "Vaporization Behavior of Fuel Droplets in a Hot Air Stream," *International Journal of Heat Mass Transfer*, **34**, 2669-2673.

Ahluwalia R., 1999, "Droplet Vaporization Model and FCC Riser Model," Argonne National Laboratory, Argonne, IL.

Bazile R. and Stepowski D., 1994, "2D Laser Diagnostics of Liquid Methanol for Investigation of Atomization and Vaporization Dynamics in a Burning Spray Jet", *Symposium (International) on Combustion Proceedings of the 25th Symposium (International) on Combustion,* Jul. 31-Aug. 5, Irvine, CA, 363-369.

Belyaev S.P. and Levin L.M., 1974, "Techniques for Collection of Representative Aerosol Samples," *Journal of Aerosol Science*, **5**, 325.

Blake T.R., 1996, "Gas Jets in Fluidized Media, Turbulent Diffusion Flames, and Condensing Vapor Jets in Liquids," *Powder Technology*, **89**, 187-195.

Bos A.S. and Ooms G., 1985, "Particle Collision Theories Applied to Agglomeration in Suspension," *Applied Scientific Research,* **42**, 265-276.

Buchanan J.S., 1994, "Analysis of Heating and Vaporization of Feed Droplets in Fluidized Catalytic Cracking Risers," *Industrial and Engineering Chemistry Research*, **33**, 3104-3111.

Bussmann M., Chandra S., and Mostaghimi J., 1997, "Droplet Impact on Arbitray Surface Geometries," *Procedding of ASME Fluids Engineering*, June 22-6, Ancouver, BC, FEDSM97-3073.

Chang S. L., Lottes S.A., Zhou C.Q. and Petrick M., 1996, "Evaluation of Multi-phase Heat Transfer and Droplet Evaporation in Petroleum Cracking Flows," *HTD-Vol. 335, Proceeding of ASME Heat Transfer Division*, **4**, 17-27.

Chang S. L., Lottes S.A., Golchert B. and Petrick M., 1998, "Interaction of Multi-phase Hydrodynamics, Droplet Evaporation, and Chemical Kinetics in FCC Riser

Reactions", *AIAA/ASME Joint Thermophysics and Heat Transfer Conference*, **1**, 261-269.

Chen M., Kontomaris K. and Mclaughlin J.B., 1998, "Direct Numerical Simulation of Droplet Collisions in a Turbulent Channel Flow. Part 1. Collision Algorithm," *International Journal of Multiphase Flow*, **24**, 1079-1103.

Chen M., Kontomaris K. and Mclaughlin J. B., 1998, "Direct Numerical Simulation of Droplet Collisions in a Turbulent Channel Flow. Part 2. Collision Rates," *International Journal of Multiphase Flow*, **24**, 1104-1138.

Chen X.-Q. and Pereira J.C.F., 1995, "Prediction of Evaporating Spray in Anistropically Turbulent Gas Flow," *Numerical Heat Transfer: An International Journal of Computation and Methodology; Part A: Applications* , **27**, 143-162.

Chen X.-Q. and Pereira J.C.F., 1996, "Computation of Turbulent Evaporating Sprays with Well-specified Measurements: a Sensitivity Study on Droplet Properties," *International Journal of Heat and Mass Transfer,* **39**, 441-454.

Chiang H. and Kleinstreuer C., 1992, "Computational Analysis of Interacting Vaporizing Fuel Droplets on a One-Dimensional Trajectory," *Combustion Science and Technology*, **86**, 289-309.

Crowe C. T., 1984, "Droplet-Gas Interaction in Counter-Current Spray Dryers," *Drying Technology*, **1**, 35-56.

Dabros T. T. G. and Van De Ven M., 1994, "Collision-Induced Dispersion Of Droplets Attached To Solid Particles," *Journal of Colloid and Interface Science*, **163**, 28-36.

Dear J.P. and Field J.E., 1988, "High-Speed Photography of Surface Geometry Effects in Liquid/Solid Impact," *Journal of Applied Physics,* **63**, 1015-1021.

Dubrovsky V. V., Podvysotsky A. M. and Shraiber A. A., 1992, "Particle Interaction in the Three-Phase Polydisperse Flows," *International Journal of Multiphase Flow*, **68**, 337-352.

Dwyer H.A., 1989, "Calculations of Droplet Dynamics in High Temperature Enviroments," *Progress in Energy Combust Science,* **15**, 131-158.

Elghobashi S. and Truesdell G.C., 1993, "Two-Way Interaction Between Homogeneous Turbulence and Dispersed Solid Particles. I. Turbulence Modification," *Physics of Fluids A Fluid Dynamics*, **5**, 1790-1801.

Elperin T., Krasovitov B., 1995, "Radiation, Thermal Diffusion and Kinetic Effects in Evaporation and Combustion of Large and Moderate Size Fuel Droplets," *International Journal of Heat Mass Transfer*, **38**, 409-418.

Estrade J.-P., Carentz H., Lavergne G., and Biscos Y., 1999, "Experimental Investigation of Dynamic Binary Collision of Ethanol Droplets – A Model for Droplet Coalescence and Bouncing," *International Journal of Heat and Fluid Flow*, **20**, 486-491.

Field M. A., 1963, "Entrainment into an Air Jet Laden with Particles," *BCURA Inf.*, Circular No. 273.

Filla M., Massimilla L. and Vaccaro S., 1983, "Gas Jets in Fluidized Beds: The Influence of Particle Size, Shape and Density on Gas and Solids Entrainment," *International Journal of Multiphase Flow*, **9**, 259-267.

Foss J.M., Frey M.F., Schamberger M.R., Peters J.E. and Leong K.H., 1989, "Collection of Uncharged Prolate Spheroidal Aerosol Particles by Spherical Collelectors-1: 2D Motion," *Journal of Aerosol Science*, **20**, 515-532.

Gakkhar R.P. and Ppakash S., 1990, "Unsteady Vaporization of Fuel Droplets in a Convective Environment with Varying Ambient Conditions," *International Journal of Heat Mass Transfer*, **33**, 1003-1012.

Gao J., Xu C., Lin S., Yang G. and Guo Y., 2001, "Simulation of Gas-Liquid_Solid 3-Phase Flow and Reaction in FCC Riser Reactors," *AIChE Journal,* **47**, 677-692.

Gavalses M., Theodorakakos A., Bergeles G. and Breon G., 1996, "Evaluation of the Effect of Droplet Collisions on Spray Mixing," *Proceedings of the Institution of Mechanical Engineers, Part C: Journal of Mechanical Engineering Science,* **210**, 465-475.

Gemmen R.S., Keller J.O. and Arpaci V.S., 1990, "Pulse Combustion: Numerical Analysis of Droplet Mass Transfer Enhancement," ASME, *Advanced Energy Systems Division (Publication) AES Thermo-Physical Aspects of Energy Conversion - 1990 Winter Annual,* Nov 25-30 1990, Dallas, TX, **16,** 81-90.

Giorges A.T.G., Wang X. and Forney L.J., 2001, "The Jet Shape of Concentric Mixers," *The Canadian Journal of Chemical Engineering,* **79**, 87-93.

Gore R. and Crowe C.T., 1989, "Effect of Particle Size on Modulating Turbulent Intensity," *International Journal of Multiphase Flow*, **15**, 279-285.

Gu W., 1995, "Evaporation of Liquid Droplets in Superheated Gas/Particle Flows," Ph.D. Thesis, Lehigh University.

Gupta A. and Rao D. S., 2001, "Model for the Performance of a Fluid Catalytic Cracking (FCC) Riser Reactor: Effect of Feed Atomization," *Chemical Engineering Science,* **56**, 4489-4503.

Hetsroni G., 1989, "Particles-Turbulence Interaction," *International Journal of Multiphase Flow*, **15**, 735-746.

Hagesaether L., Jakobsen H.A. and Svendsen H.F., 1999, "Theoretical Analysis of Fluid Particle Collisions in Turbulent Flow," *Chemical Engineering Science*, **54**, 4749-4755.

Hallett W. L.H., 2000, "A Simple Model for Vaporization of Droplets with Large Numbers of Components," *Combustion and Flame*, **121**, 334-344.

Harpole G.M., 1980, "Radiative Absorption by Evaporating Droplets," *International Journal of Heat Mass Transfer*, **23**, 17-26.

Hatta N., Fufimoto H., Kinoshita K. and Takuda H., 1997, "Experimental Study of Deformation Mechanism of a Water Droplet Impinging on Hot Metallic Surfaces above the Leidenfrost Temperature," *Journal of Fluids Engineering, Transactions. ASME,* **119**, 692-699.

Haywood R.J., Renksizbulut M. and Raithby G.D., 1994, "Transient Deformation and Evaporation of Droplets at Intermediate Reynolds Numbers," *International Journal of Heat Mass Transfer*, **37**, 1401-1409.

Hetsron G., 1989, "Particles-Turbulence Interaction," *International Journal of Multiphase Flow*, **15**, 735-746.

Hinze J. O., 1971, "Turbulent Fluid and Particle Interaction", *Progress in Heat Mass Transfer*, **6**, 433-452.

Huang L.S. and Yao S.C., 1999, "Experimental Investigation of the Impaction of Water Droplets on Cylindrical Objects", *International Journal of Multiphase Flow*, **25**, 1545-1559.

Jeelani S.A.K. and Hartland S., 1998, "Effect of Surface Mobility on Collision of Spherical Drops", *Journal of Colloid Interface Science,* **206**, 83-93.

Jenkins J.M., Jones R.L., Jones T.M. and Beret S., 1986, "Method for Fluidized Bed Polymerization," *U.S. Patent* 4,588,790.

Jiang Y. J., Umemura A. and Law C. K., 1992, "An Experimental Investigation on Collision Behavior of Hydrcarbon Droplets", *Journal of Fluid Mechanics,* **234**, 171-190.

Joseph D.D. and Lundgren T.S., 1990, "Ensemble Averaged and Mixture Theory Equations for Incompressible Fluid-Particle Suspensions," *International Journal of Multiphase Flow*, **16**, 35-42.

Johnsson H. and Johnsson F., 2001, "Measurements of Local Solids Volume-Fraction in Fluidized Bed Boiler," *Powder Technology*, **115**, 13-26.

Kawaguchi T., Tanaka T., Tsuji Y., 1998, "Numerical simulation of Two-Dimensional Fluidized Beds Using the Diserete Element Method (Comparison between the Two- and Three Dimensional Models)," *Powder Technology,* **96**, 129-138.

King D., 1992, "Fluidized Catalytic Crackers: An Engineering Review, in: D. Potter, D. Nicklin (Eds.), Fluidization VII", *Engineering Foundation*, New York, NY.

Kitron A., Elperin T. and Tamir A., 1990, "Monte Carlo Simulation of Gas-solids Suspension Flows in Impinging Streams Reactors," *International Journal of Multiphase Flow*, **16**, 1-17.

Klinzing G.E, Rohatgi, N.D., Myler C.A., Dhodapkar S. and Zaltash, 1989, "A Pneumatic Transport of Solids in an Inclined Geometry," *Canadian Journal of Chemical Engineering*, **67**, 237-244.

Kouremenos D., Pantzas C., Panagakls G. and Krikkls R., 1995, "Vaporization Behavior of Fuel Droplets in a Gas Turbine Combustor," *AES-Vol.35, Thermodynamics and the Design, Analysis, and Improvement of Energy Systems*, ASME, **35**, 261-273.

Kunii D., and levenspiel, O., 1991, "Fluidization Engineering, 2nd ed.," Butterworth-Heinemann, Boston.

Lage P.L. C. and Range R.H., 1993, "Single Droplet Vaporization Including Thermal Radiation Absorption," *Journal of Thermophysics and Heat Transfer*, **7**, 502-509.

Lasheras J. C., Villermaux E., and Hopfinger E. J., 1998, "Break-up and Atomization of a Round Water Jet by a High-Speed Annular Air Jet," *Journal of Fluid Mechanics,* **357**, 351-379.

Lee, S. L. and Durst F., 1982, "On the Motion of Particles in Turbulent Duct Flows," *International Journal of Multiphase Flow*, **8**, 333-339.

Levin A. and Hobbs P.V., 1971, "Splashing of Water Drops on Solid and Wetted Surfaces: Hydrodynamics and Charge Separation, Phil. Trans," *Royal Society of London A*, **269**, 555-585.

Leong K. H., Beard K. V. and Stukel J. J., 1985, "The Collision of Non-spherical Aerosol Particle with Small Evaporative Water Drops," *Aerosol Science and Technology*, **4**, 445-454.

Liu G. and Zhu C., 2001, "Drop-particle Collision over Leidenfrost Temperature," *Proceeding of 2001 AIChE Annual Meeting*, November 4-9, Reno, Nevada, 148K.

Lottes S.A., Duffy G.J. and Udaja P., 1993, "A Four-Lump Kinetic Model for Cracking/Coking of Recycled Heavy Oil," *Fuel*, **72**, 1331-1334.

Lun C.K.K., 2000, "Numerical Simulation of Dilute Turbulent Gas-Solid Flows," *International Journal of Multiphase Flow*, **26**, 1707-1736.

Luo H. and Svendsen H.F., 1996 "Modeling and Simulation of Binary Approach by Energy Servation Analysis," *Chemical Engineering Communication,* **145**, 145-153.

Mclaughlin J. B., 1994, "Numerical Computation of Particles-turbulence Interaction," *International Journal of Multiphase Flow,* **20**, 211-232.

Memmot, V. J. and Smoot L. D., 1978, "Cold Flow Mixing Rate Data for Pulverized Coal Reactors," *AIChE Journal,* **24**, 466-473.

Michaeldes E. E. and Liang Li, 1992, "The Effect of Turbulence on the Phase Change of Droplets and Particles under Non-equilibrium Conditions," *International Journal of Heat and mass transfer,* **35**, 2069-2076.

Mostoufi N., J. Chaouki, 1999, "Prediction of Effective Drag Coefficient in Fluidized beds," *Chemical Engineering Science*, **54**, 851-858.

Newton D., 1998, "How BP Makes Use of Its X-Ray Imaging Facility to Support Developments in Fluidized Bed Processes," *Proceeding of 1998 AIChE Annual Meeting*, November 15-20, Miami, FL, 220-231.

Nobari M. R., Jan Y.-J. and Tryggavason G., 1996, "Head-on Collision of Drops—A Numerical Investigation," *Physics of Fluids*, **8**, 29-42.

Park T. W., Aggarwal S. K. and Katta V. R., 1996, "A Numerical Study of Droplet-vortex Interaction in an Evaporating Spray," *International Journal of Heat and Mass Transfer*, **39**, 2205-2219.

Parthasarathy R. N. and Faeth G. M., 1990, "Turbulence Modulation in Homogeneous Dilute particle-Laden Flows," *Journal of Fluid Mechanics*, **220**, 485-514.

Peter E. M., Takimoto A. and Hayashi Y., 1994, "Flashing and Shattering Phenomena of Superheated Liquid Jets," *JSME International Journal, Series B,* **37**, 313-321.

Podvysotskiy A. M. and Dubrovskiy V.V., 1986, "Mass Transfer on Collision of Droplets with a Solid Spherical Particle," *Heat Transfer-Soviet Research*, **18**, 136-140.

Reveillon J. and Vervisch L., 2000, "Spray Vaporization in Nonpremixed Turbulent Combustion Modeling: A Simple Droplet Model," *Combustion and Flame*, **121**, 75-90.

Ricou F. P. and Spalding D. B., 1961, "Measurement of Entrainment by Axisymmetrical Turbulent Jets," *Journal of Fluid Mechanics*, **11**, 21-32.

Senior R.C. and Grace J.R., 1998, "Integrated Particle Collision and Turbulent Diffusion Model for Dilute Gas-Solid Suspensions," *Powder Technology*, **96**, 48-78.

Sirignano W.A., 1999, "Fluid Dynamics and Transport of Droplets and Sprays," Cambridge University Press, New York, NY.

Silverman I. and Sirignano W.A., 1994, "Multi-droplet Interaction Effects in Dense Sprays," *International Journal of Multiphase Flow*, **20**, 99-116.

Sinclair J.L. and Jackson R., 1989, "Gas-Particle Flow in Vertical Pipe with Particle-Particle Interactions," *AIChE Journal*, **35**, 1473-1486.

Skouby D. C., 1998, "Hydrodynamics Studies in a 0.45-m Riser with Liquid Feed Injection," *Proceeding of 1998 AIChE Annual Meeting,* November 15-20, Miami, FL, 238-243.

Sommerfeld M. and Qiu H.-M., 1995, "Particle Concentration Measurements by Phase-doppler Anemometry in Complex Disperesed Two-phase Flows," *Experiments in Fluids*, **18**, 187-198.

Straatsma J., Houwelingen G.V., Steenbergen A.E., Jong P.De, 1999, "Spray Drying of Food Products: I. Simulation Model," *Journal of Food Engineering*, **42**, 67-72.

Sornek R. J., Dobashi R. and Hirano T., 2000, "Effect of Turbulent on Vaporization, Mixing, and Combustion of Liquid-Fuel Sprays," *Combustion and Flame*, **120**, 479-491.

Subramanian V., 1982, "Entrainment by a Concentric Jet with Particles in the Primary Stream," *Letters in Heat and Mass Transfer*, **9**, 277-290.

Subramanian V., 1982, "Entrainment by a Concentric Jet with Particles in the Secondary Stream," *The Canadian Journal of Chemical Engineering*, **60**, 589-592.

Subramanian V. and Raman N., 1983, "The Fully Developed Region of a Two-Phase Jet," *International Communication of Heat Mass Transfer*, **10**, 413-420.

Subramanian V. and Ganesh R., 1984, "Influence of Free Stream Velocity on the Entrainment by Single- and Two-phase Axisymmetric Jets," *AIChE Journal*, **30**, 1010-1013.

Subramanian V. and Raman N., 1984, "Measurement of Velocity and Concentration for a Two-phase Turbulent Jet," *The Canadian Journal of Chemical Engineering*, **62**, 314-318.

Subramanian V. and Venkatram S., 1985, "Particle Entrainment by Axisymmetric Jets," *The Canadian Journal of Chemical Engineering,* **63**, 853-855.

Sujith R. I., Waldherr G.A., Jagoda J. I. and Zinn B.T., 1996, "On the Effect of Evaporation on Droplet Drag," *Journal of Fluids Engineering, Transactions of ASME*, **118**, 862-864.

Syamlal M., Rogers W. and O'Brien T. J., 1994, "MFIX Documentation Theory Guide," Morgantown Energy Technology Center, *DE94000087*, Morgantown, WV.

Syamlal M., 1995, "MFIX Documentation User's Manual," Morgantown Energy Technology Center, *DE95000031*, Morgantown, WV.

Tatterson D. F., Marker T. L. and Forgac J. M., 1987, "Particle Effects on Free Jet Entrainment," *The Canadian Journal of Chemical Engineering*, **65**, 361-365.

Tsuji Y., Morikawa Y., Tanaka T. and Karimine K., 1988, "Measurement of an Axisymmetric Jet Laden with Coarse particles," *International Journal of Multiphase Flow*, **14**, 565-574.

Warsito W. and Fan L.-S., 2001, "Neural Network Based Multi-Criteria Optimization Image Reconstruction Technique For Imaging Two- And Three-Phase Flow Systems Using Electrical Capacitance Tomography," *Measurement Science and Technology,* **12**, 2198-2210.

Wachters L.H.J. and Westerling N.A.J., 1996, "The Heat Transfer from a Hot Horizontal Plate to Sessile Water Drops in the Spheroidal State," *Chemical Engineering Science,* **21**, 923-936.

Wiesendorf V. and Werther J., 2000, "Capacitance Probes for Solid Volume Concentration and Velocity Measurements in Industrial Fluidized Bed Reactors", *Powder Technology*, **110**, 143-157.

Williams F.A., 1958, "Spray Combustion and Atomization," *Physics of Fluids*, **1**, 541-545.

Wu J.-S. and Faeth G. M., 1995, "Effect of Ambient Turbulence Intensity on Sphere Wakes at Intermediate Reynolds Numbers," *AIAA Journal*, **33**, 171-173.

Yang W.-C., 1974, "Correlations for solid Friction Factors in Vertical and Horizontal Pneumatic Conveyings," *AIChE Journal*, **20**, 605-607.

Yang Y., Arastoopour H. and Hariri M. H., 1993, "Agglomeration of Polyolefin Particles in a Fluidized Bed with a Central Jet, Part2- Theory," *Powder Technology*, **74**, 239-247.

Yarin L. P. and Hetsroni G., 1994, "Turbulence Intensity in Dilute Two-phase Flows-3, The Particles-Turbulence Interaction in Dilute Two-phase Flow," *International Journal of Multiphase Flow*, **20**, 27-44.

Yao S.C. and Cai K.Y., 1988, "The Dynamics and Leidenfrost Temperature of Drops Impacting on a Hot Surface at Small Angles," *Experimental Thermal and Fluid Science*, **1**, 363-371.

Yuan Z. and Michaelides E.E., 1992, "Brief Communication: Turbulence Modulation in Particulate Flows—a Theoretical Approach," *International Journal of Multiphase Flow*, **18**, 779-785.

Zhu C., Slaughter M. C. and Soo S.L., 1991, "Measurement of Velocity of Particles in a Dense Suspension by Cross Correlation of Dual Laser Beams," *Review of Scientific Instruments,* **62**, 2036-2037.

Zinchenko A.Z. and Davis R.H., 1994, "Gravity-induced Coalescence of Drops at Arbitrary Peclet Numbers," *Journal of Fluid Mechanics,* **280**, 119-148.

Zuev Yu. V. and Lepeshinskii I.A., 1995, "Two-Phase Milticomponent Turbulent jet with Phase Transitions," *Fluid Dynamics*, **30**, 750-757.

Zuo B. and Bulck E.D., 1998, "Fuel oil Evaporation in Swirling Hot Gas Streams," *International Journal of Heat and Mass Transfer*, **41**, 1807-1820.